



City Research Online

City, University of London Institutional Repository

Citation: Patterson, Emily (2015). Understanding disability glare: the effects of scattered light on visual performance. (Unpublished Doctoral thesis, City University London)

This is the accepted version of the paper.

This version of the publication may differ from the final published version.

Permanent repository link: <https://openaccess.city.ac.uk/id/eprint/13651/>

Link to published version:

Copyright: City Research Online aims to make research outputs of City, University of London available to a wider audience. Copyright and Moral Rights remain with the author(s) and/or copyright holders. URLs from City Research Online may be freely distributed and linked to.

Reuse: Copies of full items can be used for personal research or study, educational, or not-for-profit purposes without prior permission or charge. Provided that the authors, title and full bibliographic details are credited, a hyperlink and/or URL is given for the original metadata page and the content is not changed in any way.

Understanding disability glare:
the effects of scattered light on visual performance

by

Emily J. Patterson

A thesis submitted for the degree of Doctor of Philosophy at City University, London

This research was funded by the Engineering and Physical Sciences Research Council
(EPSRC) (Grant reference numbers; EP/G044538/1 and EP/I003940/1)

October 2014



**CITY UNIVERSITY
LONDON**

CityLibrary
Your space
Your resources
Your library

**THE FOLLOWING PARTS OF THIS THESIS HAVE BEEN REDACTED
FOR COPYRIGHT REASONS:**

p4, Fig 1.2
p5, Fig 1.3
p11, Fig 1.7
p38, Fig 2.4
p39, Fig 2.5

Summary

The focus of this thesis is on how light is scattered on its passage through the optics of the human eye, and the consequences for visual performance under different lighting conditions. A number of visual psychophysical measurement techniques were employed to investigate the impact of light scatter on various aspects of visual performance.

The preliminary experiments carried out were designed to explore the physical properties of scattered light in the eye. Scattered light varies in both amount and angular dependence, outcomes that relate directly to the number and size of particles involved. In this respect, scattered light is estimated using two methods: one that measures both the amount and the angular dependence of scattered light and the other that assumes constant angular dependence in all observers. The findings show that there are significant differences in angular dependence between observers and that the size of the differences correlates with errors in the estimation of the overall amount of scatter.

Experiments were then carried out to investigate the effects of increased scattered light on visual performance and whether these can explain any aspects of age-related visual degradation. To disentangle increased scattered light from the innumerable other changes that occur with ageing, the amount of scattered light in young, healthy eyes was increased using fogging filters. Increased scatter is shown to have only a small effect on chromatic sensitivity and the ability to recognise letters or other high contrast optotypes that are commonly used to assess visual acuity. Contrast sensitivity, on the other hand, can be much reduced in the presence of increased light scatter.

In addition to gaining a deeper understanding of the physical behaviour of scattered light and its effect on different aspects of vision, this work also addresses the question of how increased retinal illuminance through scattered light derived from spatially localised glare sources affects the retinal sensitivity at discrete locations away from the glare source. The results show that sensitivity to contrast in the presence of a bright glare source varies with the level of ambient luminance. A model that accounts for both optical and retinal factors that cause changes in overall sensitivity to contrast is proposed.

Sensitivity of photoreceptors to the direction of light is also examined, but found to be relatively unimportant in the prediction of sensitivity to contrast. By taking into account changes in retinal sensitivity that occur at different lighting levels, predictions in visual performance are improved significantly in comparison to models based solely on losses of image contrast due to scattered light.

Declaration

I hereby declare that this thesis:

- a) has not been submitted as an exercise for a degree at this or any other University,
- b) comprises the results of my own investigations.

I give permission to the Library to lend or copy this thesis upon request, subject to normal conditions of acknowledgement.

Signed: _____

Emily J. Patterson

Date: _____

Acknowledgements

Firstly, I would like to thank my supervisor, Professor John Barbur, for his advice and enthusiasm, but mainly for his faith in my ability to carry out my PhD. It has been a very rewarding and illuminating experience for me and I am so grateful to have been given this opportunity.

I would like to thank Yingxin Jia, Ruba Alissa, Navaz Davoudian, Edward Barratt, Peter Raynham, Steven Li and Abilene Grute for their various roles in our collaborative projects and for being so easy to work with. I would also like to thank my past and present co-members of the lab for all their help (particularly Marisa Rodriguez-Carmona, Wei Bi, and Evgenia Konstantakopoulou), as well as for a general sense of camaraderie (particularly Joe Hickey and Hanna Gillespie-Gallery).

I owe an infinite debt of gratitude to my wonderful family and my friends (especially Joe Allan and Ben Shave), who have supported and encouraged me unwaveringly. Their patience and ability to listen is admirable. Finally, I thank Gary, who has taught me so much over the course of my PhD – not only about visual science and Matlab, but also about myself. His unyielding honesty and generosity has helped me to learn and develop more than I could have imagined, and I feel lucky to have found such a good friend.

Table of contents

Summary.....	ii
Copyright declaration.....	iv
Acknowledgements.....	v
Table of Contents.....	vi
List of figures.....	xi
List of tables.....	xv
Chapter 1: Introduction.....	1
1. 1. <i>Structure of the human eye</i>	1
1. 1. 1. <i>Cornea and iris</i>	3
1. 1. 2. <i>Lens</i>	6
1. 1. 3. <i>Retina</i>	8
1. 2. <i>Functional organisation of the retina</i>	9
1. 2. 1. <i>Rod and cone photoreceptors</i>	10
1. 2. 2. <i>Retinal ganglion, bipolar, horizontal and amacrine cell</i>	11
1. 2. 3. <i>Sensitivity to spatial and temporal information</i>	14
1. 2. 4. <i>Scotopic, mesopic and photopic vision</i>	15
1. 3. <i>Retinal image quality</i>	18
1. 3. 1. <i>Optical aberrations</i>	18
1. 3. 2. <i>Diffraction</i>	20
1. 3. 3. <i>Scattered light</i>	21
1. 3. 4. <i>Sources of intraocular scattered light</i>	23
1. 3. 5. <i>Directional sensitivity of cone photoreceptors</i>	26
Chapter 2: Scattered light.....	30
2. 1. <i>Effects of light scatter on visual performance</i>	30

2. 1. 1. Disability glare.....	30
2. 1. 2. Discomfort glare.....	31
2. 2. Factors that affect scattered light.....	32
2. 2. 1. Properties of the light source and the eye.....	32
2. 2. 2. Uniformity of light scatter over the plane of the pupil.....	33
2. 2. 3. Wavelength dependence of light scatter.....	34
2. 3. Clinical applications.....	36
2. 3. 1. Age-related changes in scattered light.....	36
2. 3. 2. Cataracts.....	38
2. 3. 3. Measurement techniques.....	39
Chapter 3: Apparatus and Methods.....	48
3. 1. Flicker cancellation technique: measurement of light scatter within the eye.....	48
3. 1. 1. Theoretical basis for light scatter measurement.....	48
3. 1. 2. Apparatus.....	53
3. 1. 3. Stimuli.....	54
3. 1. 4. Calibration for light scatter internal to the display.....	56
3. 1. 5. Procedure.....	57
3. 2. Contrast Acuity Assessment (CAA) test: measurement of visual acuity and functional contrast sensitivity.....	58
3. 2. 1. Apparatus.....	58
3. 2. 2. Stimuli.....	59
3. 2. 3. Procedure.....	61
3. 3. Colour Assessment and Diagnosis (CAD) test: measurement of chromatic discrimination.....	62
3. 3. 1. Apparatus.....	62

3. 3. 2. <i>Stimuli</i>	63
3. 3. 3. <i>Procedure</i>	64
3. 4. <i>Measurement of discomfort glare thresholds</i>	65
3. 4. 1. <i>Apparatus</i>	65
3. 4. 2. <i>Stimuli</i>	65
3. 4. 2. <i>Procedure</i>	66
Chapter 4: Angular dependence of light scatter and its significance.....	68
4. 1. <i>Introduction</i>	68
4. 2. <i>Methods</i>	70
4. 2. 1. <i>Participants</i>	70
4. 2. 2. <i>Experimental design</i>	70
4. 3. <i>Results</i>	71
4. 3. 1. <i>Descriptive statistics</i>	71
4. 3. 2. <i>Comparison of k and k' obtained with measured n and $n = 2$</i>	72
4. 4. <i>Discussion</i>	75
Chapter 5. The effects of simulated ageing, using fogging filters, on visual performance.....	77
5. 1. <i>Introduction</i>	77
5. 2. <i>Experimental design</i>	79
5. 2. 1. <i>Participants</i>	79
5. 2. 2. <i>Quantifying the scattering properties of fogging filters</i>	79
5. 2. 3. <i>Binocular summation</i>	80
5. 2. 4. <i>Visual acuity, contrast sensitivity and chromatic sensitivity</i>	81
5. 2. <i>Results</i>	81
5. 3. 1. <i>Scattering properties of fogging filters</i>	81

5. 3. 2. <i>Effects of fogging filters on binocular disparity</i>	84
5. 3. 3. <i>Effects of added scattered light on visual acuity, contrast sensitivity and chromatic sensitivity</i>	88
5. 3. <i>Discussion</i>	89
Chapter 6. The effect of disability glare on functional contrast sensitivity.....	92
6. 1. <i>Introduction</i>	92
6. 2. <i>Experimental design</i>	94
6. 2. 1. <i>Participants</i>	94
6. 2. 2. <i>Disability glare measurements</i>	95
6. 2. 2. 1. <i>Apparatus</i>	95
6. 2. 2. 2. <i>Stimuli</i>	96
6. 2. 2. 3. <i>Procedure</i>	97
6. 2. 3. <i>Scattered light measurements</i>	98
6. 2. 3. 1. <i>Procedure</i>	98
6. 2. 4. <i>Scatter-based predictions of functional contrast thresholds</i>	98
6. 2. 5. <i>Combined predictions of functional contrast thresholds</i>	99
6. 3. <i>Results</i>	102
6. 3. 1. <i>Equivalent veiling luminance and scatter parameters</i>	102
6. 3. 2. <i>Disability glare – absolute functional contrast thresholds</i>	104
6. 3. 3. <i>Disability glare – predictions of functional contrast thresholds</i>	105
6. 4. <i>Discussion</i>	112
Chapter 7. Directional sensitivity of cone photoreceptors and scattered light within the eye.....	115
7. 1. <i>Introduction</i>	115
7. 2. <i>Experimental design</i>	118

7. 2. 1. <i>Participants</i>	118
7. 2. 2. <i>Functional contrast sensitivity measurements</i>	118
7. 2. 2. 1. <i>Apparatus</i>	120
7. 2. 2. 2. <i>Stimuli</i>	120
7. 2. 2. 3. <i>Procedure</i>	122
7. 2. 5. <i>Predictions of functional contrast thresholds in the presence of glare</i>	122
7. 3. <i>Results</i>	123
7. 3. 1. <i>Absolute functional contrast thresholds</i>	123
7. 3. 2. <i>Modelling contrast sensitivity with the Stiles-Crawford effect</i>	127
7. 3. 3. <i>Disability glare –predictions of functional contrast thresholds</i>	128
7. 4. <i>Discussion</i>	133
Chapter 8. <i>Discussion and conclusions</i>	137
8. 1. <i>Summary of the results</i>	137
8. 2. <i>Discussion of overall results</i>	138
8. 3. <i>Implications for underlying mechanisms</i>	140
8. 4. <i>Implications for road lighting practice</i>	144
8. 5. <i>Implications for methodology and future directions</i>	145
8. 6. <i>Synopsis</i>	147
References.....	148

List of figures

Figure 1.1. Diagram of the human eye.....	2
Figure 1.2. The five layers of the cornea.....	4
Figure 1.3. Pupil dilation and contraction.....	5
Figure 1.4. Scanning electron micrographs of bovine lens fiber cells.....	6
Figure 1.5. The three layers of the lens.....	8
Figure 1.6. A photograph of the fundus.....	9
Figure 1.7. Rod and cone photoreceptors and their signal convergence.....	11
Figure 1.8. Three-dimensional diagram of a portion of the human retina.....	13
Figure 1.9. Diagram showing a parvocellular and a magnocellular retinal ganglion cell.....	14
Figure 1.10. Illustration of ambient light levels.....	17
Figure 1.11. Example of a chromatically aberrated image.....	19
Figure 1.12. Diagram to show the path of rays as they pass through the lens periphery.....	20
Figure 1.13. (A) Diagram to show the behaviour of a wavefront when passing through a large aperture as opposed to a small one. (B) Simulation of diffraction pattern with Airy disc.....	21
Figure 1.14. Photo of oncoming car headlights to illustrate glare.....	22
Figure 1.15. (A) A simulated Descartes corona and (B) an example of a lenticular halo.....	24
Figure 1.16. Anatomy of the human lens.....	25
Figure 1.17. A pictorial representation of photoreceptor directional sensitivity.....	28
Figure 2.1. Schematic diagram of light scattering within the eye.....	31

Figure 2.2. Schematic diagram of Rayleigh and Mie –type scattering.....	35
Figure 2. 3. A simulated ciliary corona.....	36
Figure 2.4. Photo of a cataractous eye.....	38
Figure 2.5. Diagram of the three most common type of age-related cataract.....	39
Figure 2.6. Diagram to show how the Hartmann-Shack wavefront aberrometer works.....	41
Figure 2.7. A simulated three-dimensional diagram of the estimated PSF as a function of visual angle for a 60-year old with a pigmentation factor of 0.5.....	42
Figure 2.8. Charts used to test (A) visual acuity and (B) contrast sensitivity.....	44
Figure 2.9. Diagram to show the paradigm used in the flicker-cancellation technique.	45
Figure 2.10. Stimulus layout for the flicker cancellation technique using (A) direct compensation and (B) compensation comparison methods.....	46
Figure 3.1. The relationship between L_s and θ	49
Figure 3.2. Schematic diagram to show the basis for the computation of annulus size.....	50
Figure 3.3. The experimental setup for the flicker cancellation technique.....	54
Figure 3.4. A pictorial representation of the five annulus sizes used for the measurement of scattered light at different eccentricities.....	56
Figure 3.5. An observers' view of the FCS stimuli.....	61
Figure 3.6. An observers' view of the CAD stimuli.....	64
Figure 3.7. An observers' view of the night-time residential scene used in the measurement of discomfort glare thresholds.....	66

Figure 4.1. Light scatter for an 18-year old and 76-year old observer.....	72
Figure 4.2. Absolute difference in k and k' , calculated using measured n as opposed to $n = 2$, as a function of the absolute difference between measured n and 2.....	74
Figure 4.3. Comparisons between the fitted scatter function yielded when k is computed using $n = 2$ and when k is computed using the measured value of n	75
Figure 5.1. Light scatter for a young observer with and without added scatter.....	83
Figure 5.2. Mean VA thresholds as a function of light scatter.....	84
Figure 5.3. Mean FCS thresholds as a function of light scatter.....	85
Figure 5.4. Mean FCS thresholds as a function of light scatter using the dominant and non-dominant eye.....	87
Figure 5.5. Percentage increases in VA, FCS, and chromatic sensitivity thresholds in the presence of fogging filter.....	88
Figure 6.1. Observers' view of the experimental setup for the disability glare test....	96
Figure 6.2. Functional contrast sensitivity thresholds measured at the fovea and periphery, as a function of retinal illuminance.....	101
Figure 6.3. Light scatter for forty observers.....	103
Figure 6.4. Mean FCS thresholds for 40 observers.....	105
Figure 6.5. Relationship between measured FCS thresholds and model predictions based solely on scattered light.....	106
Figure 6.6. Relationship between measured thresholds and model predictions based on changes in retinal sensitivity combined with changes in scattered light.....	111

Figure 7.1. Observers' view of the experimental setup for measuring contrast sensitivity at different light levels.....	121
Figure 7.2. Mean foveal FCS thresholds for each of four measurement conditions..	124
Figure 7.3. FCS thresholds measured at the fovea and at $\pm 5^\circ$ in the periphery.....	126
Figure 7.4. FCS thresholds measured using a 3.9 mm fixed pupil diameter as well as using a dynamic feedback loop with the Applegate apodization applied to the data.	128
Figure 7.5. FCS thresholds measured using a 3.9 mm fixed pupil diameter with and without the Applegate apodization applied to the data (post-hoc).....	128
Figure 7.6. Comparison between (A) the global model predictions used in Chapter 6, (B) new model predictions, which take into account the S-C effect.....	132

List of tables

Table 4.1. Measured values of L_s at each of the five annulus eccentricities.....	71
Table 4.2. Values of n , k and k' when using measured n and when assuming that $n = 2$	73
Table 6.1. Mean k and n values for old and young observers.....	103
Table 6.2. Root mean square error as a measure of the discrepancy between observed and predicted thresholds for each of the three models.....	109
Table 7.1. Maximum and minimum pupil diameters and FCS thresholds for both observers.....	125
Table 7.2. Root mean square error as a measure of the discrepancy between observed and predicted thresholds for each of the three models.....	130

Chapter 1: Introduction

1. 1. Structure of the human eye

It is well established that vision worsens with age (Haegerstrom-Portnoy, Schneck, & Brabyn, 1999), and many older adults would attest to this. In addition to the increased prevalence of diseases that affect vision, such as glaucoma, macular degeneration and cataract (Quillan, 1999) there are many changes that occur throughout the course of normal ageing, which contribute to age-related visual loss. One of the structures most susceptible to structural changes is the lens, which is what enables us to focus on objects over a wide range of distances; this is known as accommodation. One of the most common problems that occur in the ageing eye is the decline in accommodation due to a decline in the flexibility of the lens. Such decline can be corrected for by using spectacle or contact lenses that facilitate refraction. However, there are other age-related changes within the eye that are not as easy to correct. As the eye ages, structural changes within the cornea and lens cause the transmitted light to scatter in different directions (Boynton, Enoch, & Bush, 1954; DeMott & Boynton, 1958; Hemenger, 1988; Stiles, 1929a). As a result, the light falling on the retina is distributed away from the direction of the beam of light, resulting in a poorer quality of image. When the scattering is particularly severe due to the presence of a bright light source, the scattered light forms a veil of light across the retina, causing a variable reduction in contrast over the entire image. So while some older observers may be capable of focussing on near and distant objects, they may have difficulty detecting or identifying fine spatial detail of low contrast under certain light conditions.

This chapter aims firstly to introduce the structure of the eye (shown in Fig 1.1), in relation to its adaptation for light transmission. Secondly the causes and mechanisms for light scatter in relation to the human eye will be discussed. Thirdly, the factors that affect light scatter and glare will be considered. Finally, the practical implications will be discussed and further research opportunities suggested.

Before light reaches the photoreceptive cells in the retina, it must pass through a number of structures. Some of the structures within the eye, such as the white opaque sclera and the pigmented iris, are adapted for purposes other than light transmission, however only the structures that are relatively transparent will be discussed at present.

The first surface the light encounters is the transparent tear film. This is a very thin, three-layered structure, consisting of an anterior lipid layer, a central aqueous layer, and a mucin layer (Wolff, 1946; Wolff, 1954). The lubricating film serves the purpose of controlling the constitution of the cornea, as well as cleaning away debris to ensure that the outer surface of the eye is smooth.

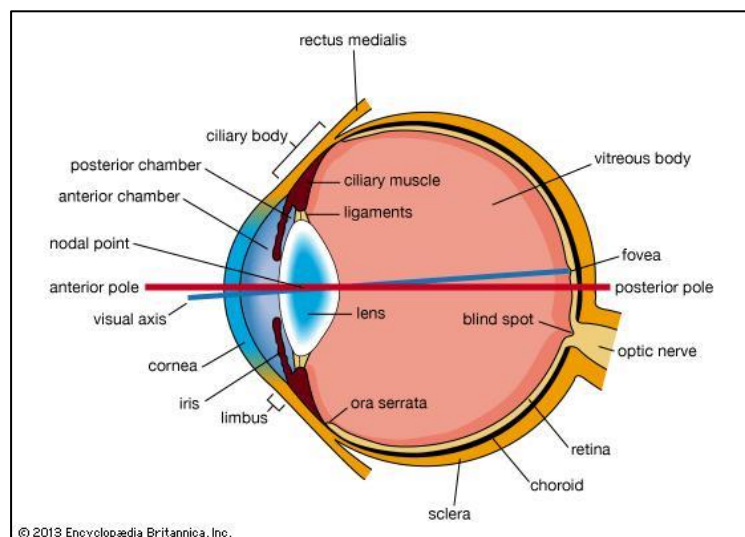


Figure 1.1. Diagram of the human eye (Perkins, 2014).

1. 1. 1. Cornea and iris

After passing through the tear film, the light enters the cornea, which is a transparent structure that acts as a lens and provides three quarters of the eye's focal power (Hubel, 1988). The cornea comprises five basic layers (Kaufman, 2002), as shown in Fig 1.2: the outermost layer acts as a barrier and is known as the corneal epithelium. The cells in this layer regenerate frequently, ensuring that minor damage to the surface of the eye is repaired quickly. Behind this is a transparent sheet known as the Bowmann's layer, which, unlike the epithelium, is made from collagen fibres rather than cells; this is the outermost part of the stroma. The stroma proper is the thickest layer of the cornea and also consists of collagen fibrils; their regular organisation and close spacing helps to ensure that only light that is being propagated in the forward direction is transmitted through the medium; this is known as destructive interference. The Stroma also contains proteoglycans, corneal nerves, salts and keratocytes; the latter are involved in repair of the collagen tissue.

Before the light reaches the final layer of the cornea, known as the corneal endothelium, it passes through Descemet's membrane — an elastic layer comprised of thin fibres, which is secreted by the endothelium itself. The endothelium acts not only as a barrier separating the stroma from the fluid that lies behind it but also as a pump that controls the level of hydration of the cornea. This is necessary because, unlike other parts of the body, there is no blood flow through the eye, which would of course restrict the amount of light that could be transmitted. Unlike the corneal epithelium, damage to the endothelium is more likely to cause long term problems, such as distortion of the wavefront of the light, resulting in aberrated images (Vaughan & Asbury, 1983).

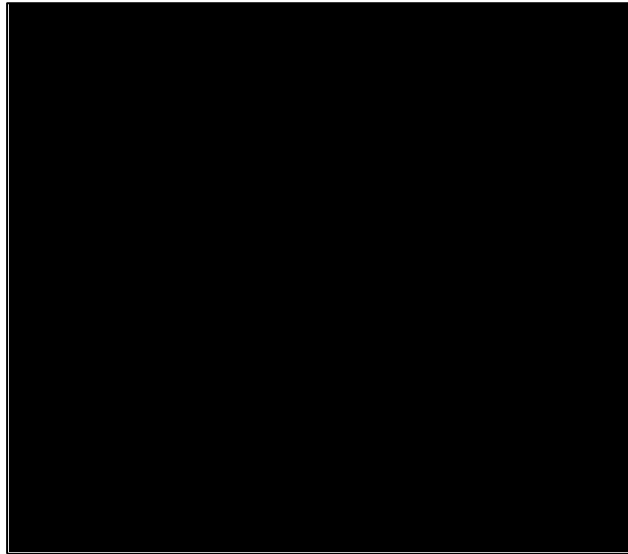


Figure 1.2. The five layers of the cornea(Trattler, 2014).

The highly organised collagen fibrils in the stroma, as well as the smooth spherical surfaces of the cornea, contribute to its transparency, making it an effective transmitter of light. However, the light is not transmitted perfectly. The single ray of light travels towards the eye at a constant speed and in a constant direction. When light comes into contact with the different surfaces of the eye, its speed changes due to variation in the refractive index of the medium. Changes in the speed of incoming light affects the route that the light takes through the medium. This is known as refraction, and the refractive power of the cornea and lens is what enables us to bring images into sharp focus on the retina. However, changes in the uniform structure of these optical components introduce unwanted changes in its optical properties, which, as shall be discussed later, are responsible for unwanted light scatter. After being transmitted through the cornea, light passes through a fluid derived from blood, which is known as the aqueous humor. This fluid serves the purpose of supplying both the cornea and lens with oxygen and nutrients, as well as removing waste.

Before entering the crystalline lens, the light passes through an aperture known

as the pupil. The size of the pupil is controlled by the action of muscles within the iris, which lead to constriction or dilation of the pupil, as shown in Fig 1.3. As the pupil dilates, more light is allowed into the eye increasing the overall retinal illuminance. Whereas a higher level of retinal illuminance has many positive effects on vision, a larger aperture also allows the individual beams of light to cross each other's paths. Rather than each point on the object forming a single point image on the retina, these image points will be spread out, resulting in a blurry image. Other aberrations exist, such as spherical aberration, coma and astigmatism, which will be discussed in more detail in section 1.3.1, also occur when the pupil is large.



Figure 1.3. Pupil dilation and contraction (*E5 the human brain.*).

Constricted pupils restrict the number of beams of light that can enter the eye, resulting in reduced aberrations, and consequently a sharper image. On the other hand, rather than the aperture creating a clear region in which the light is able to travel, individual wavelets near the edge of the aperture continue to propagate outwards; this causes bending of light, known as diffraction. The image formed by these wavelets will be positioned away from the expected point image, resulting in a

poor resolution (Freeman & Hull, 2003). Therefore, there is a trade off between the costs and benefits of large and small pupil sizes.

1. 1. 2. Lens

Both the outer and inner surfaces of the cornea are convex. Whereas the cornea has a high refractive index, which helps to focus incoming light onto the retina, the lens is the structure that enables us to accommodate and therefore must be reasonably flexible. The crystalline lens is composed of transparent fibre cells, shown in Fig 1.4. The high concentration of soluble proteins gives the lens a large refractive index (Xia, Wang, Tatarkova, Aerts, & Clauwaert, 2010), enabling it to refract light in order to focus the image on the retina.

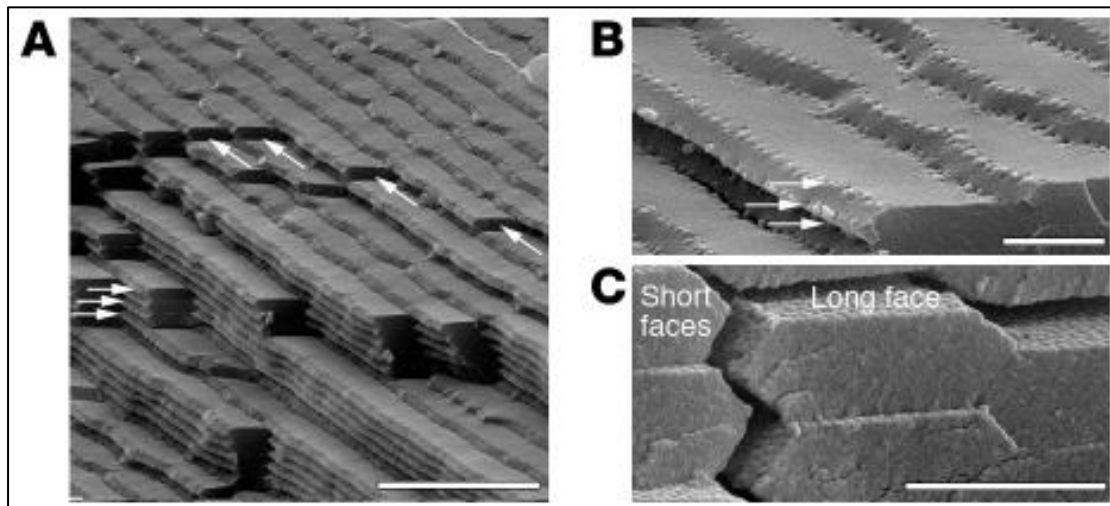


Figure 1.4. Scanning electron micrographs of bovine lens fibre cells (Song et al., 2009). There is precise alignment between the elongated fibre cells in the outermost layers of the lens (A). The arrows in (B) show where the membrane protrudes, helping neighbouring cells to interlock. Their hexagonal profile is shown in (C).

More importantly however, the ciliary muscles, connected to the lens by the zonular fibres, are able to change its shape, thereby providing variable power that enables objects to be seen clearly over a range of distances. When focusing on a close object, the ciliary muscles contract; as a result the zonules slacken, allowing the lens to become more rounded for greater focal power (Snowden, Thompson, & Troscianko, 2006). The opposite action is taken for distant objects.

The adult lens comprises of three layers (shown in Fig 1.5), which continue to develop for the first few months after birth. The outermost layer — the lens capsule — is a collagen based membrane and contributes to the elasticity of the lens (Forrester, Dick, McMenemy, & Lee, 1996). The lens capsule is synthesised by the epithelium, which is the next structure that incoming light encounters. Unlike the lens capsule, the epithelium is only present at the anterior of the lens. Epithelial cells play an important role in controlling the flow of fluid between the aqueous humor and the lens.

Finally, the main body of the lens is made up from lens fibres, which are also produced by the epithelium. The lens fibre cells form in layers, with the embryonic nucleus at the very centre, working outwards through the foetal and adult nucleus, and finally the cortex, which contains the newest cells synthesised by the epithelium. Although lens fibres are continually added throughout life, the term ‘adult nucleus’ is misleading, as most of the nuclear layers are actually fully formed by three months after birth (Augusteyn, 2010). The fibres are tightly packed, and appear to ‘lie flat’, perpendicular to the direction of the light. Again, the organisation, combined with cell transparency, maximises light transmission.

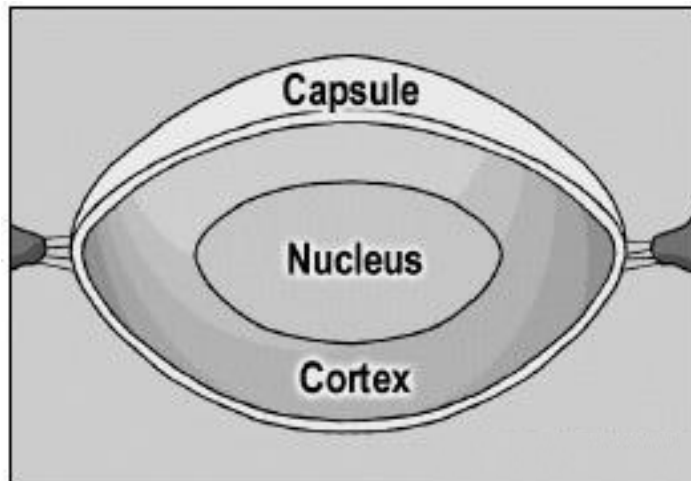


Figure 1.5. The three layers of the lens (Root, 2009).

Beyond the lens is the vitreous humor, the final part of the journey through the eye before the light reaches the photosensitive retina. The vitreous is a viscous, transparent gel-like fluid, which makes up 80% of the eye's volume (Wolfe, Kluender, & Levi, 2006).

1. 1. 3. Retina

Upon reaching the retina, some of the light will penetrate the layer of photoreceptive cells and arrive at the retinal pigment, which absorbs the light energy and can lead to a process known as photoactivation. However, some of the light is reflected back into the eye by retinal pigment, choroid and neural structures; this is known as backwards light scatter, and can be seen using double-pass imaging (Vos, 1964) (see Fig 1.6). As the eye ages, there may be degradation of the pigment due to a build-up of debris. With less pigment to absorb the light and a reduction in specularity, there is more diffuse reflection back into the eye. Fortunately, due to the

directional sensitivity of the cones, otherwise known as the Stiles-Crawford effect (Stiles & Crawford, 1933), which will be discussed in more detail later, back scatter does not have such a detrimental effect on vision as forward scatter.

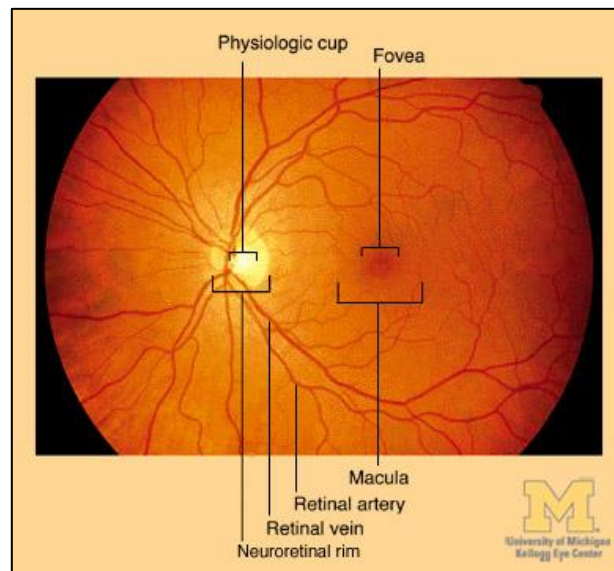


Figure 1.6. A photograph of the fundus – it is possible to obtain such images only because of the backscattering properties of the fundus (American Academy of Ophthalmology, 2014).

1. 2. Functional organisation of the retina

The retina forms a specialised part of the brain, which has become externalised, and equipped to detect light. It is composed of retinal neurons, whose purpose is to convert the incoming light to electrical signals to be sent to the brain via the optic nerve (Gregory, 1966). The majority of the retina consists of five layers, three of which are nuclear layers, containing cell bodies; the other two layers are sandwiched between, and contain the synapses that connect the neurons of the different layers. The central part of the retina, known as the fovea, however, lacks two of the three nuclear layers; the remaining nuclear layer contains the light-sensitive photoreceptors.

The human retina is made particularly impressive by its ability to function over a billion-fold illumination range (Barbur & Stockman, 2010). This achievement owes, in part, to the presence of two types of photoreceptor —rods and cones — which operate preferentially at different light levels.

1. 2. 1. Rod and cone photoreceptors

The names given to rods and cones are derived from the appearance of their outer segments, where the light-absorbing photopigments are contained. The photoreceptors are oriented with their outer segments pointed away from the pupil; therefore the light that enters through the centre of the pupil must travel through the length of the receptor before it has a chance of being absorbed by a photopigment molecule (Wandell, 1995).

The differences between rods and cones in the way that their signals converge explain some of the differences in their function (see Fig 1.7). The signals from several rods converge onto a single neuron; this makes rod-mediated system extremely sensitive to even very dim lights and, for this reason, it is associated with vision in low lighting conditions. It has been shown that the visual system is capable of responding to a single photon of light (Hecht, Schlaer, & Pirenne, 1942). There is, however, a drawback to the rods' signalling system; as each neuron encodes signals from a group of rods, it is not possible to pinpoint exactly from where the signal originates. As such, rod-mediated vision lacks fine spatial detail. The signals from cones, on the other hand, feed into several neurons; as a result, cone-mediated vision can have high spatial resolution.

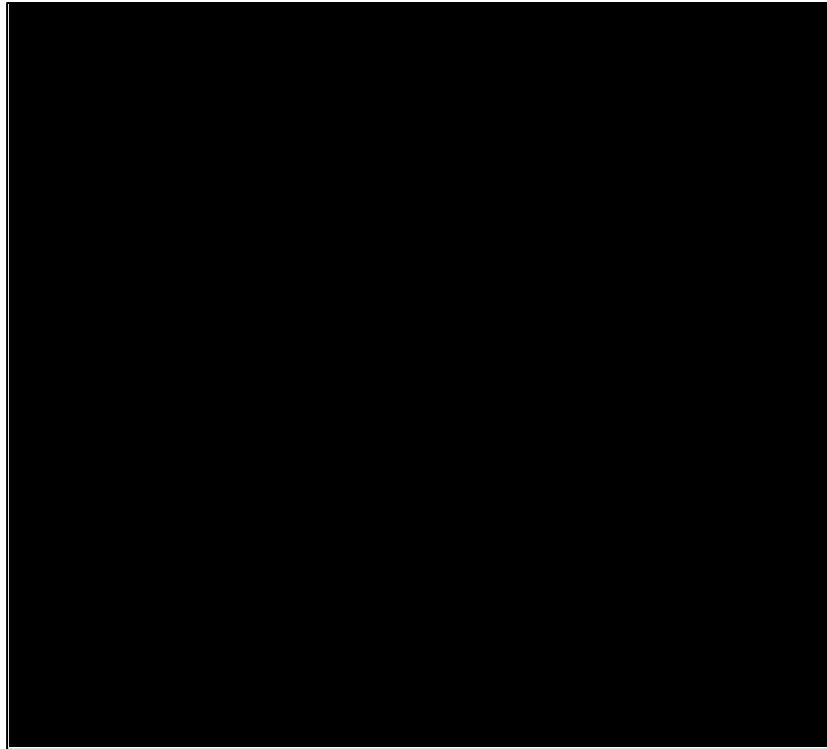


Figure 1.7. Rod and cone photoreceptors and their signal convergence (Claffey, 2012).

Another important difference between rods and cones is in the photopigments that they contain. The photopigment present in rods is of only one type — rhodopsin — whereas cones contain one of three photopigments, each responding preferentially to a different wavelength of light: short, medium and long. This enables cones to encode information, not only about the luminance of light entering the eye, but also about its spectral composition, which is what gives rise to the perception of colour.

1. 2. 2 Retinal ganglion, bipolar, horizontal and amacrine cells

As previously mentioned, the retina is composed of five basic layers, shown in Fig 1.8. Following photoactivation, the signal originating in the photoreceptor outer segment is transmitted from the outer segment to the inner segment and into the cell

body, which is situated in the outer nuclear layer: this is the layer which is furthest away from the pupil.

In the next layer, known as the outer plexiform layer, the photoreceptors make synaptic connections with both the axons and dendrites of the horizontal cells. The branches of the horizontal cells run perpendicular to the photoreceptors, forming part of a lateral pathway. Also in this layer, the photoreceptors make synaptic connections with the dendrites of the bipolar cells. Bipolar cells can be either diffuse — converging the signals from a number of photoreceptors — or ‘midget’ — receiving signals from only one photoreceptor. Midget bipolar cells are isolated to the fovea, whereas diffuse bipolars operate throughout the periphery.

The third layer is called the inner nuclear layer, where the cell bodies of bipolar, horizontal and amacrine cells are located. The adjacent layer is known as the inner plexiform layer, where the bipolar cells make synaptic connections with the dendrites of the amacrine and, sometimes in the cone pathway, directly with the ganglion cells; the latter cell bodies are located, unsurprisingly, in the ganglion cell layer, which is the fifth and final layer. Both horizontal and amacrine cells can be thought of as forming lateral pathways, as opposed to the vertical pathway of the photoreceptor, bipolar, and ganglion cells (Wolfe et al., 2006). The bipolar cells are the only cells to link the inner and outer plexiform layers; therefore the signals from all the other retinal cells must pass through them (Wandell, 1995). Similarly, the axons of the ganglion cells are the only cells to communicate with the brain, so all signals must also pass through them. The ganglion axons exit the eye at the optic disc, and the bundle of axons transmitting signals to the brain is called the optic nerve.

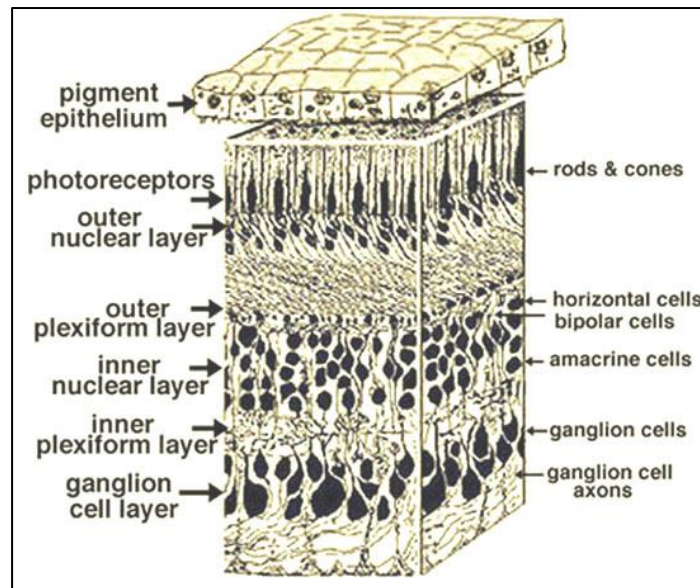


Figure 1.8. Three-dimensional diagram of a portion of the human retina. The five basic layers — outer nuclear, outer plexiform, inner nuclear, inner plexiform and ganglion cell — are shown (Kolb, 2014b).

The ratio of photoreceptors to ganglion cells is approximately 100:1; therefore some pooling of signals is needed. Ganglion cells receive input from a fixed area of the retina, known as a receptive field. They do not, however, respond equally to light in all parts of the receptive field; they have a centre-surround response pattern. Roughly half of the ganglion cells show an excitatory response when light falls on the centre and an inhibitory response when light falls on the surround; these are called ‘ON-centre’ ganglion cells, whereas ‘OFF-centre’ ganglions exhibit the opposite response. The advantage of the centre-surround response is that it enables us to detect boundaries and edges, which, in functional terms, are more important for perception (Snowden et al., 2006).

1. 2. 3. Sensitivity to spatial and temporal information

Ganglion cells come in four main types: parvocellular, magnocellular, small bistratified and shrub; the most important of these for human vision are the parvocellular — p-cells — and the magnocellular — m-cells — ganglions (see Fig 1.9). P-cells make up roughly 70%, and m-cells, roughly 10%, of all retinal ganglion cells.

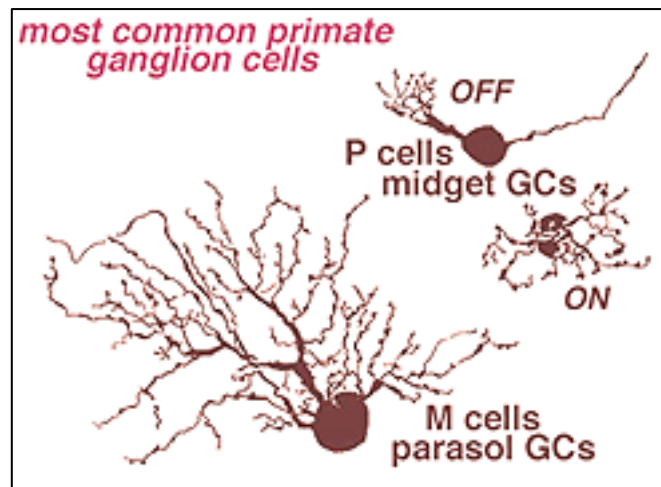


Figure 1.9. Diagram showing a parvocellular and a magnocellular retinal ganglion cell. The difference in the size of their dendritic fields is clearly illustrated (Kolb, 2014a).

Perhaps confusingly, p-cells are also known as midget, and m-cells are known as parasol ganglions; the reason for this is their appearance and the size of their receptive fields. Midgets — p-cells — have small dendritic fields and, perhaps unsurprisingly, receive input from midget bipolar cells. Parasols —m-cells — have larger, umbrella-like dendritic fields, and receive input from diffuse bipolar cells (Snowden et al., 2006; Wolfe et al., 2006).

Because parasols have larger receptive fields and pool information from a large number of photoreceptors, they are more suited to detection of dim lights.

Midgets, with their small receptive fields and limited pooling, are tuned to providing more specific information. Unlike m-cells, they have either an excitatory or inhibitory response to long-wave cone photoreceptors, and the opposite response to medium-wave cones. Therefore p-cells enable us to determine the colour and fine details of objects.

A further difference between m- and p- cells is in their firing rates. Light detected by a p-cell will cause sustained firing, giving us a continuous image. This is very useful for detecting changes in contrast over space. M-cells, on the other hand, respond only transiently to light and will return to the resting firing rate despite the light remaining constant (Wolfe et al., 2006). The effects of this can sometimes be seen when looking at the night sky; if they eyes are kept still, the stars seem to disappear, particularly in the peripheral visual field (Troxler, 1804). The transient response of the m-cells carries information about flicker or movement, helping us to detect changes over time.

To summarise, m-cells are involved largely in peripheral vision, which often involves rod and cone signals; they can function at lower contrast and provide imprecise information about light changes over time. P-cells are relevant to central, cone-mediated vision; they provide fine resolution and carry information about colour at higher light levels.

1. 2. 4. Scotopic, mesopic and photopic vision

As previously mentioned, the visual system is able to function over a large range of light levels, as shown in Fig 1.10; this is partly owing to changes in pupil

size, but mostly owing to the differences between the responses of the rod and cone pathways.

At very low levels of retinal illuminance — below 0.003 cd/m^2 — such as when a scene is lit only by starlight, vision is facilitated solely by rod photoreceptors; this is known as scotopic vision. Because of the large pooling of information in the rod pathway, we are extremely sensitive to dim, moving or flickering lights. During scotopic vision we are completely insensitive to differences in wavelengths, so we do not perceive colour, and we are unable to scrutinise fine details. Conversely, photopic vision at the fovea, which occurs — above 3 cd/m^2 — in daylight, is dictated solely by cone photoreceptors. At photopic luminance levels, we have much higher acuity and are better able to discriminate differences in colour and contrast. A further difference between scotopic and photopic vision is the spectral responsivity — the relative sensitivity to different wavelengths — of the visual system. Spectral responsivity peaks at around 505nm for scotopic and 555nm for photopic vision (Schwiegerling, 2004).

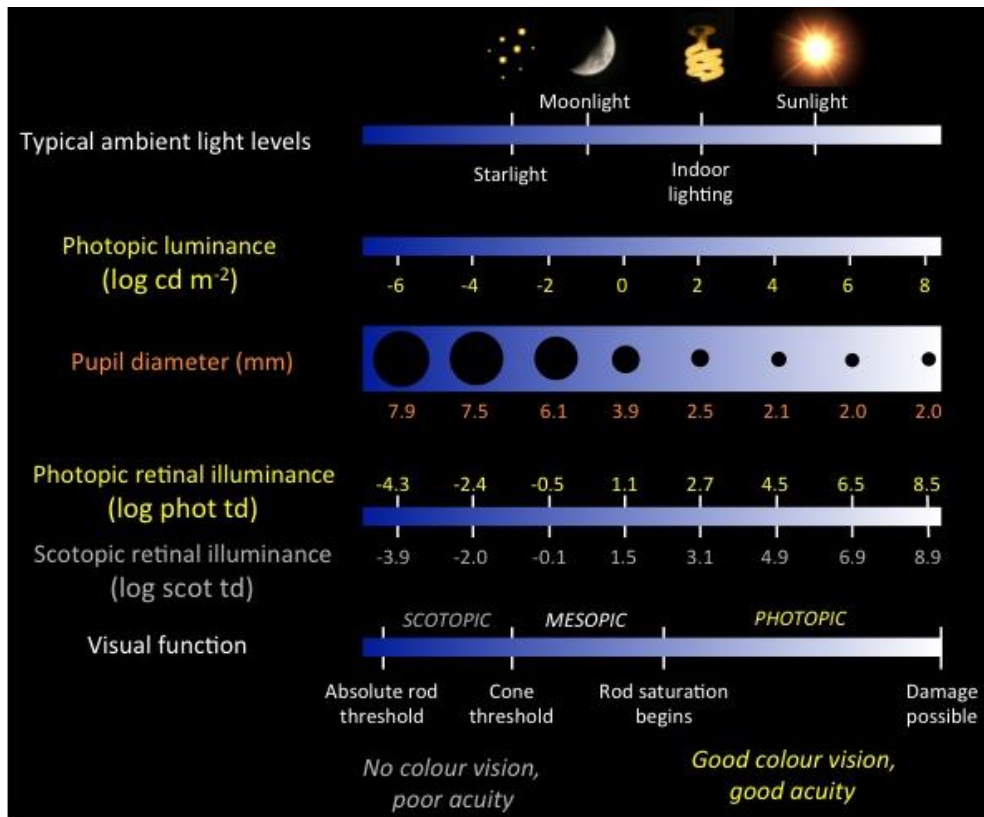


Figure 1.10. Illustration of ambient light levels (Barbur & Stockman, 2010)

Visual performance in both scotopic and photopic ranges can be reasonably well estimated using our existing knowledge of how rods and cones respond to light. The situation becomes more complicated in the intermediate — mesopic — range. Mesopic vision involves both rods and cones and small changes in either the amount or the spectral composition of light produce large changes in visual performance. As a consequence, whereas spectral responsivity curves exist for both photopic (International Commission on Illumination, 1926) and scotopic (International Commission on Illumination, 1952) ranges, no single curve exists for the mesopic range. The International Commission on Illumination have put forward recommendations for mesopic photometry, which employ a number of different curves to predict visual performance within this range (International Commission on Illumination, 2010).

It is very difficult to estimate with accuracy visual performance under mesopic lighting conditions, because the relative contribution of rod and cones will vary throughout the range (Walkey et al., 2005; Walkey, Harlow, & Barbur, 2006a; Walkey, Harlow, & Barbur, 2006b).

1. 3. Retinal image quality

1. 3. 1. Optical aberrations

The eye, though well adapted for forming images on the retina, is not a perfect optical system. Although, quite often they go unnoticed, aberrations occur that result in a lower quality image. Chromatic aberration occurs because different wavelengths travel at different velocities depending on the medium through which they are travelling. When light enters the lens, which is denser and has higher refractive power than air, short wavelengths, i.e. blue light, travel slower than long wavelengths, i.e. red light. If white light enters the lens at an angle, the blue light, which is travelling slower, will be refracted more than the red light; this can result significant changes in image plane position and size, as illustrated in Fig 1.11. In spite of large chromatic aberration in the human eye, there are very few situations in which we are able to see this effect. There are many possible reasons for our inability to notice chromatic aberrations: one is that the largest discrepancy between wavelengths occurs at the extreme ends of the spectrum, where luminous efficiency is lowest (Millodot, 1982). Blue light is also filtered out partially through absorption by the lens (Ruddock, 1965; van den Berg, IJspeert, & de Waard, 1991) and macular pigment (Hammond, Wooten, & Snodderly, 1998; Landrum & Bone, 2001) and the blue light that does reach the retina contributes little to foveal vision due to low density of S-cones at the fovea

(Curcio et al., 1991). Additionally, the luminance channel receives input from only the M- and L- cones (Snowden et al., 2006).



Figure 1.11. Example of a chromatically aberrated image.

Spherical aberrations, which are caused by the shape of the lens, also affect image quality. As with chromatic aberrations, when light enters at an angle, the change in velocity causes the rays to change direction. Because the light encounters two interfaces as it passes through the lens — one upon entry and one upon exit — there will be two changes in direction. Regular lenses have an optical axis, which is the point, or area, in which the two interfaces are parallel to each other, and light travels through the medium in a straight line. Towards the edges of an oval-shaped lens, i.e. further away from the optical axis, the light is refracted to a greater extent; the result is that these light rays do not have the same focal point as the more central rays and the image becomes blurred, as shown in Fig 1.12.(A). Spherical aberration therefore increases with pupil size as more of the light will be incident further away from the optical axis. However, the human lens is slightly flatter in the periphery, lessening the amount of refraction and thereby compensating partially for spherical aberration (Millodot, 1982), (see Fig 1.12.(B)).

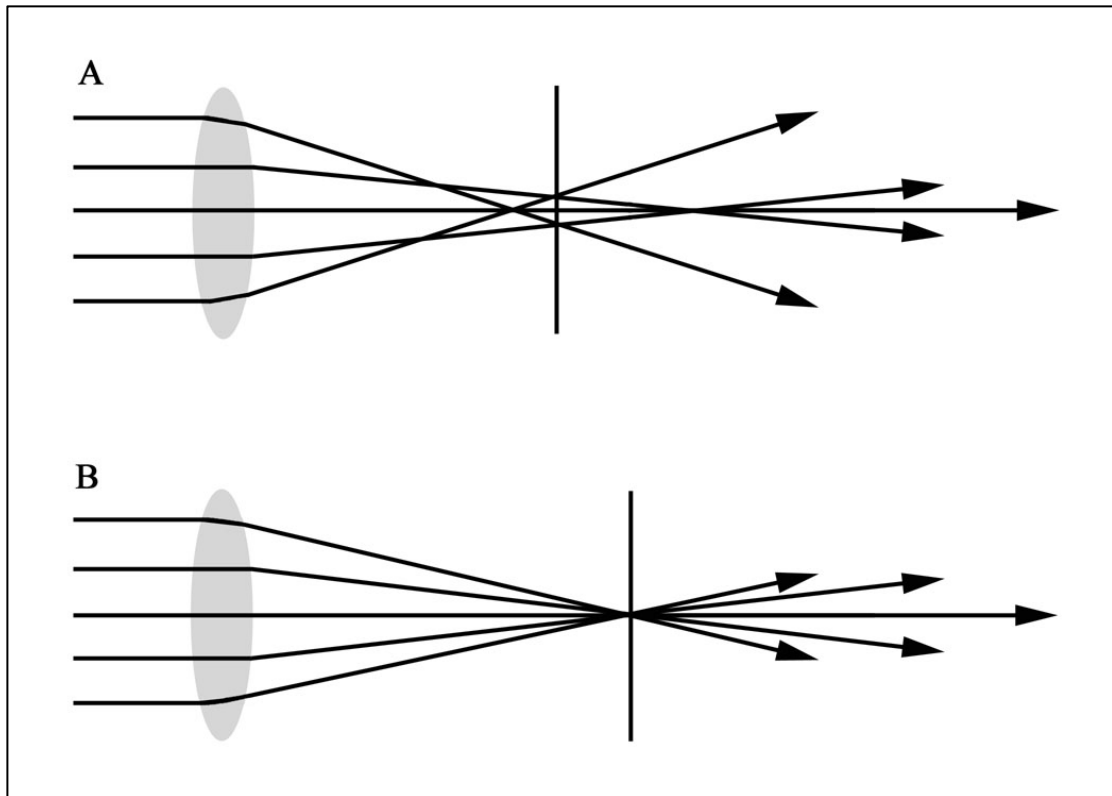


Figure 1.12. (A) Diagram to show the path of the rays as they pass through the lens periphery, resulting in spherical aberration. (B) In the absence of spherical aberration, all the rays converge at the same focal point (Wopereis, 2010).

1. 3. 2. Diffraction

Light can be thought of as being formed of both waves and particles. The particles in this case are known as photons and each particle carries one quantum of energy (Wolfe et al., 2006). However, it is the wave nature of light that leads to a reduction in the quality of the retinal image: diffraction. Diffraction occurs because every point on a wavefront acts as a secondary source of a new wave. When a wavefront is disrupted by, for example, the edges of an aperture such as the pupil, the direction of propagation is altered; rather than stopping at the aperture, some light continues to propagate outwards, around the edges of the aperture. The image that

results from a point source of light passing through a small aperture is that of a bright central disc, surrounded by concentric rings that decrease in luminance with eccentricity, known as the airy disc (see Fig 1.13). Because diffraction occurs only at the edges of an aperture, the image resulting from a smaller pupil will show less diffraction proportionally than that from a large pupil (Millodot, 1982). Diffraction therefore shows the opposite effect to other optical aberrations with changes in pupil size.

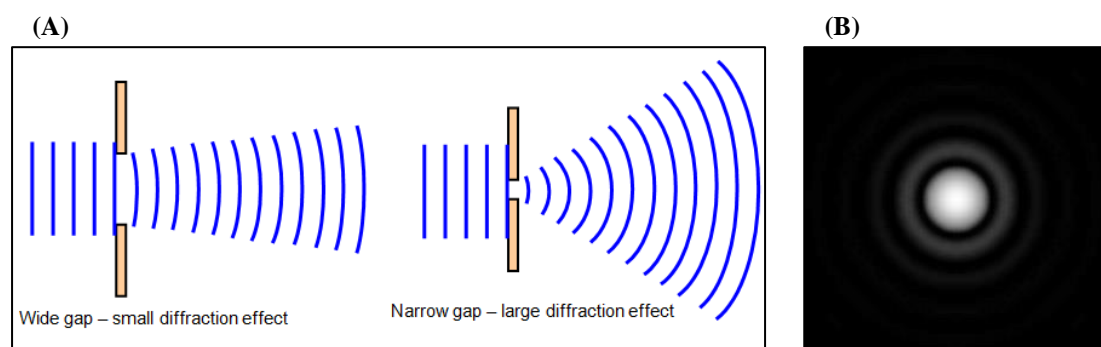


Figure 1.13. (A) Diagram to show the behaviour of a wavefront when passing through a large aperture as opposed to a small one (Gibbs, 2013). (B) Simulation of diffraction pattern with Airy disc.

1. 3. 3. Scattered light

As light travels through the atmosphere, it encounters particles suspended in the air, and when a photon of light comes within close vicinity of one of these particles its direction of propagation changes. Rather than the light being transmitted, reflected, refracted or diffracted, it is briefly captured by the particle, before being released in a different direction. Each particle therefore acts as a secondary source of radiation (Raman, 1978).

Intraocular light scatter occurs when the scattering particles are within the

structure of the eye itself and its effect on the retinal image is comparable to extraocular light scatter. The effects of intraocular light are often experienced as a halo or spikes emanating from a bright light source (Simpson, 1953); this occurs noticeably in the presence of oncoming car headlights whilst driving at night. In extreme cases, the amount of scattered light is so great that the observer is unable to see objects in other areas of the visual field; this is known as disability glare. A large amount of intra-ocular light scatter can make every day visual tasks more challenging, and many tasks, such as night-time driving (see Fig 1.14), potentially dangerous.



Figure 1. 14. Photo of oncoming car headlights to illustrate glare.

The overall amount of scatter in a given eye will depend upon the distribution and size of scattering particles within the ocular medium, predominantly the cornea and lens. Whereas there will occasionally be foreign particles in the vitreous humor — known as floaters — which are formed of biodebris suspended temporarily in the fluid, these are not usually a cause for concern and contribute very little in terms of light scatter. It was mentioned earlier that the structure and composition of both the cornea and lens maximises light transmission. However, as the light passes between adjacent cells and tissue, and interacts with particles within the medium, there will

inevitably be some deviation in the direction of propagation, albeit minimal in young healthy eyes (DeMott & Boynton, 1958).

1. 3. 4. Sources of intraocular scattered light

The cornea contributes around 30% of the total forward light scatter (Vos & Boogaard, 1963), and its contribution tends not to vary within an individual's lifetime. However, large increases in corneal light scatter occur when the tissue becomes damaged, for example after infection or surgery (De Brouwere, Ginis, Kymionis, Naoumidi, & Pallikaris, ; De Brouwere, 2008; Elliott, Fonn, Flanagan, & Doughty, 1993). Particles on the surface of the cornea can also scatter incoming light, leading to the appearance of coloured bands around bright light sources, known as Descartes coronas (see Fig 1.15.(A)). These coronas are, however, transient and tend only to appear for a few minutes after waking (Simpson, 1953).

The scatter contribution of the lens is similar to that of the cornea (Vos, 2003b) but is more susceptible to change over one's lifetime. As already discussed, the lens has a crystalline structure, and is composed of regularly packed fibres. The radial fibres in the periphery act as a circular grating, which cause the light rays to deviate. The resulting image is that of a white disc — known as an aureole — surrounded by a number of coloured bands made up from irregular rays. The coloured bands progress through the colours of the visible spectrum with violet closest to the centre and red at the outside; this is known as a lenticular halo (see Fig 1.15.(B)). The narrower the radial lens fibres, the further the rays are displaced from the centre of the retina. The diffractive effect of the fibres is limited to the periphery of the lens; a light source must therefore subtend an angle at the lens large enough for the light to reach

the fibres that cause the halo (Hemenger, 1992; Simpson, 1953). Scattering in the lens can also be caused by the formation of particles within the lens (Spector, Li, & Sigelman, 1974). This will be discussed in further detail in Chapter 2.

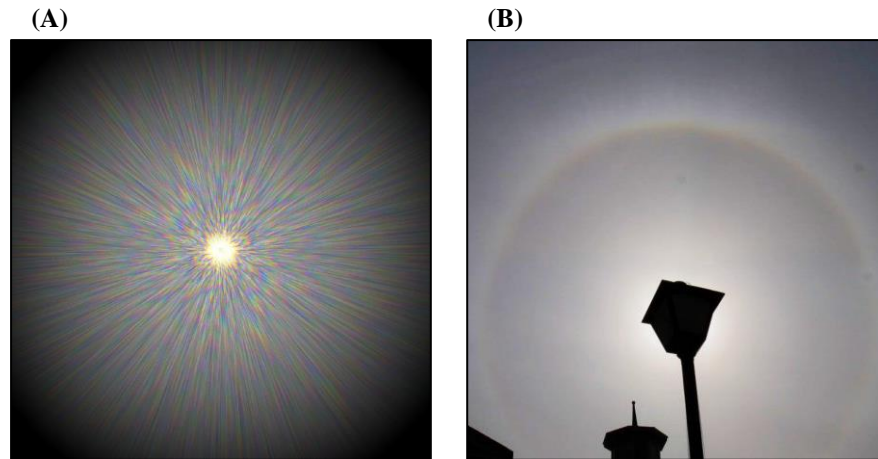


Figure 1.15. (A) A simulated Descartes corona (van den Berg, Hagenouw, & Coppens, 2005), and (B) an example of a lenticular halo.

The contribution of the nuclear region (see Fig 1.16) to the total amount of light scatter is relatively small in young eyes and increases gradually until around the age of forty, after which, scatter increases rapidly. It has been suggested that nuclear scatter is caused by the presence of large protein macromolecules, whose refractive indices differ from the surrounding lens fibres. It is the increasing size and number of these protein aggregates that is responsible for the sharp increase in scattered light in older age (Ben-Sira, Weinberger, Bodenheimer, & Yassur, 1980; Spector et al., 1974).

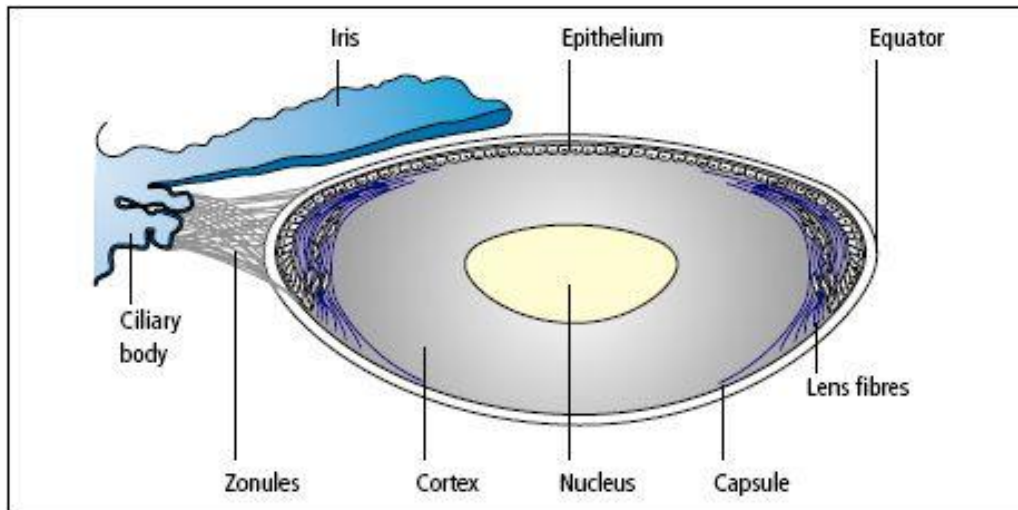


Figure 1.16. Anatomy of the human lens (James & Bron, 2011).

Structural changes elsewhere in the eye may also have an effect on the amount of light scatter that is absorbed (Ijspeert, de Waard, van den Berg, & de Jong, 1990). For example, the iris, although pigmented, is not perfectly opaque; as a result, some light is scattered through it (Coppens, Franssen, & van den Berg, 2006; van den Berg, Ijspeert, & de Waard, 1991).

Another structure to consider is the fundus, as the light must pass through the neural network that comprises the retina before it reaches the photoreceptors. A small portion of light is absorbed by the neural structures and any that is scattered does not have a significant distance to travel before it reaches the photoreceptors; therefore the effect of forward scatter is minimal. However, a significant amount of light is reflected / scattered back into the eye; as such, this type of scattering is known as backward light scatter. The contribution of the fundus to total light scatter is around 40% (Vos, 2003b) but, as we shall consider later, the Stiles-Crawford effect reduces the effective contribution of backward scatter to the glare veil in the resultant retinal image. The back-scatter from the fundus is due to the presence of microscopic neural structures in the retina, the vascular structures that make up the choroid, as well as

retinal pigments.

Macular pigment, which is present in the Henle fibres of the photoreceptors, just in front of the retina is a factor that affects the amount of back-scatter. This pigment helps to protect the photoreceptors from damage caused by high-energy, short-wave light. It apparently does this, firstly by absorbing short wavelength light and, secondly, by quenching the chemically active, free radicals, both of which could potentially damage the tissue (Hammond et al., 1998; Stringham, Garcia, Smith, McLin, & Foutch, 2011). By acting as an antioxidant and a short-wave filter, the pigment not only protects the retina, but also reduces chromatic aberration. Unlike the pigmentation in the iris, macular pigment is dietary-derived. Leafy green vegetables are rich in the component carotenoids, lutein and zeaxanthin, so there is evidence that a healthy diet may help to preserve visual function (Hammond et al., 1998). Whether macular pigment has a significant impact upon the amount of scattered light reaching the photoreceptors is a topic for debate (Cerviño, Gonzalez' Meijome, Linhares, Hosking, & Montes-Mico, 2008; Luria, 1972; Stringham et al., 2011; Wolffsohn, Cochrane, Khoo, Yoshimitsu, & Wu, 2000). However, because the pigment absorbs short-wave light, a larger amount of macular pigment is likely to result in a smaller amount of short-wave scatter.

1. 3. 5. Directional sensitivity of cone photoreceptors

In order to optimise the image on the retina, it is important that the amount of scattered light reaching the photoreceptors is minimised. Firstly, as already mentioned, the corneal and lenticular structures are highly organised; the long collagen fibres are densely and uniformly packed, and their spacing is smaller than

the wavelength of light. Any light not travelling forward is prevented from being propagated through the optical media by destructive interference (Michael, van Merl, Vrensen, & van den Berg, 2003; Trokel, 1962); as a result, much of the light that is scattered in the anterior part of the eye is prevented from reaching the photoreceptors.

Secondly, the photoreceptors themselves, particularly in the fovea, are able to filter out much of the scattered light that reaches them. Cone photoreceptors are sensitive to the direction of propagation of incident light rays so that light travelling along the axis of the cone is much more likely to illicit a response from the photoreceptor than light approaching from an angle (Stiles & Crawford, 1933), as shown in Fig 1.17. As such, a light source of fixed size and intensity will appear brighter when the beam enters through the centre, as opposed to the margin, of the pupil. It has been suggested that this is because the inner segment of each cone acts as a funnel, collecting and reflecting the incident photons onto the photopigments in the outer segment. Light that enters the funnel from an angle does not get as well reflected onto the pigment, and is therefore not as easily detected (Enoch & Fry, 1958; O'Brien, 1951). In this way, much of the wide-angle scattered light can be ignored by the visual system. Similarly, back-scatter from the retina will have little effect on the retinal image, as the majority will not approach the photoreceptors along their axes.

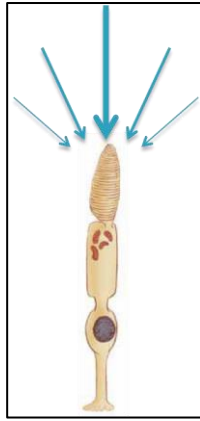


Figure 1.17. A pictorial representation of photoreceptor directional sensitivity.

Research has shown that directional sensitivity is greatest in the parafoveal region (Enoch & Hope, 1973). On the other hand, cone density is greatest at the fovea, and it is unclear whether or not the increased directional sensitivity in the parafovea compensates for the rapid decrease in cones. There is also evidence of directional sensitivity of rods (Van Loo & Enoch, 1975), although the effect is very small. It has been suggested that the reason for the differences between rods and cones in their strength of directional sensitivity is that rods only function in very low light levels, where there would not be sources of bright light; directional sensitivity is therefore only a helpful feature for cone-mediated vision (Walraven, 2009).

Throughout this chapter, the human eye has been considered in terms of its structure and function. It has been shown that its specialised transparent structures, including the cornea and lens, facilitate the transmission and focusing of light onto the retina. The moderation in the amount of light entering the eye, via changes in pupil size, as well as the receptive properties and positioning of photoreceptors in the retina, enable the visual system to function over a large range of lighting levels. Additionally, owing to the differences in communication between retinal cells according to their type and location, the visual system is able to acquire different information about the spectral, temporal and chromatic properties of light signals.

Finally, scattered light was briefly introduced and discussed in relation to the different structures within the eye. The next chapter will explore scattered light in further detail, particularly with regard to its properties and measurement.

Chapter 2: Scattered light

2. 1. Effects of light scatter on visual performance

2. 1. 1. Disability glare

Disability glare is the term given to the general phenomenon in which visual performance is hindered by the presence of a light source. The Commission Internationale de l'Éclairage defines disability glare as “glare that impairs the vision of objects without necessarily causing discomfort” (International Commission on Illumination, 1987). In Vos’s excellent review of the literature, he defines disability glare as “the masking effect caused by light scattered in the ocular media which produces a veiling luminance over the field of view” (Vos, 2003b). In the presence of a glare source, light scattered within the ocular media will spread non-uniformly over the retina; the illumination produced can be likened to a veil of lights that ends up over the background. As such, the effect on visual performance of the glare source at any point on the retina can be quantified in terms of its equivalent veiling luminance. This was achieved experimentally by Holladay (Holladay, 1926; Holladay, 1927), and again later by Stiles (Stiles, 1929a) and Stiles and Crawford (Stiles & Crawford, 1934; Stiles & Crawford, 1937).

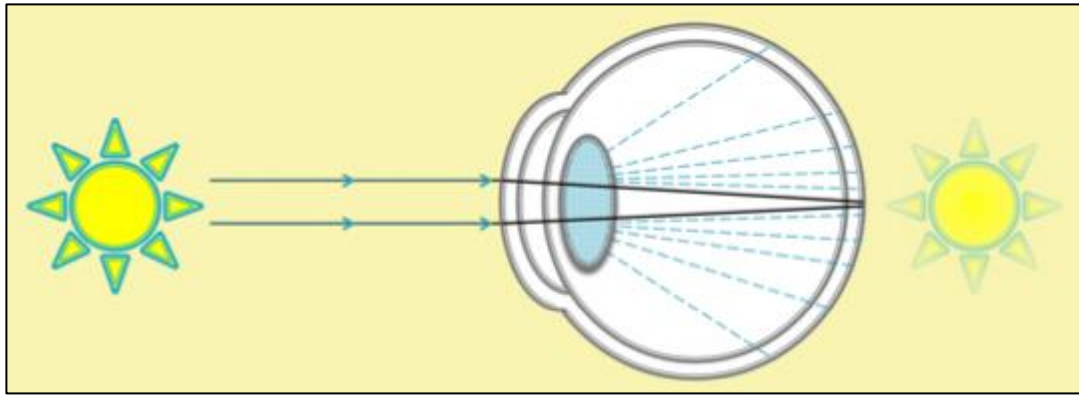


Figure 2. 1. Schematic diagram of light scattering within the eye

2. 1. 2. *Discomfort glare*

Discomfort glare is the term used to describe the subjective sensation of discomfort in the presence of a bright light source. The CIE's definition is the reverse of disability glare, i.e. "glare that causes discomfort without necessarily impairing the vision of objects" (International Commission on Illumination, 1987). Vos, on the other hand, further splits up the umbrella term into 'discomfort glare' and 'dazzling glare': discomfort glare is "the clumsily distracting effect of peripheral light sources" and dazzling glare is distinguished by the over-exposure of light, which may or may not be painful, often leading to rapid, pre-attentive avoidance reactions (Vos, 2003b). He suggests that the discomfort felt in the presence of bright light likely originates not in the retina, which has no pain receptors, but in the iris sphincter, which controls the size of the pupil in response to light exposure.

2. 2. Factors that affect scattered light

2. 2. 1. Properties of the light source and the eye

Since the 1920s, researchers have been attempting to determine how the eccentricity of a glare source relates to the amount of light-scatter in the human eye (Holladay, 1927; Stiles, 1929a; Stiles & Crawford, 1937). Experiments using enucleated lenses have shown that the angular dependency of young and old samples is very similar, suggesting that most of the light travelling through the lens is scattered only once (van den Berg & Ijspeert, 1995).

The Stiles-Holladay formula predicts that the equivalent luminance at a given eccentricity away from the scatter source is inversely proportional to the square of its visual angle; this explains the appearance of the ciliary halo that surrounds bright light sources, which decreases rapidly in intensity with increasing distance from the source. The formula has since been adapted to take into account age and iris pigmentation (Ijspeert et al., 1990; van den Berg, 1995). The age and pigmentation-adjusted model is comprised of a baseline function — dependent on the angle between the glare source and the line of sight — to which is added an age function and a pigmentation function. As already discussed, scattered light is higher in older, lightly pigmented eyes, so the age and pigmentation additions unsurprisingly increase predicted light scatter.

The CIE General Disability Glare Equation has been elaborated as follows (International Commission on Illumination, 2002):

$$Eq. 2. 1. \quad \frac{L_s}{E_g} = \frac{10}{\theta^3} + \left[\frac{5}{\theta^2} + \frac{0.1p}{\theta} \right] \times \left[1 + \left(\frac{A}{62.5} \right)^4 \right] + 0.0025p$$

Where:

L_s is the equivalent luminance at an eccentricity, \square , away from the glare-source (cd/m^2). This is known as the equivalent veiling luminance.

E_g is the illuminance at the plane of the pupil, produced by the glare-source (lm/m^2).

θ is the angular eccentricity of the glare-source in relation to the target (degrees).

p is the eye pigmentation factor, ranging from 0 for black eyes to 1 for light eyes.

A is age in years.

With increasing pupil size, more light is able to enter the eye and illuminate the retina. Light scatter is directly proportional to the total light flux, increasing as a percentage of the total amount of light entering the pupil. It should therefore be possible to accurately estimate the amount of light scattered across the retina as long as the luminance and pupil size is known. However, prediction accuracy is based on the assumption that the scattering is uniform over the pupil.

2. 2. 2. Uniformity of light scatter over the plane of the pupil

Under the assumption that light scatter is uniform over the plane of the pupil, the ratio between direct light captured from an object in the visual field and that captured from the scatter source remains constant and independent of pupil size. When measured in this way, the proportion of scattered light varies very little as the pupil size changes with ambient light level. However, in the extreme periphery of the lens the proportion of scattered light can be larger (Franssen, Taberner, Coppens, & van den Berg, 2007). Experiments using dilated pupils have also shown that the far

periphery contributes more scatter than the centre in older observers and long-term contact lens wearers (Barbur, Edgar, & Woodward, 2010). It is worth noting, however, that the relationship between pupil size and scattered light changes less than 0.2 log units for pupil sizes between 2 and 7mm (Franssen et al., 2007). The effects of uniformity of scattered light over the plane of the pupil is further complicated by directional sensitivity (Stiles & Crawford, 1933) of the photoreceptors, which will be discussed in more detail in chapter 7.

2. 2. 3. Wavelength dependence of light scatter

When light encounters a new surface, the direction of propagation is influenced by a number of factors. In the case of reflection, the direction is determined by the local angle of incidence of the light. Refracted light travels forwards and its path is determined by both the angle of incidence and the ratio of the relative indices at the boundary. Scattered light, also travels in the forwards direction but is determined by the relationship between the size of the scattering particles and wavelength of the incident light (Duree, 2011).

Intra-ocular scatter can be described using both Rayleigh and Mie models (Costello, Johnsen, Gilliland, Freel, & Fowler, 2007), shown in Fig 2.2. Rayleigh-type scattering differs from Mie-type scattering in both origin and behaviour. Rayleigh scatter is caused by particles of a similar size to the wavelength of the incoming light and propagates outward in many different directions. In contrast, Mie-type scattering is caused by particles larger than the wavelength of light and most is propagated in the forwards direction. There is a small amount of Rayleigh-type scattering within the eye (Coppens et al., 2006), however most can be accounted for by Mie-type scattering

(Whitaker, Steen, & Elliott, 1993). It is likely that irregularities within the lens fiber lattice, as well as the presence of macromolecules — particles that are larger than the wavelength of the incoming light — are responsible for the majority of intraocular scattered light (Hemenger, 1988; Hemenger, 1992; Whitaker et al., 1993; Wooten & Geri, 1987). An increase in the number of macromolecules in the lens is thought to be the cause of increased light scatter in older observers (Coppens et al., 2006; van den Berg & Ijspeert, 1995). It has also been suggested that macromolecules are present from early on in the development of the eye, but that changes in the refractive index of the surrounding cytoplasm could lead to the increase in scatter seen with age (Costello et al., 2007). In any case, any age-related increases in scattered light are likely to be relatively independent of wavelength. On the other hand, factors such as iris pigmentation and yellowing of the lens with age can affect the wavelength of the ‘effective’ scatter reaching the retina, due to changes in light absorption and transmission (Thaung & Sjöstrand, 2002). Wavelength dependence of light scatter will be discussed in further detail in Chapter 5.

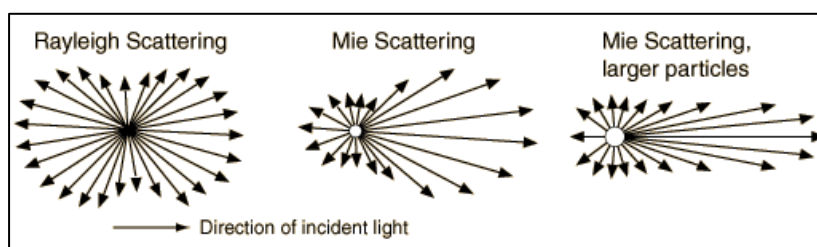


Figure 2.2. Schematic diagram of Rayleigh and Mie –type scattering (Nave, 2012).

2. 3. *Clinical applications*

2. 3. 1. *Age-related changes in scattered light*

The cornea's contribution to intraocular light scatter, although not insignificant (Vos & Boogaard, 1963), tends not to vary within an individual's lifetime; the same is also true of the aqueous and vitreous (van den Berg, Thomas J.T.P., 1995). The scattered light contributed by the lens on the other hand is strongly affected by aging.

As previously mentioned, scattering is caused partially by particles within the lens (Spector et al., 1974), whose numbers increase as the eye ages, disrupting the uniformity of the fibre cell lattice (Ben-Sira, Weinberger, Bodenheimer, & Yassur, 1980). The scatter caused by such particles results in the appearance of a relatively uniform white disc that surrounds a bright light source, which decreases in intensity with increasing eccentricity; this is known as a ciliary corona (Simpson, 1953), as shown in Fig 2.3. When the number of scattering particles increases dramatically, as in the case of cataract (de Waard, IJspeert, van den Berg, & de Jong, 1992), transmission of light by the lens, and thereby retinal illuminance, is reduced (Kline & Schieber, 1985).



Figure 2.3. A simulated ciliary corona.

The relative contribution of the different regions of the crystalline lens has been investigated both *in vitro* and *in vivo*. The anterior capsule contributes a small amount of light scatter in young and old eyes alike (Ben-Sira et al., 1980), whereas scattering in the cortex is greater and increases gradually with age. In comparison to the innermost nuclear regions, the fibre cell structure of the cortex is less uniform (Spector et al., 1974). It has been suggested that cortical scattering is caused primarily by the fibre architecture of the lens, or more specifically, differences in the refractive index between cell membranes and cytoplasm (Hemenger, 1988; Hemenger, 1992). It is suggested that the increase in scatter that occurs with age is due to the increasing size of the cortex region throughout one's lifetime.

The contribution of the nuclear region to the proportion of light scatter is relatively small in young eyes; it increases gradually until around the age of forty, and then continues to increase more rapidly. Nuclear scatter is likely to be caused mainly by the presence of large protein macromolecules, the increasing number of which is responsible for the sharp increase in scattered light in older age (Ben-Sira et al., 1980; Spector et al., 1974).

Structural changes elsewhere in the eye may also have an effect on the relative amounts of light that are scattered or absorbed (Ijspeert et al., 1990). The pigments in the iris absorb light, forming the aperture that is the pupil. However, some light is able to penetrate the iris, particularly when there is less pigment, as is the case for people with albinism or light blue eyes (Coppens et al., 2006; de Waard et al., 1992; Franssen, Coppens, & van den Berg, 2006; Kruijt, Franssen, Prick, van Vliet, & van den Berg, 2011; van den Berg et al., 1991). The rogue light rays are not focussed

correctly, but fall randomly on the retina. The light-absorbing pigments within the iris have been found to decrease with increasing age (Schmidt & Peisch, 1986; Weiter, Delori, Wing, & Fitch, 1986). As melanin, the pigment present in the iris, absorbs short-wave light more strongly, increase in light scatter due to pigmentation loss is likely to be predominantly in the long-wave part of the spectrum.

2. 3. 2. *Cataracts*

Cataract is the general term used to describe lens opacity, an example of which is given in Fig 2.4. The only treatment currently available for cataract is to have the lens removed and replaced with an artificial intraocular lens.



Figure 2.4. Photo of a cataractous eye (STAAR Surgical Company, 2014).

There are a number of different types of cataract; senile cataract is the most common, but cataracts can also occur in association with other diseases or following damage to the eye. Cataracts are caused by swelling, tissue death and protein alteration within the lens, all of which lead to disruption of the highly organised fibre lattice, which ordinarily facilitates light transmission. As a cataract develops, vision becomes progressively more blurred due to the reduction in light transmission, as well

as an increase in the proportion of light that is scattered as it passes through the lens (Vaughan & Asbury, 1983).

The amount of forward light scatter depends upon the location of the cataract, as well as its stage of progression. Posterior subcapsular cataracts tend to be associated with higher levels of forward scatter, and hence greater contrast loss, than either nuclear or cortical cataracts (de Waard et al., 1992) (see Fig 2.5).

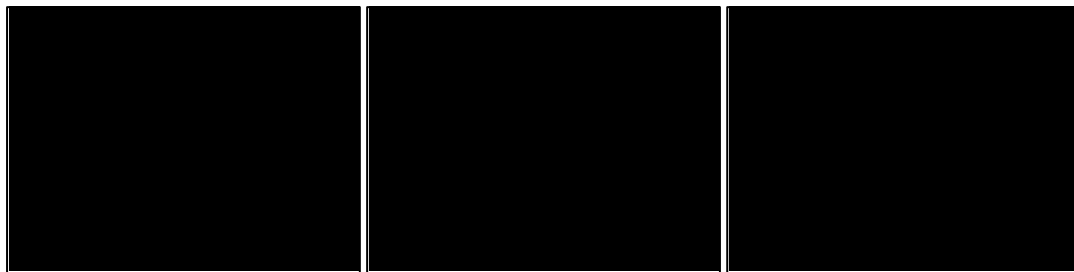


Figure 2.5. Diagram of the three most common type of age-related cataract. Nuclear cataracts (A) are the most common type and originate in the centre of the lens. Posterior subcapsular cataracts (B) are associated with large and rapid increases in scattered light. Cortical cataracts (C) originate in the outside of the lens (Alcon, 2014).

2. 3. 3. *Measurement techniques*

The techniques used to investigate scattered light can be separated into two main categories: optical and psychophysical. Optical techniques have the advantage of being objective, thereby eliminating human error, and can be further split into two categories: single-pass and double-pass, the former being conducted generally in vitro, the latter, in vivo.

Single pass measures, as the name suggests, involves light passing through the structure only once, whereas double-pass methods record the light after it has passed forward and then backward through the eye. Single-pass methods enable the

measurement of light after it has passed through a structure, such as the lens, using a photometer (Ben-Sira et al., 1980) or photomultiplier (Boynton et al., 1954; van den Berg & Ijspeert, 1995). Such techniques are very useful when attempting to identify the scattering properties of specific parts of the eye in isolation. Using excised eyes, however, necessitates careful and efficient removal, storage and mounting in order to avoid altering the structure and confounding the measurement post-mortem (Boynton et al., 1954; DeMott & Boynton, 1957; DeMott & Boynton, 1958).

Double-pass measures, such as those obtained by slit-lamp examination or Hartmann-Shack Wavefront Aberrometry (see Fig 2.6.), measure light reflected back through the pupil from the retina. The equipment consists of an array of lenses, mirrors and beam-splitters, which differentiate the incoming and outgoing beams travelling through the pupil (Westheimer & Liang, 1995). The images obtained using a Hartmann-Shack Wavefront Aberrometer provide information about the wavefront of the beam that exits the pupil. Although forward light scatter cannot be inferred directly from double-pass measurements (Boynton et al., 1954), the images obtained can be used to estimate the amount of scattered light in the eye.

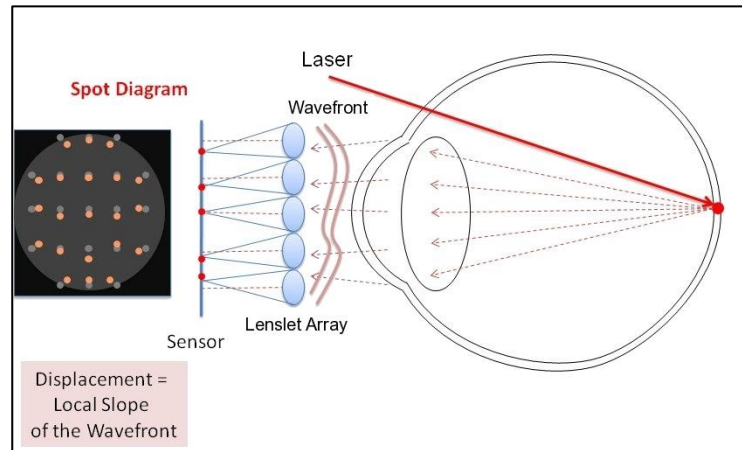


Figure 2.6. Diagram to show how the Hartmann-Shack wavefront aberrometer works. The light reflected from the back of the eye is captured over discrete regions of the pupil and compared to what would be expected in the absence of aberrations; the amount and nature of displacement reveals information about the wavefront aberrations of the eye (Vitorpamplona, 2010).

One way of describing the amount and distribution of scattered light within the eye is by using the point spread function (PSF) (Vos & van den Berg, 1999). The light arriving at the retina from a point source of light spreads out from the central point. In a poor optical system, there will be a larger spread of light, which is associated with a large PSF (Hodgkinson & Greer, 1994). The PSF of the human eye varies with age and pigmentation (an example is shown in Fig. 2.7.) and, when convolved with an image, can be used to estimate the effects on visual performance.

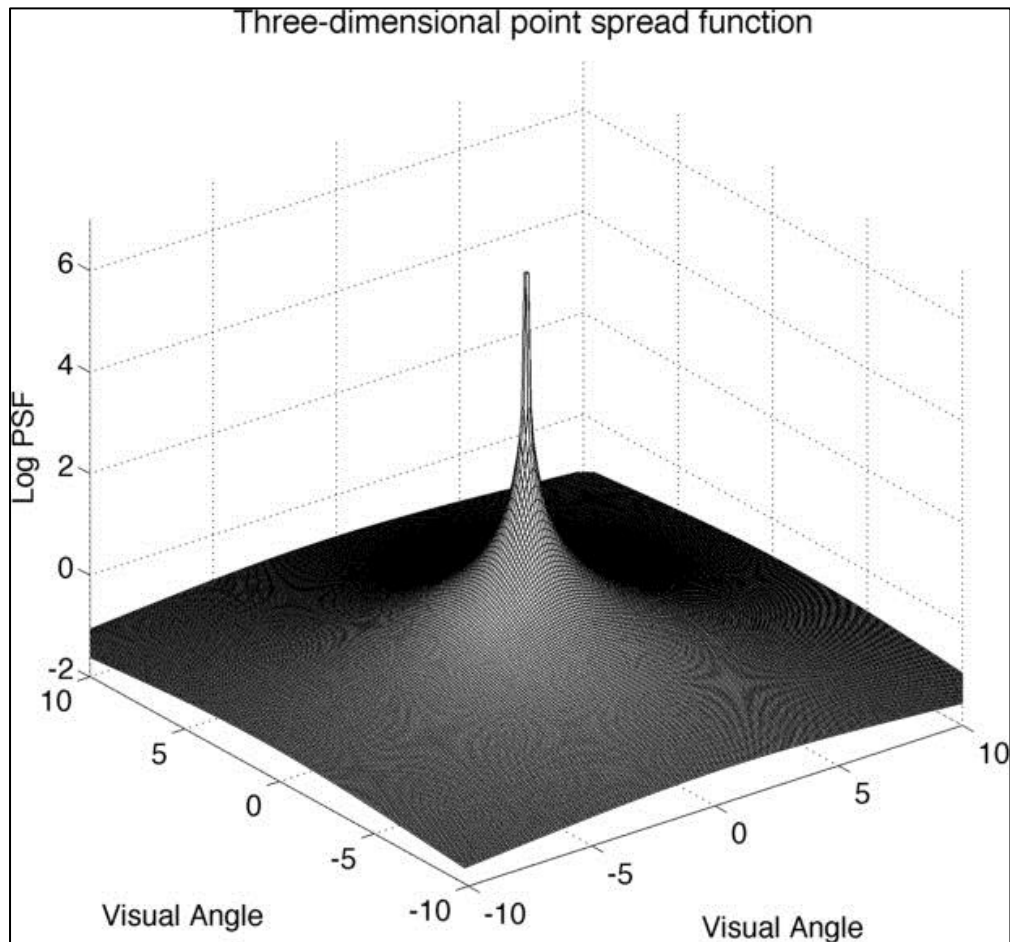


Figure 2.7. A simulated three-dimensional diagram of the estimated PSF as a function of visual angle for a 60-year old with a pigmentation factor of 0.5.

One notable disadvantage of optical, as opposed to psychophysical, techniques is that they are not representative of the overall effect on visual performance. As already mentioned, factors such as pigment density, cone directional-sensitivity, neural efficiency and so on, all have the potential to alter the impact of scattered light on vision. Psychophysical measurements, on the other hand, provide an indication of how scattered light interacts with the visual system as a whole. Such measures do, however, rely on observers' subjective experiences, and their ability to communicate using accurate and consistent responses; psychophysics is therefore susceptible to

inaccuracies and variability caused by human error. Much effort has in recent years been focussed on improving the validity and reliability of such techniques (van den Berg, Franssen, Kruijt, & Coppens, 2013).

Visual acuity and contrast sensitivity tests are widely used in visual assessment, as shown in Fig 2.8. These measures can provide some indication of levels of small-angle scattered light, simply because poor vision is likely to coincide with large amounts of scatter. For wide-angle scattered light, visual acuity correlates poorly, and can lead to inaccurate assessments. These tests have been used in conjunction with sources of glare in an attempt to provide a more direct measure, but they have been found to show large variability (van den Berg & IJspeert, 1991; van den Berg et al., 2013) and poor correlation with other measures (Elliott, Hurst, & Weatherill, 1990; Elliott & Bullimore, 1993; Haegerstrom-Portnoy, 2005; Prager, Urso, Holladay, & Stewart, 1989).

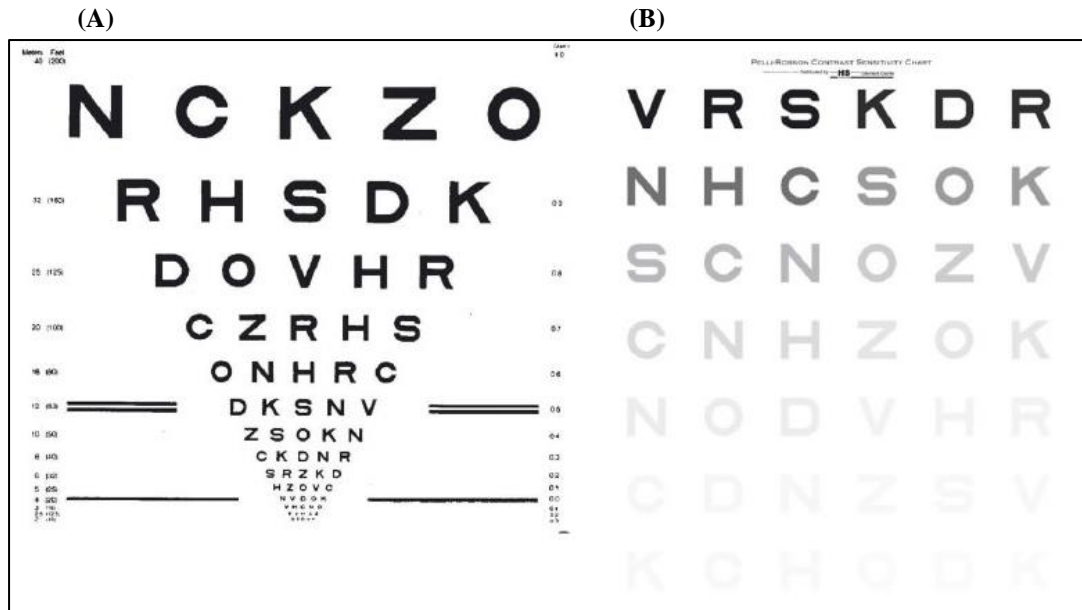


Figure 2.8. Charts used to test (A) visual acuity (Ferris, Kassov, Bresnick, & Bailey, 1982) and (B) contrast sensitivity (Pelli, Robson, & Wilkins, 1988).

One psychophysical method for quantifying scattered light within an individual's eye uses a flicker cancellation technique, originally developed by Le Grand and later refined by van den Berg and Spekreijse (van den Berg & Spekreijse, 1987) and Barbur et al (Barbur, de Cunha, Harlow, & Woodward, 1993; Barbur, Chisholm, & Harlow, 1999). The technique uses a dark central target disc, usually subtending less than 1° visual angle at the plane of the pupil (see Fig 2.10 (A)); light scattered over an area this size tends to appear reasonably uniform. Modulating the luminance of an annular glare source gives the impression that the target is flickering, due to the scattered light falling on the centre of the retina. Over a small area, the effects of scattered light can be replicated simply by modulating the luminance of the target.

The aim of the task is to adjust the maximum luminance of the target so that it is equivalent to the veiling luminance resulting from scattered light when the glare

source is on; when the target luminance and glare source luminance are modulated sinusoidally in counter-phase, the perception of flicker is extinguished, as shown in Fig 2.9. By using glare annuli of different eccentricities, it is possible to estimate not only the amount, but also the angular distribution of the light scatter within the eye.

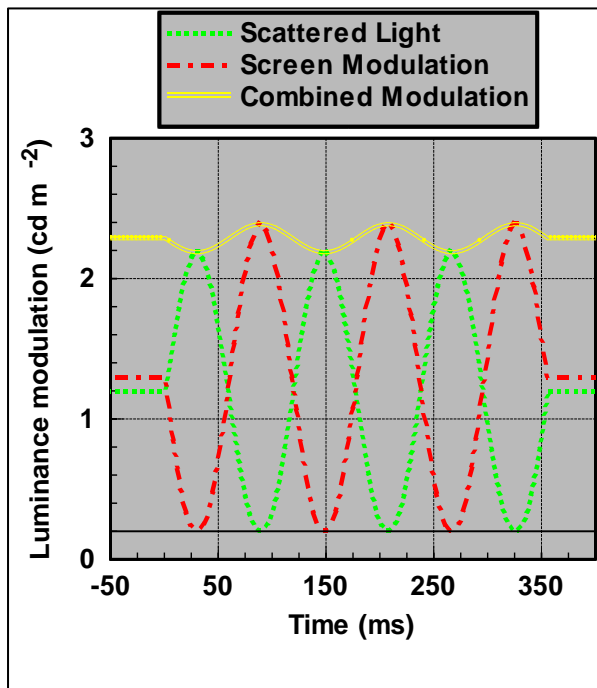


Figure 2.9. Diagram to show the paradigm used in the flicker-cancellation technique. Luminance of the target and scatter source are modulated sinusoidally in counter-phase. The luminance is increased so that the retinal illuminance generated by the target directly compensates for that generated by the scatter source.

Unfortunately, although the flicker-cancellation method is capable of yielding accurate and reliable results, the paradigm requires thorough explanation, demonstration and practice, which is not always viable in a clinical setting. A variation — the Compensation Comparison method (Franssen et al., 2006; van den Berg & Coppens, 2005) — was developed to tackle this problem. Instead of using one central target and asking participants to identify when they cease to detect flicker, the test target is split into two halves (see Fig 2.10 (B)). The luminance of one of the test field halves is modulated in counter-phase with the scatter source (as in the original flicker-cancellation technique) whereas the luminance of the other half is not

modulated. Consequently, both half-fields will appear to flicker; for the former this is caused by the combination of light scatter and luminance modulation whereas for the latter this is caused by scattered light only. The maximum luminance of the modulating half-field is different for each presentation and the observer's task is to identify the half-field that appears to flicker strongest. A psychometric curve is fitted to the test results according to the observer's responses in each presentation, which yields the straylight parameter.

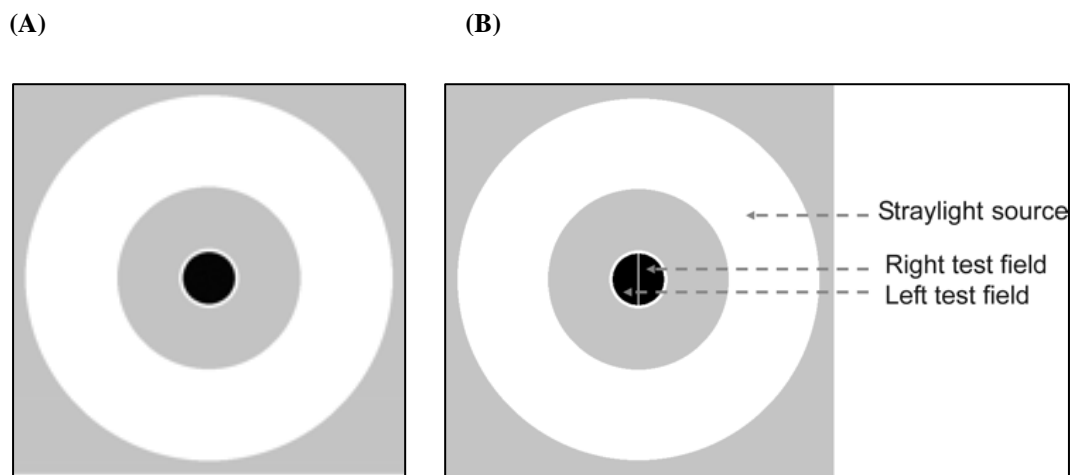


Figure 2.10. Stimulus layout for the flicker cancellation technique. The observer is required to judge the amount of flicker over the dark central disc. The direct compensation method requires that the observer make judgements over sequential presentations (A) whereas the compensation comparison method (B) requires the observer to compare the flicker over the right and left test field presented simultaneously.

As observers compare two simultaneously, as opposed to consecutively, presented fields, the task is more intuitive and may be more appropriate for clinical use (Franssen et al., 2006). However, information about the angular distribution of scattered light is not obtained using the Compensation Comparison method (van den Berg & Coppens, 2005). The question of whether the angular distribution of scattered

light is important with respect to the overall accuracy of measurement will be the topic of the next chapter.

Chapter 3: Apparatus and Methods

3. 1. Flicker cancellation technique: measurement of light scatter within the eye

3. 1. 1. Theoretical basis for light scatter measurement

The equivalent veiling luminance of an object that generates the same retinal illuminance as the light scattered from a glare source can be predicted using the following equation, which is derived from the classic Stiles-Holladay equation, based on the work of Holladay (Holladay, 1926; Holladay, 1927), Stiles (Stiles, 1930) and later Stiles and Crawford (Stiles & Crawford, 1937):

Eq. 3. 1.
$$L_s = Ek\theta_e^{-n}$$

Where:

L_s is the luminance of an external source that is expected to generate the same retinal illuminance as that resulting from light scattered by the glare-source (cd/m^2). This is known as the equivalent veiling luminance.

k is the straylight parameter. This value is proportional to the amount of light scattered within the eye. A large k value indicates a greater amount of light scatter.

E is the illuminance at the plane of the pupil, produced by the glare-source (lm/m^2).

θ is the angular eccentricity of the glare-source in relation to the target (degrees).

n is the scatter index. This value is inversely proportional to the angular distribution of scattered light within the eye. A large n indicates a narrow angle of scattered light.

k and n are constants for a given eye. There is a linear relationship between L_s and θ when plotted on a logarithmic scale, as shown in Fig 3.1, and k and n are given by the

gradient and intercept respectively. These parameters can therefore be used to estimate the amount of light scattered by a glare-source of known eccentricity and pupil-plane illuminance.

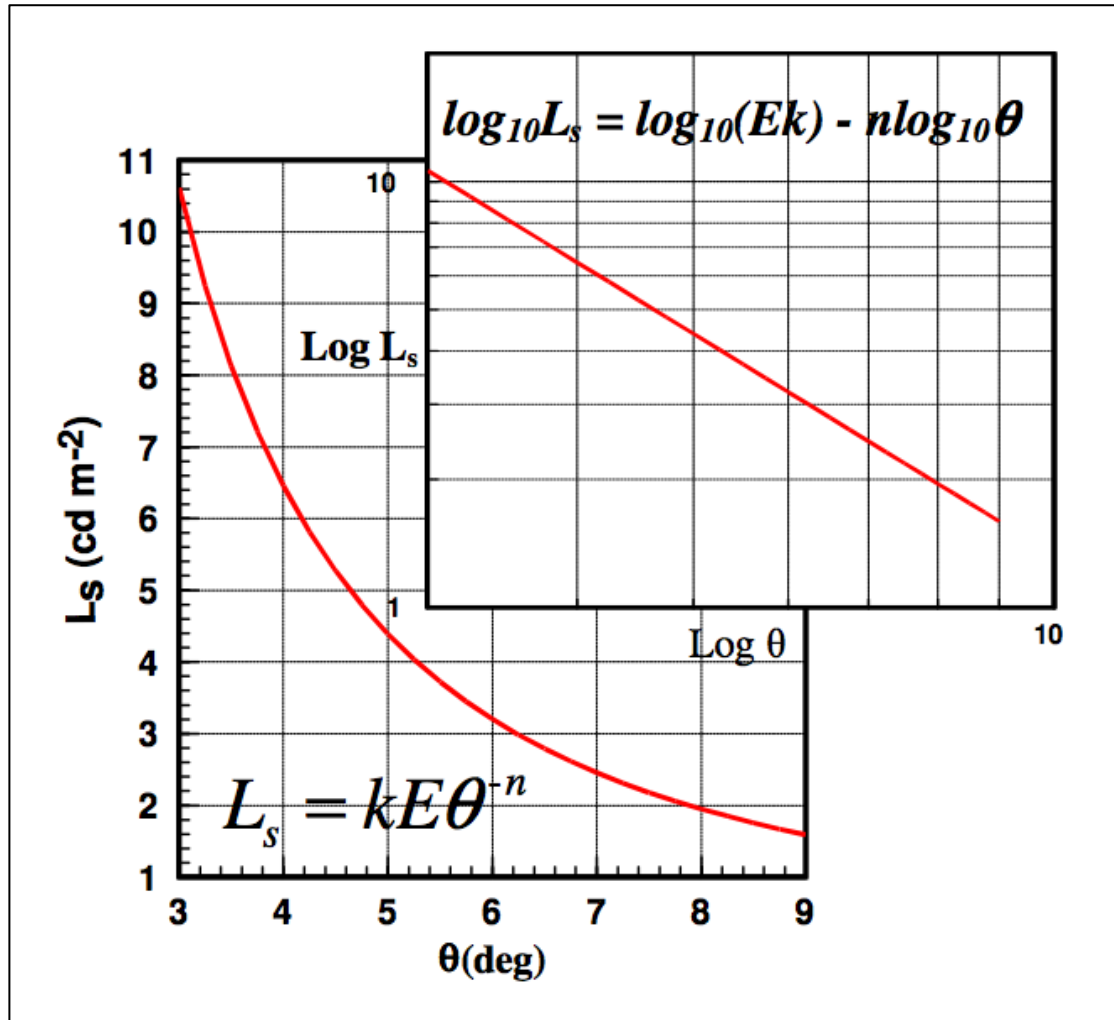


Figure 3.1. The relationship between L_s and θ plotted on both linear and logarithmic scales (Kvansakul, 2005).

To ensure that the absolute level of scattered light within the eye is sufficiently high to be measured at large eccentricities, the illuminance generated at the plane of the pupil must also be high. In this case, either an extremely high luminance or a large

area of glare source is needed. As high-resolution visual displays are often incapable of generating the luminance levels needed, a compromise is reached by increasing the width, and thereby the area, of the glare source annuli, S_A . A schematic diagram to illustrate the calculation of source size is shown in Fig. 3.2.

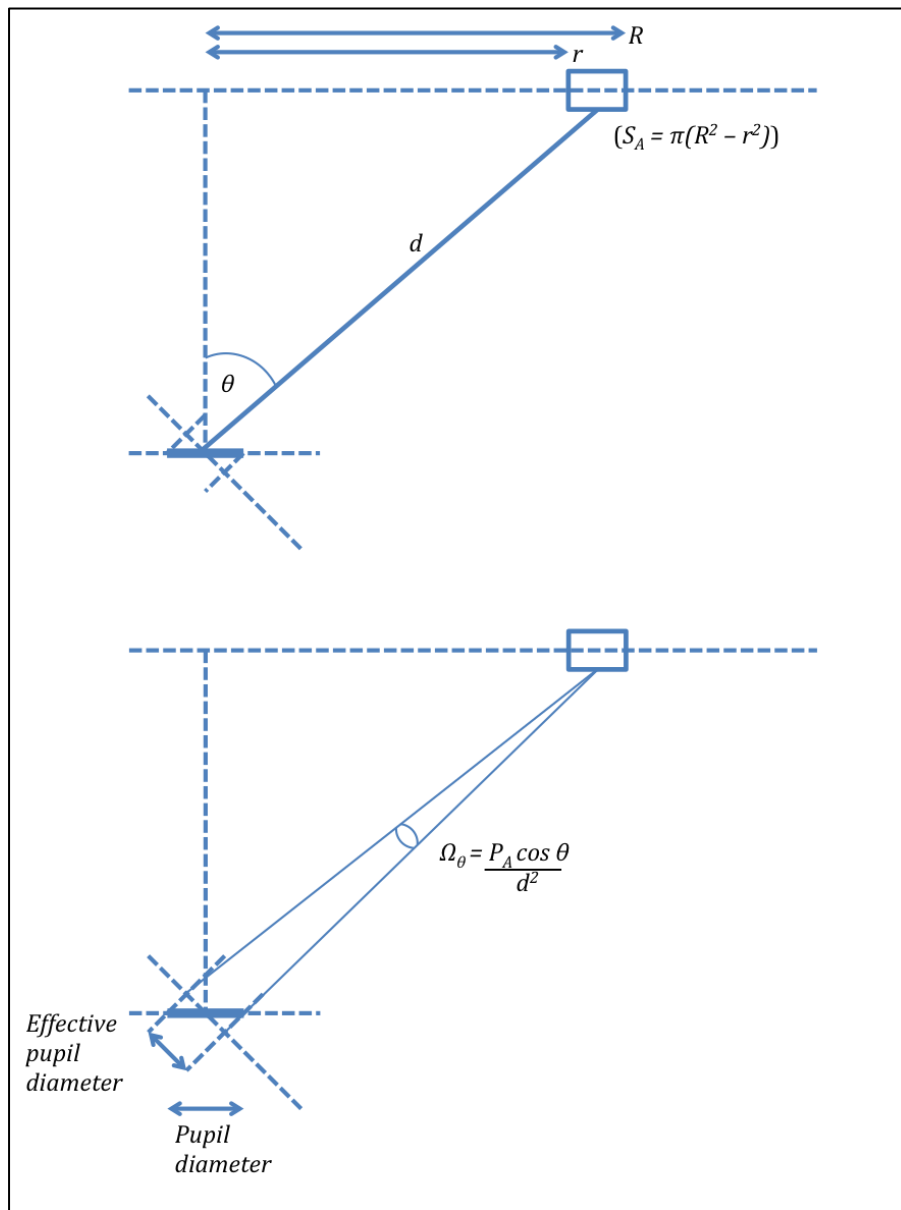


Figure 3.2. Schematic diagram to show the basis for the computation of annulus size so as to ensure that the illuminance in the pupil plane is independent of annulus eccentricity (modified from a previously published diagram (Kvansakul, 2005)).

Eq. 3. 2.
$$S_A = \pi(R^2 - r^2)$$

Where R is the outer radius and r is the inner radius of the annulus.

According to Lambert's cosine law, the intensity of a Lambertian source is directly proportional to the cosine of the angle between the line of fixation and the source, θ . The intensity of the light reaching the plane of the pupil is given by:

Eq. 3. 3.
$$I_\theta = L S_A \cos\theta$$

Where L is the luminance of the glare source and S_A is the source area.

Because the glare source is off the line of fixation and the light enters the pupil from an angle, the effective area of the pupil will be reduced.

The effective solid angle subtended by the pupil at a given point on the annulus, Ω_θ , is therefore given by:

Eq. 3. 4.
$$\Omega_\theta = \frac{P_A \cos\theta}{d^2}$$

Where P_A is the pupil area and d is the distance between the pupil and the source. The flux captured by the eye is then given by:

Eq. 3. 5.
$$\phi = \Omega_\theta I_\theta$$

The size of each scatter source is adjusted to maintain a constant level of illuminance in the plane of the pupil. For the CRT display employed in this test, the typical error in pupil plane illuminance is less than 1% when computed with respect to the mean illuminance. The phosphors of the display approximate extremely well the light emission properties of a Lambertian source over the angular range of interest.

A broad annulus does not have a unique eccentricity like a point source or a thin annulus. It is therefore necessary to derive an equation for the ‘effective eccentricity’, θ_e , of each broad annulus employed in the test. The effective eccentricity is defined as the angular radius of a narrow ring that would produce the same pupil-plane illuminance and result in the same amount of scattered light over the central test target as the broad annulus.

The formula used by the program was derived in earlier studies and involves integration of the scattered light contributed by each point in the extended annulus. The effective eccentricity is, however, a function of the scatter index, n , as shown below:

$$\text{Eq. 3. 6.} \quad \theta_e = \frac{1}{n} \log \left(\frac{\sin^2 \theta_2 - \sin^2 \theta_1}{F(n)} \right)$$

Where θ_1 and θ_2 are the inner and outer radii of the annulus and $F(n)$ is given by:

$$\text{Eq. 3. 7.} \quad F(n) = \int_{\theta_1}^{\theta_2} \frac{\sin 2\theta}{\theta^n} \delta\theta$$

The relative contribution to light scatter of the inner and outer edges of the extended annulus will vary depending on the angular distribution of light scatter within the eye, which relates nonlinearly to the scatter index, n . A large value of n is indicative of a narrow angular distribution of scattered light, which corresponds to a large difference in light scatter contribution between the inner and outer edges of the annulus. Because the inner part of the annulus would be contributing significantly more scattered light, the effective eccentricity, θ_e , would be smaller than in the case of a small n .

Assuming that $n = 2$ in the first instance, the program computes θ_e . By plotting $\log_{10}(L_s)$ against $\log_{10}(\theta_e)$ and using linear regression, a new value of n is extracted. In

this way, θ_e and n are calculated iteratively until the value of n no longer differs between insertion and extraction from the calculation.

The straylight parameter, k , is proportional to the amount of scattered light within the eye. By integrating k from 2° to 90° , it is possible to obtain an ‘integrated’ index that is proportional to the total amount of scattered light in the eye. The lower limit of 2° was chosen as the empirical scatter function (Eq. 1.) does not predict accurately small angle scatter, becoming infinitely large towards 0° .

Eq. 3. 8.
$$k' = \int_2^{90} k\theta^{-n}\delta\theta$$

The integrated straylight parameter, k' , has the advantage of being less variable with repeated measurements with the same eye when compared to k (Barbur, Edgar, & Woodward, 1995). Its independence from n also allows comparisons to be made between observers.

3. 1. 2. Apparatus

The light scatter test was implemented at City University over several years as part of a series of programs developed for use on the P_Scan pupillometer system (Alexandridis, Leendertz, & Barbur, 1992.). The latter employs a 50 cm NEC SuperBright monitor for the generation of visual stimuli³⁰. The observer views the centre of the display at a viewing distance of 0.7 m. A chin and forehead rest is used to position the observer's head while the participant fixates on the centre of the display. A hood is positioned over the head-rest to minimise the amount of external light reaching the observer. The experimental setup is shown in Fig 3.3.



Figure 3.3. The experimental setup for the flicker cancellation technique. The display in the foreground of the photo is used to set up and control the experiment, while the participant is seated on the right and views the far display through the hood.

To calibrate the display, the luminance of each phosphor for each of the 1024 gun voltage values is measured automatically using the LMT 1009 luminance meter. Both the display luminance calibration data and the chromaticity co-ordinates of the display phosphors are stored in a calibration file, which is used when the experimental program is loaded. In order to maintain stable display operation, the maximum luminance of the display for white light (i.e., chromaticity co-ordinates, $x = 0.305$, $y = 0.323$) was limited to 100 cd/m^2 .

3. 1. 2. Stimuli

The scatter stimulus consists of three concentric circles: a central dark target disk, an isolation annulus and an outer scatter source. The background luminance is set at 5 cd/m^2 , with chromaticity coordinates of $x = 0.169$, $y = 0.085$; the low luminance reduces the scatter from the background itself while the dark blue colour helps to delineate the scatter source. The luminance of the isolation annulus was set at 25 cd/m^2 , with chromaticity $x = 0.450$, $y = 0.450$, selected to reduce spatial spreading of perceived flicker around the target. An annular scatter source of specified

eccentricity is generated on the display together with a central disc, subtending 0.8° , which forms the test target; both the target and the scatter source have chromaticity coordinates of $x = 0.290$, $y = 0.317$, in order to reach the maximum luminance of the screen. The light scatter stimulus consists of a burst of sinusoidal flicker at a frequency of 8.6 Hz, with a mean luminance of 50 cd/m^2 and modulation of 100%. Upon detection of flicker, the pupil constricts even when the time averaged light flux remains unchanged. However, the pupil response triggered by high frequency flicker has a relatively long latency (Troelstra, 1968) and using a burst of flicker of duration ~ 350 ms ensures that the pupil remains relatively unchanged during the stimulus.

While the glare annulus is flickering, the luminance of the test target is modulated sinusoidally in counter-phase. Whereas the mean luminance of the test target is adjusted between presentations, that of the scatter source remains unchanged.

The test uses light scatter annuli at five different eccentricities and the size of each was adjusted to ensure equal pupil-plane illuminance across conditions. From smallest to largest eccentricities, the inner radii measured 56, 105, 155, 200, 300 pixels; outer radii measured 405, 415, 431, 450, and 506 pixels (see Fig 3.4). The effective radius of each annulus for each participant was calculated by the program. Once the flicker-null point was found for each annulus, the next annulus would be presented in a random order. One run consisted of five repetitions for each of the five annuli. Scatter parameters were computed based on means for each of the five annuli.

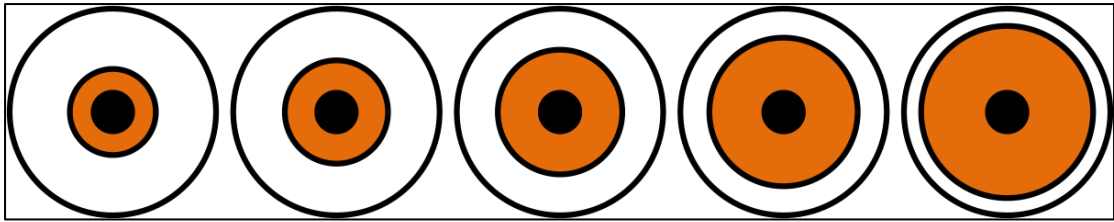


Figure 3.4. A pictorial representation of the five annulus sizes used for the measurement of scattered light at different eccentricities. The ‘effective’ radius i.e. that of a thin annulus that would contribute the same level of illuminance in the plane of the pupil, is calculated by the program.

The purpose of the yellow isolation annulus is to help define the test target; its luminance must be sufficiently high to ensure that the detection of flicker is confined largely to the test target. Both the isolation annulus and the scatter source produce internal scatter within the monitor, some of which ends up over the black disc, located at its centre, adding a steady pedestal of light. This pedestal does not affect the measurement of light scatter since it remains steady throughout the test, but the height of the pedestal increases as the isolation annulus becomes larger. The compromise adopted in this scatter test was to adjust the luminance of the isolation annulus for each scatter source eccentricity so as to ensure that the internal light scatter at the centre of the annulus was constant and independent of the size of the annulus. The colour of the isolation annulus was chosen to be yellow (chromaticity co-ordinates: 0.45, 0.45) which also helps visually to define the achromatic test target. A large, dark, blue, uniform background field of low luminance is used to maintain steady state of light adaptation and fills the display area outside the scatter source annulus.

3. 1. 3. Calibration for light scatter internal to the display

An LMT 1009 luminance meter with a measuring field aperture of 20 min arc was used to calibrate the display luminance and to measure the internal light scatter

within the display. Some of the light originating from the glare source will be scattered within the display and fall on the test stimulus; this scatter will undergo the same temporal modulation as the scatter source. If uncorrected, the amount of scattered light in the eye will be overestimated and its angular distribution distorted by the angular dependence of the scattered light internal to the monitor. A simple technique was therefore developed to correct for this effect by measuring the luminance of the screen over the test target for each of the scatter sources employed in the test. The luminance of the isolation annulus was set to zero and photometer readings at the centre of the test target were obtained for each scatter source eccentricity. The internal scatter within the photometer head itself can also be large under such conditions. By placing a small black velvet absorber at the centre of the display to block out any direct light from the test target and again measuring the luminance for each scatter source eccentricity, a measure of the light scattered within the photometer head was obtained. The new luminance readings provided a measure of the light scattered within the photometer head, which was used to correct the internal light scatter produced by the scatter source. For example, the corrections applied for internal scatter following the most recent calibration were 0.42, 0.32, 0.17, 0.14 and 0.10 cd/m^2 for the smallest to largest annuli respectively. The corrections are applied automatically to each estimate of scattered light, reflecting the combined effects of scatter within the eye and internal scatter within the display.

3. 1. 4. Procedure

Participants are given a minimum of three minutes to dark-adapt, after which, they are asked to fixate on the central disc during each presentation and provide oral

feedback on their perception of flicker. The test can be carried out either monocularly or binocularly.

The experimenter adjusts the mean luminance of the test target after each presentation by means of two response buttons. Adjustments are made to increase or decrease the mean luminance of the test target so as to minimise the observer's perception of flicker at the test target. Since the dioptics of the eye inevitably scatter some of the light from the test target, the equivalent veiling luminance may be slightly overestimated. However, the error is expected to be small since a large percentage of the light scattered would normally remain within the area of the test target. The typical duration of the test is 10-15 mins.

3. 2. Contrast Acuity Assessment (CAA) test:

measurement of visual acuity and functional contrast sensitivity

3. 2. 1. Apparatus

The Visual Acuity (VA) and Functional Contrast Sensitivity (FCS) test was developed at City University, London (Chisholm, Evans, Harlow, & Barbur, 2003) and provides a functional measure of contrast sensitivity. The VA and FCS tests were again implemented on the P_Scan pupillometer apparatus, which employs a 50 cm NEC SuperBright monitor for the generation of visual stimuli. In addition, the P_Scan system enables simultaneous, binocular measurement of pupil size and the point of regard every 20 ms (Alexandridis et al., 1992.). Chin and forehead rests were used to position the observer's head. The observer viewed the centre of the display through a large, infrared reflecting mirror oriented at 45° with respect to the viewing direction, from a viewing distance of 1.6 m. A black, wooden hood was positioned over the

head-rest and camera equipment, thereby minimizing the amount of external light reaching the observer's eye.

Glare was introduced using two four-primary LED units (produced by PerkinElmer) driven by a TTI Precision DC PSU (model TSX3510). The LED units were vertically stacked and surrounded by black felt to reduce dispersion of light and create the impression of a single glare-source location positioned horizontally, 10° to the right of fixation. The combined spectral power distribution of the LED lights had a chromaticity of $x = 0.278$, $y = 0.286$ (CIE, 1931).

3. 2. 2. Stimuli

The test stimulus consists of a Landolt ring presented against a uniform background. For the visual acuity (VA) test, the target has high negative contrast with respect to the background and the measured variable is target size. For the functional contrast sensitivity (FCS) tests, the target size is superthreshold and it has positive luminance contrast with respect to the background; in this case, the measured variable is target luminance, from which the contrast is calculated. The FCS test measures Weber contrast, defined as:

Eq. 9.
$$\frac{L_t - L_b}{L_b}$$

Where L_t is the luminance of the target and L_b is the luminance of the background measured in cd/m^2 .

The Landolt ring has a gap oriented in one of four directions at $\pm 45^\circ$ to the horizontal and vertical. Generally, a supra-threshold target gap size is chosen to ensure that small fluctuations of accommodation and differences in higher order

ocular aberrations, which can cause large inter-observer differences when assessing the limit of spatial resolution, would not confound significantly the measurement of contrast sensitivity. The CAA test therefore measures the luminance contrast threshold needed to detect and discriminate correctly the orientation of the gap in the Landolt ring.

For the following studies, unless otherwise stated, the target was presented either at the centre of the display or $\pm 5^\circ$ from fixation, along the horizontal meridian. For FCS measurements, a supra-threshold target gap size of $4'$ was chosen at the foveal location and peripheral targets were scaled in size to maintain similar contrast visibility across the three target locations. Based on threshold measurements for four young participants at a display luminance of 26 cd/m^2 , the target gap size was set at $8'$ for peripheral targets. The chromaticity co-ordinates of both the target and background were set to $x = 0.305$, $y = 0.323$ (CIE, 1931). Example stimuli are shown in Fig 3.5.

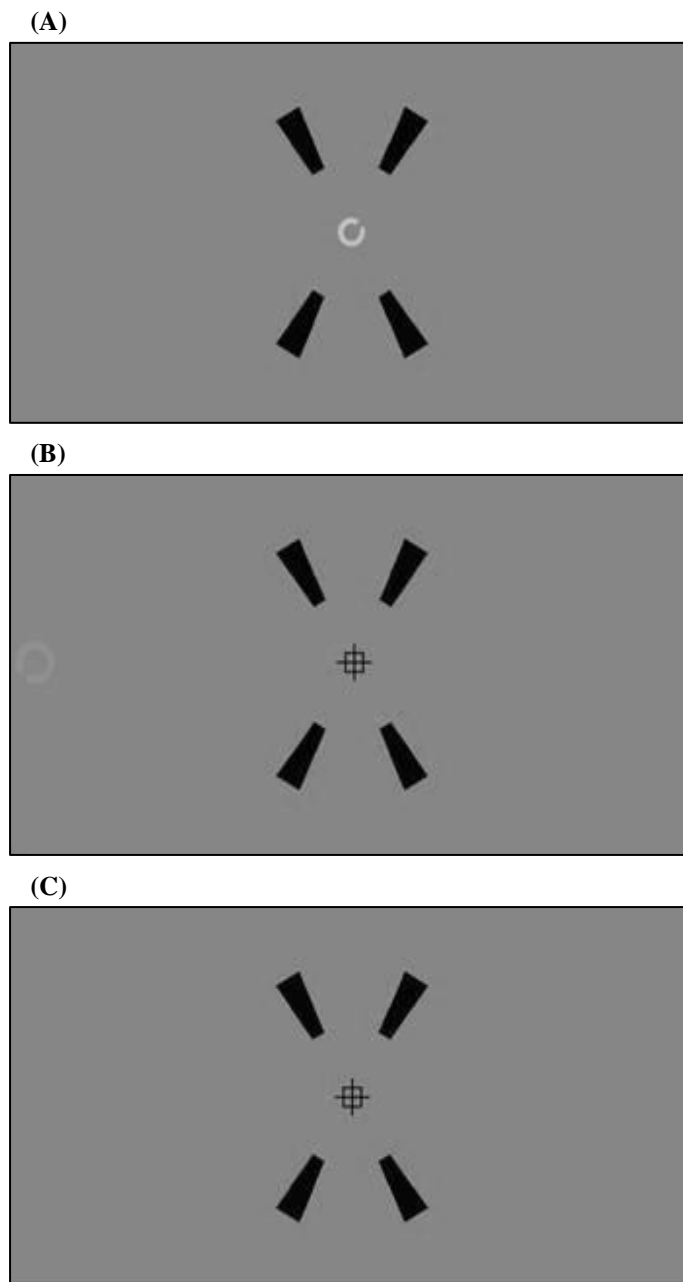


Figure 3.5. An observers' view of the FCS stimuli. The target consists of a superthreshold-sized Landolt C target. The observer's task is to identify the orientation of the gap by means of a response keypad, using a four-alternative, forced-choice procedure

(A) shows a foveal high contrast target. (B) shows a peripheral (-5°) low contrast target. (C) shows the fixation guides that appear before stimulus presentation.

3. 2. 3. Procedure

The observer fixated at the centre of the screen, regardless of target location. Guides were used to maintain fixation and to minimise accommodation fluctuations. Fixation guides were presented for 150 ms followed by a delay of 800 ms, during which the screen was uniform, before the presentation of the stimulus, lasting 80 ms.

The short duration of target presentation ensures that observers will be unable to make complete saccades in order to fixate on peripheral targets.

Thresholds were obtained using a two-up, one-down staircase procedure and the independent variable, i.e. stimulus size or contrast, was adjusted automatically according to the participant's response. This reduces the likelihood of a reversal resulting simply from correctly guessing the target orientation, without actually seeing the target, to 1/16.

The task used a four-alternative forced choice procedure. Target orientation was varied in a random order and the participants' task was to indicate, in their own time, the orientation of the Landolt C using a response keypad. Unless otherwise stated, the test was carried out binocularly and, as the same stimuli were presented to each eye, pupil diameter was measured monocularly.

3. 3. Colour Assessment and Diagnosis (CAD) test:

measurement of chromatic discrimination

3. 3. 1. Apparatus

The Colour Assessment and Diagnosis (CAD) test was developed at City University, London (Barbur, Rodriguez-Carmona, & Harlow, 2006; Rodriguez-Carmona, Harlow, Walker, & Barbur, 2005). The test is based on background luminance perturbation techniques developed to isolate the use of colour signals (Barbur, Harlow, & Plant, 1994).

The CAD test employed in this study was implemented on a high resolution NEC 10-bit PA241W 24" colour-stable display. Chin and forehead rests were used to position the observer's head. A black wooden hood was positioned over the head-rest and camera equipment, thereby minimizing the amount of external light reaching the observer.

3. 3. 2. *Stimuli*

The test stimulus consists of a colour-defined, square outline moving diagonally across an achromatic chequered-array background, shown in Fig 3.5. The target and the background are isoluminant, as specified by the CIE (x,y) 1931 standard observer. Thresholds are measured along 16 directions in colour space, measuring red-green and yellow-blue chromatic sensitivity. Both the target and background are comprised of random, dynamic, luminance contrast noise, which isolates the colour signal so that responses cannot be made using luminance contrast signals (Barbur & Ruddock, 1980). The stimulus subtends 3.3° by 3.3° visual angle and is surrounded by a background adaptation field, the chromaticity co-ordinates of which are $x = 0.305$, $y = 0.323$ (CIE, 1931). Example stimuli are shown in figure 3.6.

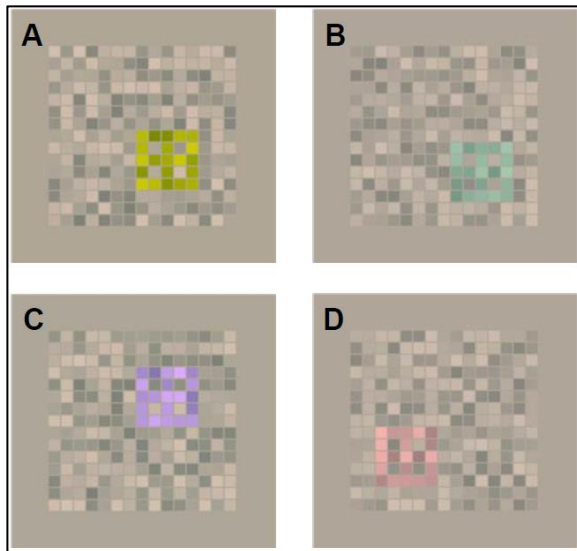


Figure 3.6. An observers' view of the CAD stimuli. The stimulus consists of a moving chromatic target within an achromatic background; both the target and background utilise dynamic luminance contrast noise to isolate the chromatic signal. Thresholds are measured along 16 directions in colour space. (A) shows one of two yellow hues; (B) shows one of six green hues; (C) shows one of two blue hues; (D) shows one of six red hues.

3. 3. 3. Procedure

The observer fixated at the centre of the screen, where there was a small fixation dot to help maintain fixation. After stimulus presentation, the screen became uniform and the observer heard a short beep to indicate that they should make their response.

Chromatic detection thresholds were measured using a two-up, one-down staircase procedure and the saturation of the coloured target was adjusted automatically according to the participant's response. This reduces the likelihood of a reversal resulting simply from correctly guessing the target orientation, without actually seeing the target, to 1/16. A full run consisted of 1 staircase for each of the 16 directions in colour space.

The task used a four-alternative forced choice procedure, whereby the participant responded to the direction of movement of the target along the diagonal. Direction of movement was varied in a random order and the participants responded

using a response keypad. Unless otherwise stated, the test was carried out binocularly.

3. 4. Measurement of transient discomfort glare thresholds

3. 4. 1. Apparatus

Equipment was also developed in our laboratory for measurements of discomfort glare thresholds. The glare source consisted of a four-primary LED unit (produced by PerkinElmer), with a light homogeniser mounted in front to produce a spatially uniform beam. A multi-aperture wheel enabled variation in glare source size. Conventional lamps were used to vary the ambient luminance of the area surrounding the unit, which was otherwise in a darkened room. In order to record pupil diameter, a 50 Hz Pulnix camera was mounted to the left of the participant. Viewing distance was 1 m from the glare source.

3. 4. 2. Stimuli

The stimulus consisted of a large photograph of a night-time residential street scene, as shown in Fig 3.7, mounted onto a board; within this was a hole through which the glare source was visible. The purpose of the glare source was to produce transient discomfort glare. The stimulus had a duration of 300 ms; 600 ms prior to stimulus onset, three short 50 ms, dim flashes were used to attract the observers attention.



Figure 3.7. An observers' view of the night-time residential scene used in the measurement of discomfort glare thresholds. The glare source was presented through an aperture in the centre of the image. Small red fixation spots were positioned at -0° , -3° , -6° and -12° to aid peripheral fixation.

The effects of changes in target size, background luminance and eccentricity were examined separately. Five different target sizes were used, measuring 0.28° , 0.62° , 1.04° , 1.33° and 1.73° ; all were presented at the fovea and the background luminance was set to 2.6 cd/m^2 . To investigate the effect of background luminance, three background luminances, 0.26 cd/m^2 , 2.6 cd/m^2 and 26 cd/m^2 were used; the source size was kept constant at 1.33° and, again, all targets were presented at the fovea. Finally, four eccentricities, 0° , 3° , 6° and 12° , were investigated using a constant background luminance of 2.6 cd/m^2 and a source size of 1.33° .

3. 4. 3. Procedure

The observer was asked to fixate either on the centre of the screen or at the eccentricities stated above; a small red circular target was used for each of the three peripheral fixation points. Participants were given verbal notice and asked to blink prior to glare source presentation. Observers indicated the presence or absence of discomfort, using a two-alternative forced choice procedure, on a keypad.

Pupil diameter was measured prior to stimulus onset and used to calculate the

retinal illuminance, i.e. the dependent variable. Stimulus intensity was modulated according to a one-up, one-down staircase; the step size was reduced at each of the 9 reversals used. The mean value of log retinal illuminance from the last 6 reversals was taken as the discomfort glare threshold.

Chapter 4: Angular dependence of light scatter and its significance

4. 1. Introduction

The angular dependence of scattered light is usually described by a power law, θ_e^{-n} , whereby θ_e represents the eccentricity of the scatter source and n is defined as the scatter index. The empirical light scatter equation, $L_s = E k \theta_e^{-n}$, describes the luminance of an external source, L_s , needed to match the retinal illuminance generated by the scatter source. The latter is therefore directly proportional to the illuminance level, E (measured in lumens / m²), in the plane of the pupil generated by the scatter source. The parameter k describes the amount of light scattered in the eye; a large k is indicative of a greater amount of scattered light. The value of the scatter index, n , determines its angular distribution, with a large n corresponding to a narrower spread of scattered light.

A value of 2 for n is often used to describe the angular dependence of scattered light from 1° to 30° (van den Berg & Ijspeert, 1992; van den Berg, 1986), but values in the range [1.5 to 2.8] have been reported (Fry & Alpern, 1953; Holladay, 1926; International Commission on Illumination, 2002; Stiles & Crawford, 1937). It is not, however, clear whether this variation reflects true changes in the angular distribution of scattered light in the eye or is simply the effect of measurement errors arising from using different experimental techniques (DeMott & Boynton, 1957).

The aim of this study was to assess the extent to which the variability in parameters describing the scatter function of the eye represents genuine differences between individuals, or whether it can be explained solely by instrumentation and

measurement errors. A large age range was recruited in order to assess age related changes. A secondary aim was to compare the variability of k with that of the integrated straylight parameter, k' .

In this context, two major problems that may limit the accuracy of light scatter measurements are addressed; the first being the fact that light scattering may not always be uniform over the pupil. Secondly, random errors that affect the measured L_s values may limit the accuracy of n and k . In addition to observer-related errors in setting a flicker-null threshold, other factors can also affect the accuracy of light scatter measurements. Differences in the level of illumination in the plane of the pupil can affect the accuracy of measured L_s values. In a typical set up for light scatter measurements, there are two principal sources of instrumental error that can cause variation in the amount of light that is measured as scattered light in the eye: one being the display device that is employed to generate the scatter source and the other being the photometer head that is used to calibrate for equality of pupil plane illuminance for different scatter source eccentricities.

Visual displays offer great advantages in terms of variable stimulus geometry and the generation of sinusoidal flicker modulation. The use of spatially extended annuli also generates increased levels of scattered light that can be measured using flicker-nulling techniques at low luminance levels when the operation of the display can be kept stable. By using the methodology given in Chapter 3.1, it is also possible to extract accurately the angular dependence of light scatter in the eye despite the fact that the scatter source no longer has a unique eccentricity.

4. 2. Methods

4. 2. 1. Participants

Five female and six male participants took part in the study. All participants undertook an ocular examination, which was conducted by an optometry undergraduate on-site. The examination involved refraction and a slit-lamp examination. Visual acuity was corrected using participants' own glasses or contact lenses. All participants had corrected visual acuity of 6/9 or better. Only those with good general health and without the presence of ocular disease, damage, surgery or intraocular lenses in either eye were recruited. Older participants with lens opacity were not excluded from the analysis, as this was deemed to constitute normal ageing. No exclusions were made based on outlying results.

4. 2. 2. Experimental design

The experiment utilised the flicker cancellation technique as described in Chapter 3.1. The test was also modified to use only one scatter annulus, as in most clinical tests, with the parameters n , k and k' being computed on the assumption that $n = 2$. This is the mean value typically expected for normal young observers (van den Berg & Ijspeert, 1992). The annulus of effective eccentricity 7.3° (corresponding to ring number 4 of 5) was presented in this case.

Each participant completed both the full test and the single annulus version, each consisting of five experimental runs; this enabled comparison of the two light scatter estimates.

4. 3. Results

4. 3. 1. Descriptive statistics

Values of n and k were calculated from measured values of L_s as described in section 3.1.1. Measured L_s values are given in Table 4.1 for all participants whose data were available.

Table 4.1. Measured values of L_s at each of the five annulus eccentricities

Inner radius (pixels)	Light scatter values								
	VJ	LR	SL	EP	DL	GL	JB	NA	LC
56	1.86	1.98	1.85	1.96	1.97	2.26	2.80	2.37	5.29
105	1.52	1.33	1.17	1.89	1.09	1.35	2.08	1.59	3.37
155	1.03	0.79	0.87	1.42	0.84	0.99	1.73	0.91	2.11
200	0.73	0.68	0.65	1.00	0.81	0.69	1.42	0.72	1.12
300	0.52	0.34	0.43	0.61	0.53	0.36	0.95	0.36	0.52

Measured values of n using the full test varied from 1.66 to 2.72 (mean = 2.19) for 11 subjects. Measured n values were found to be significantly different from the value of 2, $t(10) = 28.3$, $p < .00$.

Larger values of n were found for older observers, with a mean value of 1.95 for those aged under fifty years and 2.39 for those aged fifty years and over. This suggests that the angular distribution of light scatter within the eye decreases with age, in contrast to previous literature in which no effect was found (Fisher & Christie, 1965). However, a smaller angular distribution is consistent with theories that age-

related increases in scatter are caused by larger particles in the lens (Costello et al., 2007; Spector et al., 1974; Thaug & Sjöstrand, 2002; van den Berg & Ijspeert, 1995; Wooten & Geri, 1987). This finding is also coherent given that the lens tends to become more yellow with age, and is likely to absorb some wide-angle short-wave scatter (Steen, Whitaker, Elliot, & Wild, 1994; van den Berg & Ijspeert, 1995).

Similarly, k and k' , as yielded by the full test, both show age differences, with mean values of 9.89 and 6.04 respectively for the young group, and 32.49 and 6.12 for the older age group. This is consistent with previous work that has shown an increase in the amount of scatter within the eye over the age of fifty years (Harrison, Applegate, Yates, & Ballentine, 1993; Hennelly, Barbur, Edgar, & Woodward, 1998). A comparison of the youngest and oldest observers from the current sample is shown in Fig 4.1.

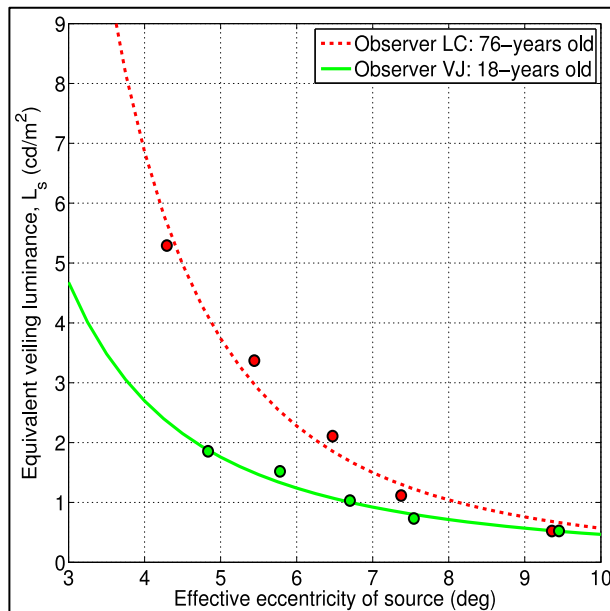


Figure 4.1. Light scatter as a function of effective eccentricity of the scatter source, given by $L_s = kE\theta^{-n}$. Each data point represents the light scatter measurement at the given eccentricity for each observer. The luminance of the target needed to compensate for the retinal illuminance generated by the scatter source is higher for the 76-year old when compared to the 18-year old observer.

4. 3. 2. Comparison of k and k' obtained with measured and fixed ($n = 2$) n values.

There were errors in the estimation of k when only a single annulus was used,

i.e. when n is assumed to be 2, as shown in Table 4.2. Although error values ranged from 18.28% to 95.81% (mean = 58.40%), the difference between the two sets of k was not statistically significant, $t(10) = 2.0$, $p = .075$. This is likely to be due to the large age range and hence the larger variability in the values of k for the full test (standard error = 5.77). There was, however, an observable positive correlation between the deviation in n from 2 and the resulting difference in k between the full versus single annulus tests, $r(11) = 0.9$, $p < .000$.

Table 4.2. Values of n , k and k' when using measured n and when assuming that $n=2$.

<i>Observer</i>	<i>Age</i>	<i>Measured n</i>	<i>k (using measured n)</i>	<i>k' (using measured n)</i>	<i>k (assuming n = 2)</i>	<i>k' (assuming n = 2)</i>
<i>VJ</i>	<i>18</i>	<i>1.92</i>	<i>8.98</i>	<i>4.76</i>	<i>10.75</i>	<i>4.88</i>
<i>LR</i>	<i>19</i>	<i>2.33</i>	<i>16.03</i>	<i>4.24</i>	<i>10.30</i>	<i>4.68</i>
<i>SL</i>	<i>23</i>	<i>2.11</i>	<i>10.99</i>	<i>4.14</i>	<i>8.98</i>	<i>4.08</i>
<i>EP</i>	<i>25</i>	<i>1.72</i>	<i>7.89</i>	<i>6.26</i>	<i>14.00</i>	<i>6.37</i>
<i>DL</i>	<i>40</i>	<i>1.70</i>	<i>5.55</i>	<i>4.56</i>	<i>10.86</i>	<i>4.94</i>
<i>GL</i>	<i>50</i>	<i>2.43</i>	<i>20.85</i>	<i>4.74</i>	<i>7.59</i>	<i>3.45</i>
<i>JB</i>	<i>53</i>	<i>1.66</i>	<i>9.60</i>	<i>8.65</i>	<i>15.01</i>	<i>6.82</i>
<i>NA</i>	<i>59</i>	<i>2.51</i>	<i>25.44</i>	<i>5.14</i>	<i>8.01</i>	<i>3.64</i>
<i>AL</i>	<i>65</i>	<i>2.46</i>	<i>26.82</i>	<i>5.78</i>	<i>10.77</i>	<i>4.89</i>
<i>LV</i>	<i>70</i>	<i>2.58</i>	<i>42.98</i>	<i>7.78</i>	<i>11.92</i>	<i>5.42</i>
<i>LC</i>	<i>76</i>	<i>2.72</i>	<i>69.24</i>	<i>10.43</i>	<i>17.42</i>	<i>12.47</i>

k' values appeared to be more resistant to changes in n , with error values ranging from 1.40% and 30.39% (mean = 15.16%), and the difference between the two sets of k' values was not significant, $t(10) = 1.15$, $p = .276$. As for k values, there was a significant correlation between the deviation in n from 2 and differences in k , $r(11) = 0.8$, $p < .001$. These results are shown graphically in Fig 4.2.

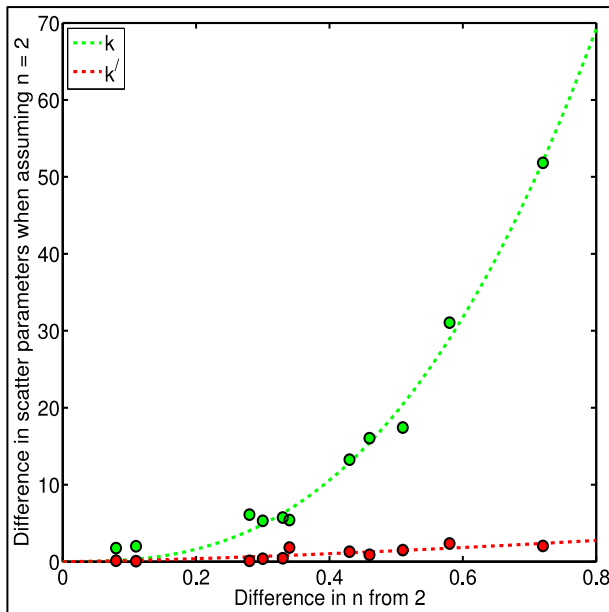


Figure 4.2. Absolute difference in measured scatter parameters – k and k' – calculated using measured n as opposed to $n = 2$, as a function of the absolute difference between measured n and 2. As the deviation of n from 2 increases, there is an increase in the error of both k and k' , although k is the more susceptible of the two measures to error.

The effect that the deviation in n from 2, and the coincident error in the measurement of k , has on the appearance of the curves is shown in Fig 4.3.

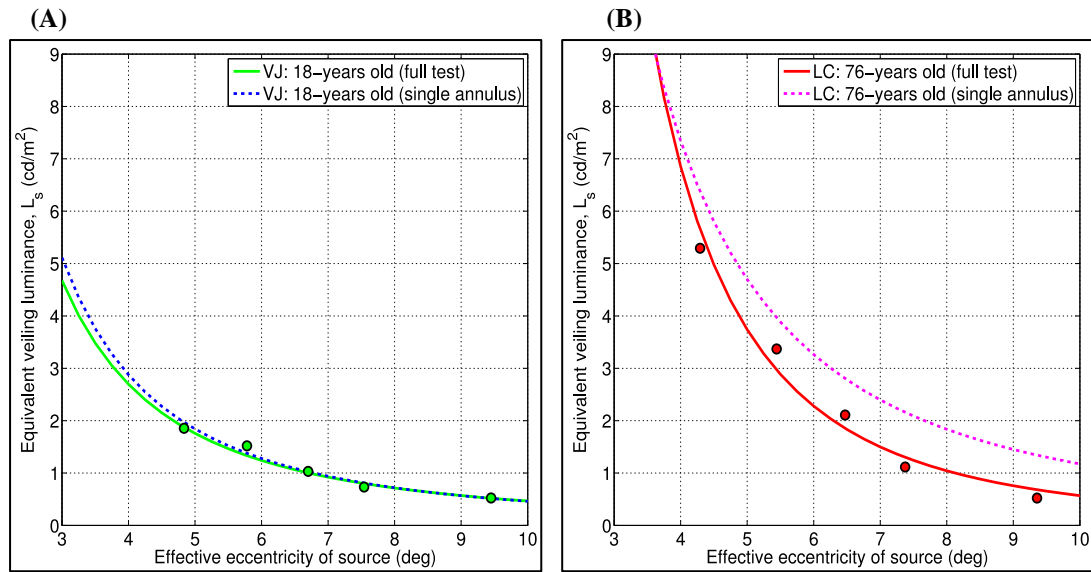


Figure 4.3. Comparisons between the fitted scatter function yielded when k is computed using $n = 2$ and when k is computed using the measured value of n . For the observer with the smallest deviation in n from 2 (A), the difference between the two functions is small. For the observer with the largest deviation in n from 2 (B), there is a large difference between the two curves.

4.4 Discussion

This study aimed to establish the importance of angular distribution in the measurement of scattered light within the eye. The results show that values of n are often significantly different from 2, usually assumed to be the standard normal value for a young observer, and that this cannot be attributed entirely to measurement errors; this replicates previous findings using similar methodology (Kvansakul, 2005). Deviation in n from 2 is likely to reflect genuine differences in the angular distribution of scatter. n values also show a slight positive increase, and therefore a decrease in angular distribution, with age. This may be due larger scattering particles in older lenses, or the absorption of wide-angle short-wave light scatter by the yellowing lens. Further investigation is required to determine the precise cause of age-

related increases in n .

The flicker cancellation technique has been used previously to show that n values are affected in patients with conditions associated with increased light scatter, such as keratoconus, cataract, corneal dystrophy. Such conditions can lead to variations in the uniformity of light scattered over the area of the pupil (Hennelly, Barbur, Edgar, & Woodward, 1997). In light of the current findings, it would be of further interest to determine the extent to which uniformity of scatter over the pupil is affected in non-pathological ageing.

The findings from this study suggest that the total amount of forward light scatter within the eye, as described by integrated straylight parameter, k' , shows less variation than k . Measured changes in k therefore reflect fluctuations in the angular distribution of scattered light as well as the effect that measurement errors have on the computation of n and k . The k' parameter combines the effect of changes in n and k and shows much lower variability. Although k' cannot be used to describe changes in the angular dependence of scattered light, its significantly smaller variability makes it more appropriate for use in clinical studies.

When n is assumed to have a value of 2, there is a positive correlation between the resulting difference in the values of k obtained using the full tests and the single annulus test; the same is true for k' . This demonstrates that, in order to examine accurately the full scatter function of the eye, it is advisable to measure both the amount and distribution of scattered light whenever possible.

Chapter 5.

The effects of simulated ageing, using fogging filters, on visual performance

5. 1. Introduction

As well as being uncomfortable and irritating, scattered light can seriously impair visual performance. Such impairment could be particularly dangerous when driving, for example, when sunlight reflects from the road, causing disability glare. In order to develop measures to reduce forward light scatter and its effects, it is crucial to understand which aspects of visual function are affected most. The amount of scattered light within the eye increases in old age (de Waard et al., 1992; Hennesly et al., 1998; Spector et al., 1974; Vos, 2003a) and with the onset of certain clinical conditions such as cataracts (de Waard et al., 1992; Elliott,), corneal dystrophy (van den Berg, 1986), keratoconus (Jinabhai, O'Donnell, Radhakrishnan, & Nourrit, 2012) and retinitis pigmentosa (Alexander, Fishman, & Derlacki, 1996). However, it is difficult to isolate the effects of increased scattered light from other factors that are coincident with ageing and clinical conditions.

The purpose of the following exploratory studies was to manipulate the level of forward scatter within the eye, independently of other factors associated with degradation of the optical media, by placing 'fogging' filters in front of healthy young eyes. Firstly, it was necessary to quantify the scattering properties of the fogging filters by comparing scatter measurements with and without the fogging filters. The intention was then to determine the extent to which binocular summation may provide a greater advantage when images of reduced contrast, as a result of increased scatter, are involved.

The intention was to ascertain the relative impact of scattered light on different measures of visual performance. Visual acuity (VA) is a commonly used metric for describing the quality of vision, and is used as part of many assessments to determine an individual's ability to carry out certain tasks, such as driving; in fact the DVLA standards apply only to VA and field of vision. However, it is well known that scattered light affects mostly sensitivity to contrast (Stiles, 1929b). As light does not scatter equally at all wavelengths, it was also of interest to measure the effects of scatter on chromatic sensitivity (Strutt, 1971). Although it is possible to produce spectrally biased stimuli using the flicker-cancellation technique, it is not feasible to produce a stimulus with sufficient luminance while restricting the spectral content to a narrow band of wavelengths. In addition, previous studies have reported little wavelength dependence of light (Coppens et al., 2006; Whitaker et al., 1993; Wooten & Geri, 1987). On the other hand, chromatic sensitivity declines in old age and it is unclear how much of an impact increased scatter has on the loss of sensitivity.

The aim of the current chapter was to gain an improved understanding of the functional impact of scattered light by investigating the effects on three performance measures — VA, functional contrast sensitivity (FCS) and chromatic sensitivity — as well as exploring the extent of binocular summation for measurements of VA and FCS when the image in one eye is degraded by scattered light.

5. 1. Experimental design

5. 2. 1. Participants

One female participant, aged 23 years, undertook all the measurements in the study. Two further female participants, aged 28 and 29 years, completed the quantification of the filters (5. 2. 2.) and visual performance measurements (5. 2. 5.). All participants were refracted by an optometrist on-site and visual acuity was corrected using participants' own glasses or contact lenses. All participants were free from ocular disease, damage, surgery or intraocular lenses in either eye. No exclusions were made based on outlying results. No exclusions were made based on visual acuity, as the target size was well above average threshold.

5. 2. 2. Quantifying the scattering properties of fogging filters

This study aimed to simulate increased scattered light within the eye by using Tiffen Pro-Mist Diffusion Filters. The filters were placed in front of the eyes of young participants to simulate the effects of ageing on scattered light within the eye, thereby removing potential confounding variables associated with ageing.

The purpose of the first part of this study was to quantify the scattering properties of a number of fogging filters. The flicker cancellation technique for measuring scattered light within the eye (Chapter 3. 1) was used to quantify the scattering properties of five fogging filters (Tiffen Pro-Mist Diffusion Filters: 0.125, 0.25, 0.5, 1, and 2). Tiffen filters are made using a process that involves laminating the filter substrate between 2 pieces of optical glass, grinding flat to a tolerance of 1/10,000th of an inch, and then mounting to precision metal rings. The filter number indicates the power of diffusion, with larger numbers corresponding to greater filter

density. Further details about these filters including how they are tested can be found on the company website (Tiffen, 2015). One female 23-year-old observer completed five runs with and without each of the five filters. A further two female observers completed two runs in the absence and presence of the strongest filter only (Tiffen Pro-Mist Diffusion Filter: 2). In all cases, the filter was placed over the right (dominant) eye.

Once the results were obtained, the mean values from the five runs were entered back into the program so that the scatter function could be fitted to the data. The fitted functions were then used in the analysis. Comparisons in the presence and absence of fogging filters were then made on the following performance measures:

5. 2. 3. Binocular summation

The aim of this part of the study was to examine the extent to which binocular viewing is advantageous over monocular viewing. In order to achieve this, visual acuity (VA) and functional contrast sensitivity (FCS) thresholds were obtained using the CAA (Chapter 3. 2) under binocular and monocular conditions. Both VA and FCS were measured in the absence and in the presence of all five fogging filters, with six runs completed for each of the twelve conditions. The filter was positioned over the right (dominant) eye.

In order to compare the effects of eye dominance on binocular summation in sensitivity to contrast, further testing was undertaken using the strongest filter only (Tiffen Pro-Mist: 2). Twelve runs of the contrast sensitivity assessment were completed in the absence and presence of the filter positioned in front of the right and

left eye. All tests were completed under both binocular and monocular viewing conditions. One 23-year-old female observer completed all the tests.

5. 2. 4. Visual acuity, contrast sensitivity and chromatic sensitivity

The purpose of this part of this study was to assess the effects of added scattered light on three measures of visual performance: VA, FCS and chromatic discrimination thresholds. Scattered light was assessed as in Chapter 3. 1, VA and FCS were assessed using the CAA test (Chapter 3. 2), and colour vision was assessed using the CAD test (Chapter 3. 3). Three young female observers undertook all the assessments monocularly using the right (dominant) eye. For both conditions, i.e. with and without fogging filter (Tiffen Pro-Mist 2), one run of the scatter assessment, six runs of the acuity assessment, six runs of the contrast assessment and three runs of the colour assessment were completed.

5. 3. Results

5. 3. 1. Scattering properties of fogging filters

The results from the scatter test showed a general increase in the amount of scattered light corresponding with increasing filter strength for the one observer tested. Fitted values of k and k' increased progressively from 17.87 and 5.31 (respectively) in the absence of any filters to 59.10 and 12.25 in the presence of the strongest filter. There was also a statistically significant correlation between filter strength and k , $r(6) = 0.87$, $p < .05$, as well as k' , $r(6) = 0.87$, $p < .05$. For ensuing analyses, filter strength will be considered in terms of the k' value of the eye and filter combined.

Fitted values of n ranged from 2.25 in the absence of any filters and progressively increased to 2.49 in the presence of the strongest filter. The correlation between filter strength and the value of n was, however, not statistically significant, $r(6) = 0.80$, $p = .054$. These findings suggest that the filters do not have a significant effect on the angular distribution of scattered light.

For all three observers, there was a clear increase in the amount of scattered light in presence of the strongest filter (Tiffen Pro-Mist: 2) when compared with standard monocular viewing. Mean fitted values of k and k' increased by 65.89% and 95.50% respectively whereas n decreased by 3.31% in the presence of the filter. A comparison between the scatter results for one of the three observers with and without the strongest fogging filter (Tiffen Pro-Mist: 2) and the average normal observer is shown in Fig 5.1.

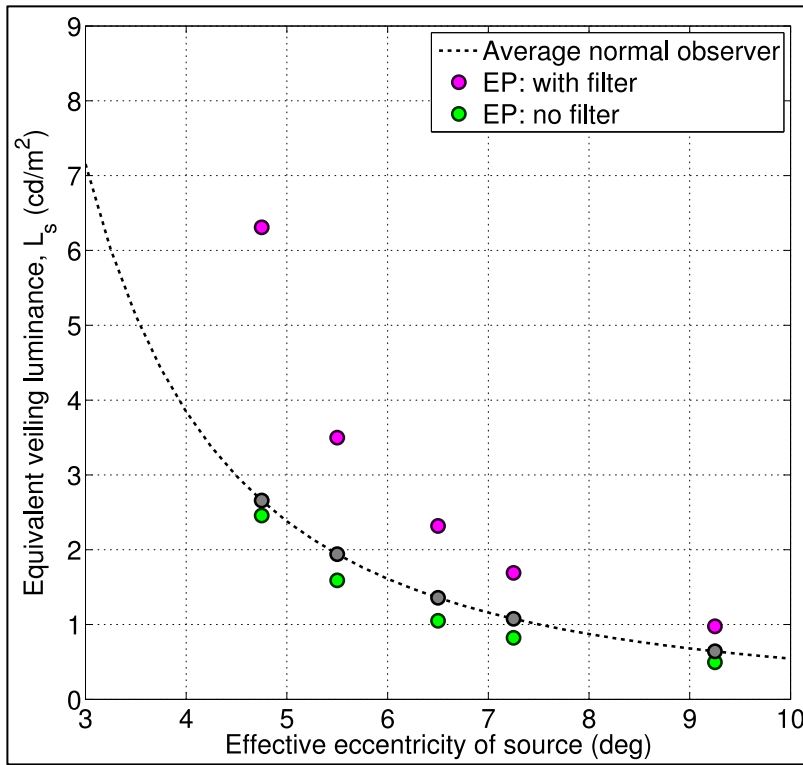


Figure 5.1. Light scatter as a function of effective eccentricity of the scatter source, given by $L_s = kE\theta^{-n}$. The test was carried out on a visual display, using an annular source of scatter and a disc-like central target. The scatter test employs five glare source eccentricities and the measured data are used to compute the parameters k and n , which relate to the amount and angular distribution of scattered light in the eye respectively. The addition of the strongest fogging filter (Tiffen Pro-Mist: 2) leads to a significant increase in scattered light.

5. 3. 2. Effects of fogging filters on binocular summation

The results from the VA tests in the absence and presence of all five fogging filters, shown in Fig 5.2, revealed a binocular advantage, as all the monocular thresholds were higher than the corresponding binocular thresholds, $F(1) = 17.71$, $p < .00$. Although there was also a significant main effect of filter strength (defined in terms of k' values), $F(5) = 2.42$, $p < .05$, there was no statistically significant correlation between filter strength and visual acuity thresholds under either binocular, $r(36) = 0.33$, $p = .051$, or monocular, $r(36) = 0.24$, $p = .159$, conditions. This is in agreement with previous literature, which has found a poor relationship between measures of scattered light and VA.

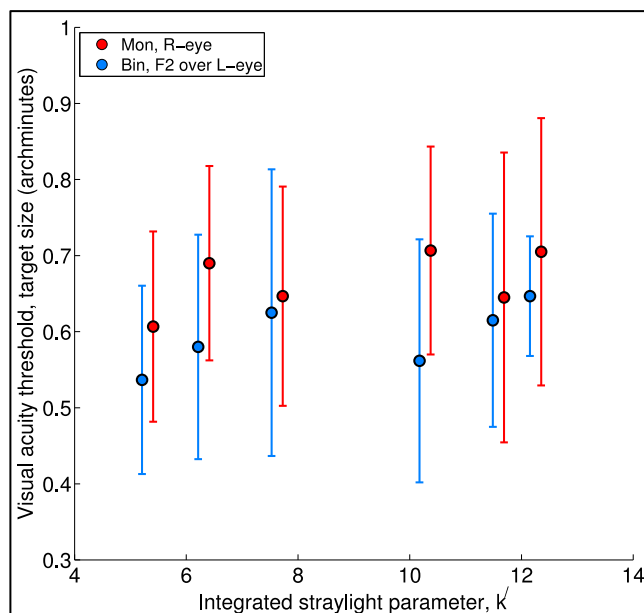


Figure 5.2. Mean VA thresholds as a function of light scatter, as defined by measured k' values in the presence of fogging filters. VA thresholds are given as the diameter of the Landolt C in minutes of arc. The two left-most data points represent thresholds in the absence of any filters. The error bars represent ± 2 standard errors of the mean. Although the k' values were the same for each pair of data points, for clarity the data are displayed adjacently.

The results from the FCS tests in the absence and presence of all five fogging filters shown in Fig 5.3, also revealed a binocular advantage, $F(1) = 163.28$, $p < .00$. There was also a main effect of filter strength, $F(5) = 70.75$, $p < .00$, as well as statistically significant correlations between filter strength and contrast sensitivity thresholds, $r(36) = 0.87$, $p < .000$ and $r(36) = 0.80$, $p < .000$ for binocular and monocular viewing conditions respectively.

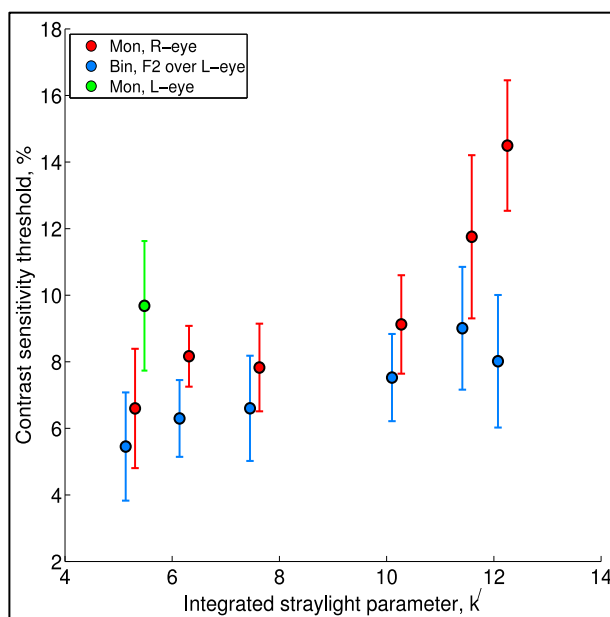


Figure 5.3. Mean FCS thresholds as a function of light scatter, as defined by measured k' values in the presence of fogging filters. FCS thresholds are given as percentage contrast difference. The three left-most data points represent thresholds in the absence of any filters. The error bars represent ± 2 standard errors of the mean. Although the k' values were the same for each pair of data points, for clarity the data are displayed adjacently.

It was of interest to determine the degree of degradation needed in order to extinguish the advantage of binocular viewing. Comparisons were made between monocular thresholds taken with the non-dominant (left) eye and binocular thresholds taken with each of the five filters positioned in front of the dominant (right) eye. Monocular performance with the first three (i.e. weakest) filters placed in front of the dominant

eye was significantly better than unhindered performance using the non-dominant eye only, $t(5) = 8.43$, $p < .000$ and 4.99 and 4.56 , $p < .01$ respectively. The fourth filter resulted in equivalent performance in monocular and unhindered monocular viewing, $t(5) = 1.25$, $p = .276$. The fifth (i.e. strongest) filter resulted in poorer binocular performance than under unhindered monocular viewing conditions, $t(5) = 3.12$, $p < .05$; this can be seen in Fig 5.3. These findings would suggest that, for this particular observer, an increase in scattering of over 100% is needed in order to negate the effects of binocular summation.

Further analysis was undertaken in order to ascertain the effects of eye dominance on FCS thresholds in the presence and absence of the strongest two filters (Tiffen Pro-Mist: 2). Thresholds were measured in the presence and absence of the fogging filter for both eyes, as shown in Fig 5.4. As expected, the presence of the filter resulted in a statistically significant degradation of monocular FCS for both the dominant, $t(11) = 9.03$, $p < .000$, and non-dominant, $t(11) = 8.52$, $p < .000$ eyes. Mean thresholds increased from 6.93 to 13.22 for the right eye and from 9.79 to 18.45 for the left, equating to an approximate doubling of thresholds in the presence of the strongest filter; it was therefore expected that there would be little binocular advantage. The comparisons of interest were between monocular viewing with the non-dominant eye and binocular viewing with the filter over the dominant eye and vice versa, i.e. the same eye remains unhindered for each comparison. When comparing the unhindered performance of the dominant eye, there was no binocular advantage using the strongest filter, $t(11) = 1.02$, $p = .328$. However, there was a small but statistically significant advantage of binocular viewing when the non-dominant eye was unhindered, $t(11) = 2.92$, $p < .05$. These findings indicate that eye

dominance can affect the extent to which binocular summation is beneficial, under conditions in which the image in one eye is severely degraded.

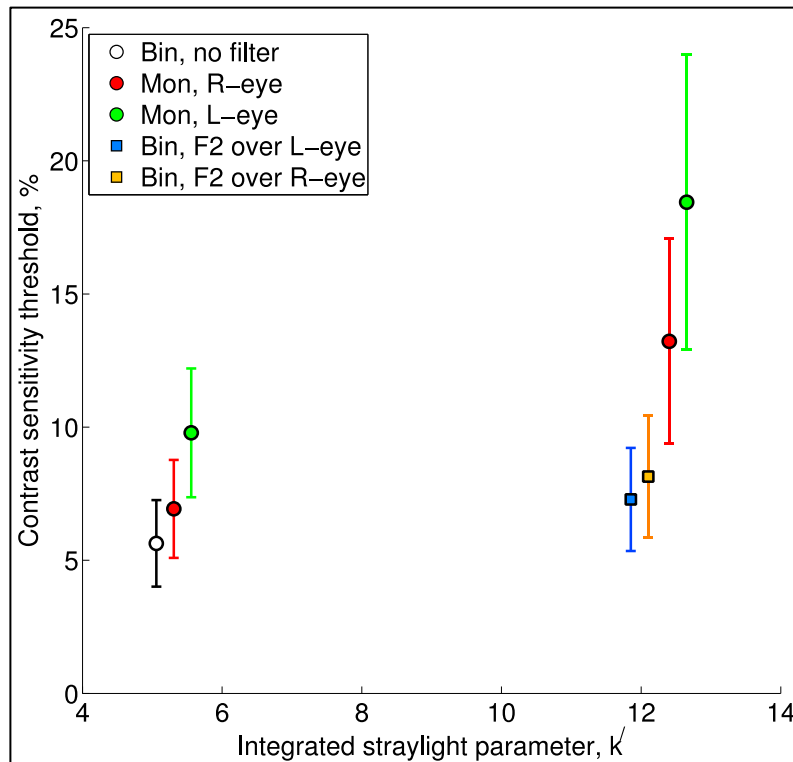


Figure 5.4. Mean FCS thresholds as a function of light scatter, as defined by measured k' values.

The three data points on the left represent thresholds in the absence of the fogging filter; the four data points on the right represent thresholds in the presence of the strongest fogging filter (Tiffen Pro-Mist: 2). Red data points represent thresholds taken with the right (dominant) eye only; green represents the left (non-dominant) eye only. FCS thresholds are given as the percentage contrast difference. The error bars represent ± 2 standard errors of the mean. Although the k' values were the same for the three data points on the left and for the four data points on the right, for clarity the data are displayed adjacently.

5. 3. 3. *Effects of added scattered light on visual acuity, contrast sensitivity and colour vision*

Three measures of visual performance from three observers revealed that large amounts of added scattered light leads to a worsening of visual acuity, contrast sensitivity and, to some extent, chromatic sensitivity, as shown in figure 5.5.

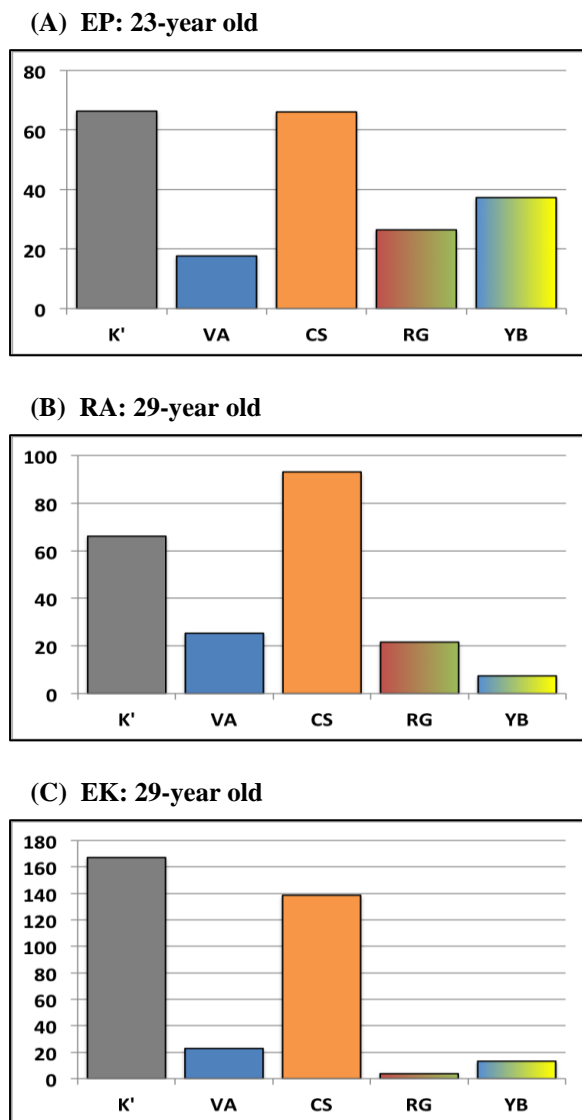


Figure 5.5. Percentage increases in thresholds in the presence of the strongest (Tiffen Pro-Mist: 2) fogging filter. Results for each of the three observers are given. Increases in scattered light are given in terms of the scatter parameter, k' . Increases in VA are given as the percentage increase in threshold target size for a high contrast Landolt C target. Increases in functional CS are given as percentage increase in threshold contrast for a superthreshold-sized Landolt C target. Increases in chromatic discrimination thresholds are given as the percentage increase in CAD units for both red-green (RG) and yellow-blue (YB) chromatic discrimination.

In the presence of the strongest fogging filter (Tiffen Pro-Mist: 2) thresholds increased, on average, by 22.38% for visual acuity, 94.16% for contrast sensitivity

and 19.17% for chromatic sensitivity. T-tests revealed that for each observer, the increase in visual acuity and contrast sensitivity thresholds was statistically significant $t(5) = [3.41 - 5.99], p < .05$.

Chromatic sensitivity was assessed separately for red/green and yellow/blue opposing channels in colour space. Increases in red/green chromatic sensitivity thresholds were not statistically significant for any of the three observers. Increases in yellow/blue colour thresholds were significant for two of the three observers, $t(2) = 7.42$ and $9.16, p < .05$; the thresholds did, however, remain within the range of values expected for someone with normal colour vision.

5. 4. Discussion

The aim of the exploratory studies in this chapter was to gain a greater understanding of the functional effects that increased scattered light has upon various aspects of visual performance. Fogging filters were used to simulate the effects of increased scatter without introducing confounding variables associated with ageing. Initial assessment of five fogging filters showed that the levels of scatter increased with increasing filter strength. They also demonstrated little change in angular dependence of scattered light, rendering them appropriate for use in simulating the effects of ageing.

Firstly, the effects of scattered light on visual acuity and contrast sensitivity were assessed using monocular thresholds. It was found that there was little effect of increased scattered light on visual acuity. This was to be expected, as previous studies have shown that visual acuity does not correlate well with other measures of scattered light and disability glare (Elliott et al., 1990; Elliott & Bullimore, 1993; Prager et al.,

1989). Only when scatter reached very high levels, i.e. approximately double that of the eye itself, was there a significant effect on visual acuity. The effects of increased scattered light on contrast sensitivity were larger, with increasingly larger thresholds observed with increasing filter strength. This finding was also to be expected, as it is well known that scattered light reduces the contrast of the retinal image by adding light to the object and the background.

For both measures, there was a clear advantage of binocular over monocular viewing, which is consistent with previous literature (Hume, 1978). As the presence of the fogging filter had a large effect on contrast sensitivity — the strongest filter having roughly doubled the threshold — it was of interest to assess the extent to which binocular viewing is beneficial when the image in one eye is degraded by scattered light. It was found that the amount of scattered light needed in order to nullify the benefits of binocular summation was more than double that already present within the ocular media. Although binocular inhibition can occur at high spatial frequencies in those with severe unocular cataracts (Pardhan & Gilchrist, 1991), our findings did not reveal any effects of binocular inhibition; it is, however, possible that the image was not sufficiently degraded for competition between the two images to occur. Binocular summation and inhibition may also be affected by eye dominance. The current results show that a binocular advantage was present when the non-dominant eye was unhindered, even when the amount of scattered light in the dominant eye was roughly doubled. When the dominant eye was unhindered, however, there was no binocular advantage when the non-dominant image was degraded. In order to determine the universality of these effects, it would be necessary to repeat these tests using participants with different degrees of eye dominance.

The current results showed that the addition of scattered light had little effect on colour vision. Red/green chromatic sensitivity thresholds were not affected and any increase in thresholds along the yellow/blue channel did not exceed those expected for the normal trichromatic observer. Intraocular light scatter follows the Rayleigh wavelength dependence of scattered light, with shorter wavelengths being scattered more. However, because the iris is not completely opaque, some light at the long wave end of the spectrum is added. In addition, the yellowing of the lens that occurs in older age results in a larger absorption of short wave light (Norren & Vos, 1974), thereby increasing the relative amount of long wave scatter. As a result, there is little wavelength dependence of scattered light (Whitaker et al., 1993; Wooten & Geri, 1987) and little effect on chromatic sensitivity (Coppens et al., 2006).

It is, of course, worth noting that all the stimuli were presented in photopic viewing conditions. Previous research has shown that all three aspects of visual performance are affected by luminance (Blackwell, 1946; Brown, 1951; Schlaer, 1937; Yebra, García, Nieves, & Romero, 2001). In order to gain a fuller understanding of the effects of light scatter on these performance measures, it would be necessary to repeat these experiments at different levels of illumination. These exploratory studies have shown that the largest effect of scattered light on visual performance was in terms of sensitivity to contrast. It was therefore of interest to investigate further the effects of scattered light and disability on contrast sensitivity under different lighting conditions.

Chapter 6. The effect of disability glare on functional contrast sensitivity

6. 1. Introduction

In the presence of a bright source of light, it is common for an observer to experience problems with spatial vision. Although there is a good understanding of how the properties of the glare-source affect the physical behaviour of light, the effects of scattered light on visual performance remain poorly understood, particularly at low light levels. It is known that the ‘veiling luminance’ produced by the glare source reduces the contrast, and thereby the quality, of the retinal image. Understanding the visual response, however, is complicated by changes in the sensitivity of the retina with light level (van den Berg, 1991).

It is well established that the retina responds differently according to the level of ambient lighting (Barbur & Stockman, 2010; Mainster & Turner, 2012; Stockman, Langendorfer, Smithson, & Sharpe, 2006). Increased light levels on the retina produce a much larger improvement in sensitivity to contrast in the mesopic range than a similar increase in the photopic range (Barbur & Stockman, 2010; Blackwell, 1946); one might therefore expect glare to have a positive effect on visual performance under mesopic conditions.

Some studies using high intensity glare have found little evidence of improvement in contrast sensitivity due to increasing adaptation luminance (Aguirre, Colombo, & Barraza, 2011). Interestingly though, others have found the effects of disability glare to be less severe than would be predicted using measures of scattered light and, in some cases, to even improve visual performance (de Waard et al., 1992; Fisher & Christie, 1965; van den Berg, 1991). It was suggested that the phenomenon

may be owing to the increased luminance of the surround field (de Waard et al., 1992), that there could be a threshold to the disability glare effect (Fisher & Christie, 1965), or that the addition of scattered light might cause the dark-adapted retina to light-adapt (van den Berg, 1991). However, a systematic explanation and a model of how such preferential effects of increased retinal sensitivity might interact with the detrimental effects of reduced image contrast on the retina has not yet been put forward.

In order to establish the overall effect on sensitivity to contrast of the two conflicting factors, functional contrast thresholds were measured at different eccentricities, under different background luminance levels and at different glare-source intensities. In addition, the light scatter function of the eye (i.e., the amount as well as the angular distribution of light scattered within the eye) was measured for each observer, enabling prediction of retinal image contrast in the presence of glare. If glare-induced changes in visual performance depend solely on the contrast of the retinal image, one would expect threshold predictions based on scattered light to be highly accurate. On the other hand, if retinal sensitivity to contrast improves in the presence of glare, one would expect scatter-based predictions to over-estimate contrast thresholds.

6. 2. *Experimental design*

6. 2. 1. *Participants*

24 female and 29 male participants took part in the study. All participants undertook an ocular examination, which was conducted by an optometrist on-site. The examination involved ophthalmoscopy and refraction; in addition, general health, ocular health, medication and family ocular health were recorded. Visual acuity was corrected using participants' own glasses or contact lenses. Exclusion criteria were based on the presence of ocular disease, damage, surgery or intraocular lenses in either eye; 10 participants were excluded on this basis. Three participants who experienced extreme difficulty performing either task were also excluded. Older participants with early-stage cataract — grade 1, nuclear cataract or less — were not excluded from the analysis, as this was deemed to constitute normal ageing. No exclusions were made based on outlying results. No exclusions were made based on visual acuity, as the target size was well above threshold. Of the 53 participants who took part, 13 were excluded as a result of the criteria employed and the results from the remaining 40 observers (17 female and 23 male), were used in the final analysis. The age of the final sample ranged from 21 to 68, with a mean age of 42 years. There were 26 participants below the age of 50 years and 14 above.

This study was approved by the Senate Research and Ethics Committee at City University London, and adhered to the principles of the Declaration of Helsinki. All participants provided written consent to take part in the study.

6. 2. 2. *Disability glare measurements*

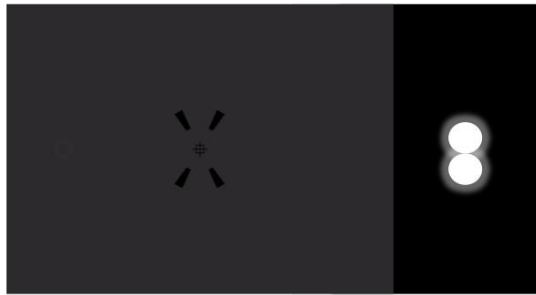
Contrast thresholds were measured under binocular viewing conditions using the CAA test, described in Chapter 3.2.

6. 2. 2. 1. *Apparatus.* Glare was introduced using two (Perkin Elmer, four primary) LED units driven by a TTi Precision DC PSU (model TSX3510). The LED units were stacked vertically and surrounded by black felt to reduce dispersion of light and create the impression of a single glare-source location positioned horizontally, 10° to the right of fixation (Fig 6.1). The combined spectral power distribution of the LED lights had a chromaticity of $x = 0.278$, $y = 0.286$ (CIE 1931).

(A) Screen luminance = 1cd/m^2 , glare intensity = 0lm/m^2



(B) Screen luminance = 2.6cd/m^2 glare intensity = 1.35lm/m^2



(C) Screen luminance = 26cd/m^2 , glare intensity = 19.21lm/m^2

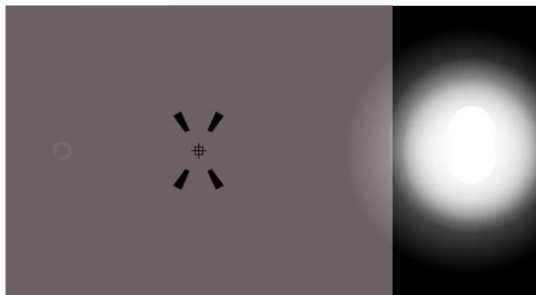


Figure 6.1. Observers' view of the experimental setup. The functional contrast sensitivity test was carried out on a CRT monitor. The glare source was positioned to the right of the monitor, 10° from fixation. The Landolt C target was presented at three locations — at fixation and $\pm 5^\circ$ — which corresponded to angular eccentricities of 15° , 10° and 5° with respect to the glare source.

The screen luminance was at (A) 1cd/m^2 , (B) 2.6cd/m^2 or (C) 26cd/m^2 . The task was performed under (A) no glare, (B) low intensity glare: 1.35lm/m^2 or (C) high intensity glare: 19.21lm/m^2 . Pupil size was measured continuously and the mean value during the test was used to calculate retinal illuminance.

6. 2. 2. 2. *Stimuli.* An observer's view of the stimuli is shown in Fig 6.1. A Landolt C target of positive luminance contrast was employed. The target was presented either at the centre of the display or $\pm 5^\circ$ from fixation, along the horizontal meridian. Consequently, the eccentricity of the target with respect to the glare-source was 5° , 10° or 15° . Each run consisted of three randomly interleaved staircases: one for each target location. One run yielded three contrast threshold measurements as well as one estimate of average pupil diameter. In total, the subjects completed 360 runs.

The luminance conditions followed a three by three design. Three background luminance levels were used to cover the high mesopic and the low photopic range: 1, 2.6 and 26 cd/m^2 (as shown in Fig 6.1(A, B and C, respectively). Three glare levels were used: No Glare — glare-source switched off — (Figure 1(A)), Low Glare — 1.35 lm/m^2 — (1(B)) and High Glare — 19.21 lm/m^2 — (1(C)). Runs for each of the nine lighting combinations were presented in a random order.

A supra-threshold target gap size of 4' was chosen at the foveal location to ensure that small fluctuations of accommodation and differences in higher order ocular aberrations that can cause large inter-observer differences when assessing the limit of spatial resolution would not confound significantly the results of this study. Peripheral targets were scaled in size to maintain similar contrast visibility across the three target locations. The scaling factor was determined using threshold measurements for four young participants at a display luminance of 26 cd/m^2 . Target gap size was set at 4' for central targets and 8' for peripheral targets.

6. 2. 2. 3. *Procedure.* Participants were given a minimum of three minutes to dark-adapt while the test was explained, demonstrated and practiced. Each participant completed one experimental run for each of the nine luminance conditions. As each run consisted of three staircases — one for each eccentricity — completion of the test yielded 27 contrast thresholds and nine estimates of pupil diameter. The luminance conditions were set at the beginning of each run, and participants were instructed to avoid looking directly at the glare-source.

The test was carried out binocularly and, as the same stimuli were presented to

each eye, pupil diameter was measured monocularly. The typical duration of the test (9 runs) was 1 hour 40 mins.

6. 2. 3. *Scattered light measurements*

Scattered light was measured using the flicker-cancellation technique, described in Chapter 3.1.

6. 2. 3. 1. *Procedure.* Participants were given a minimum of three minutes to dark-adapt. Each participant completed two full runs and the mean scatter parameters were used in the final analyses. Only one participant was unable to complete both runs, and the value for the single run was used in the analysis. Participants were asked to fixate on the central disc during each presentation and to indicate verbally the presence or absence of flicker. The test was carried out binocularly. The typical duration of a single test was 12 mins.

6. 2. 4. *Scatter-based predictions of functional contrast thresholds*

Equation 6. 1, as described in Chapter 3.1, is used to estimate the equivalent ‘veiling luminance’ that can be attributed to scattered light on the retina:

Eq. 6. 1.
$$L_s = kE\theta^{-n}$$

In the absence of glare, measured Weber contrast of the Landolt C target, C_{m0} , is calculated using:

Eq. 6. 2.
$$C_{m0} = \frac{L_t - L_b}{L_b}$$

Where L_t is the luminance of the target and L_b is the luminance of the background.

In the presence of glare, light scatter, L_s , is added to the retina at locations that correspond to both the target and background. This reduces the ‘real’ retinal image contrast, C_r , like so:

Eq. 6. 3.
$$C_r = \frac{(L_t + L_s) - (L_b + L_s)}{L_b + L_s} = \frac{L_t - L_b}{L_b + L_s}$$

On the assumption that, at threshold, an observer requires the same retinal image contrast to resolve the gap in the presence of glare, C_{mg} , as in the absence of glare, C_{m0} , then it follows that:

Eq. 6. 4.
$$C_{m0} = C_r = \frac{L_t - L_b}{L_b + L_s}$$

And hence:

Eq. 6. 5.
$$L_t = C_{m0}(L_b + L_s) + L_b$$

Once the stimulus luminance needed to achieve a retinal image contrast of C_{m0} in the presence of glare is known, it is possible to calculate the corresponding stimulus contrast as measured on the display. As in Equation 6.2, the predicted measured stimulus contrast becomes:

Eq. 6. 6.
$$C_{mg} = \frac{C_{m0}(L_b + L_s) + L_b - L_b}{L_b} = \left(C_{m0} \frac{L_s}{L_b} \right) + 1$$

6. 2. 5. Combined predictions of functional contrast thresholds

As equation 6 does not take into account improvements in retinal sensitivity

that occur due to increased retinal illuminance, it was not surprising to discover that predictions based only on scattered light over-estimated the detrimental effect of glare. In an attempt to improve upon existing scatter-based predictions, the formula was altered to incorporate a model that predicts contrast thresholds as a function of adaptation luminance. The model was derived from data collected previously (Connolly & Barbur, 2009) and is shown in Fig 6.2. Contrast thresholds were recorded at various adaptation luminance levels and a function was fitted to the data, which are best described using an equation of the form:

$$Eq. 6. 7. \quad C_e = (b_1 \times \text{exponent}(-b_2 \times \log_{10}(E)) + b_3) \times 100$$

Where:

C_e is the expected contrast threshold at a given retinal illuminance, E , given as a percentage.

E is the ‘effective’ retinal illuminance at the point of interest on the retina (Trolands).

b_1 , b_2 and b_3 are constants. The model was applied to measured data, both at the fovea and at 5° in the periphery, yielding different constants for the two retinal locations. The foveal constants were $b_1 = 44.24$, $b_2 = 2.37$ and $b_3 = 2.88$; peripheral constants were $b_1 = 45.02$, $b_2 = 1.81$ and $b_3 = 4.50$.

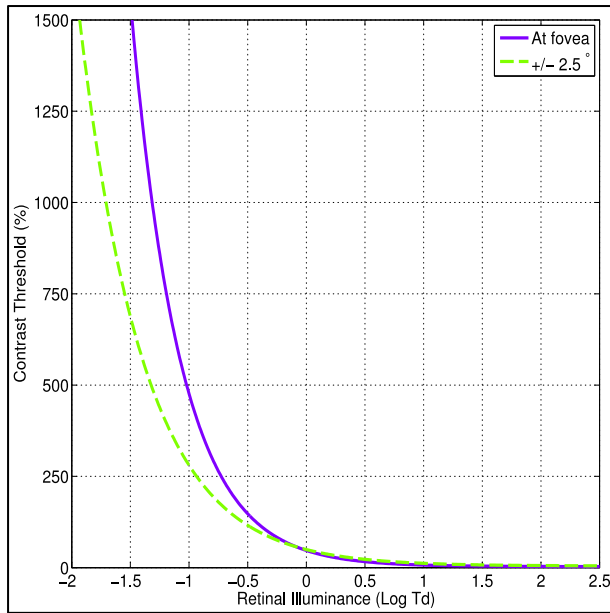


Figure 6.2. Functional contrast sensitivity thresholds measured at the fovea and 2.5° in the periphery, as a function of retinal illuminance, for a 30-gap Landolt ring stimulus. Pupil size was monitored continuously and this measurement was used to adjust the luminance of the display to maintain constant retinal illuminance. The results show that sensitivity to contrast increases asymptotically with log increase in retinal illuminance.

Using Equation 6.7, the ratio between the threshold expected in the absence of glare, C_{e0} , and that in the presence of glare, C_{eg} , was found using the corresponding change in effective retinal illuminance for each observer. The following equation provides a new ‘baseline’ contrast, C_{m0}' , which accounts for the expected change in retinal sensitivity:

$$Eq. 6. 8. \quad C_{m0}' = C_{m0} \frac{C_{eg}}{C_{e0}}$$

The new baseline, C_{m0}' , replaces the measured contrast in the absence of glare, C_{m0} , in Equation 6. 6 to yield new predictions that take into account the loss of contrast caused by scattered light and the corresponding change in retinal sensitivity to contrast:

$$Eq. 6. 9. \quad C_{mg}' = C_{m0}' \left(\frac{L_s}{L_b} + 1 \right)$$

In an attempt to understand more fully the effects of adaptation luminance on visual performance in the presence of glare, the combined predictions were calculated using two types of luminance values. The first type of luminance value, which shall

be referred to as local luminance, was calculated at the precise location of the target. The second type, which shall be referred to as global luminance, used the mean luminance from across the whole display. Although the visual system is by no means bound by the display area, the motivation behind using this second, 'global' measure of luminance was to provide a value that remained constant across target locations; it was hoped that this comparison would reveal whether visual performance was more reliant on local changes in retinal illuminance or changes in the adaptation state of the retina as a whole.

6. 3. Results

6. 3. 1. Equivalent veiling luminance and scatter parameters

The light scatter test yielded values for the scatter parameter, k , and the scatter index, n , as shown in Table 6.1. These constants were utilised in Equation 6.1 in order to calculate the equivalent veiling luminance, L_s , of the glare-source. Higher L_s values indicate a greater amount of scattered light within the eye. Mean L_s values for glare-sources of different eccentricities are plotted in Fig 6.3. It is clear from the scatter plot that observers over the age of fifty years are more likely to have a greater amount of scattered light within the eye.

Large k values indicate a greater amount of scattered light within the eye. As expected, those aged fifty years or older had significantly larger k values (mean = 57.14) than younger participants (mean = 33.46), $t(38) = 3.90$, $p < .01$. In agreement with previous literature, this finding indicates that scatter within the eye increases over the age of fifty years (Harrison et al., 1993; Hennelly et al., 1998; Spector et al., 1974).

Small n values indicate a large angular distribution of light scatter within the eye. There was no significant difference in n values between old (mean = 2.11) and young (mean = 1.98) observers. The mean values are comparable to the often used value of 2 (van den Berg, 1986).

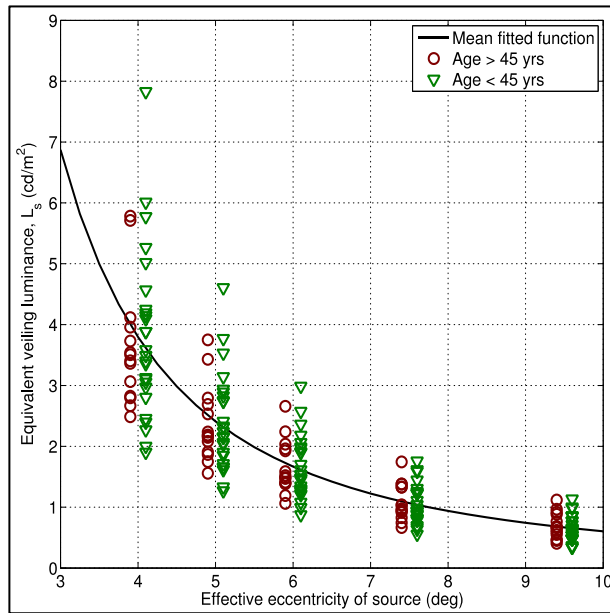


Figure 6.3. Light scatter as a function of effective eccentricity of the scatter source, given by $L_s = kE\theta^{-n}$. Each data point represents the mean fitted light scatter measurement (from two runs) at the given eccentricity for one of forty observers. In general, older subjects exhibit higher levels of scattered light when compared to the younger participants. Although the same effective eccentricities were used for each age group, for clarity the data are displayed adjacently.

Table 6.1. Mean k and n values for old and young observers

	Mean		Standard Deviation	
	< 50 yrs	> 50 yrs	< 50 yrs	> 50 yrs
$L_s = kE\theta^{-n}$				
Age (years)	33.5	57.1	8.4	5.1
k , scatter parameter	12.7	24.0	6.2	12.2
n , scatter index	1.98	2.11	0.26	0.35

6. 3. 2. Disability glare – absolute functional contrast thresholds

Contrast thresholds were obtained at three different eccentricities, for three different backgrounds, in the absence of glare and in the presence of two levels of glare. The three variables, each with three levels, therefore equate to 27 conditions. Mean contrast thresholds for each condition are shown in Figure 6. 4.

In order to rule out confounding variables such as eye dominance or gaze aversion, the contrast thresholds for targets on the left and right of fixation in the absence of glare were compared. As expected, there were no significant differences between left and right contrast thresholds at any of the background luminance levels tested.

In the absence of glare, contrast thresholds for foveal targets, corresponding to a glare-source eccentricity of 10°, were significantly higher than for peripheral targets. This finding suggests that the original scaling overcompensated for the expected loss of spatial vision in the periphery. This can be explained by the fact that the scaling was based on measurements made at a photopic background luminance of 26 cd/m², and that the decline in performance of rods is lower than that of cones at low luminance levels. Whereas this is worth bearing in mind for scaling in future experiments, it has little bearing on the current analyses, as comparison of absolute thresholds was not the aim of the investigation.

observers who were over the age of fifty years were found to have elevated levels of scattered light within the eye, a corresponding increase in contrast thresholds was expected. A 2×3×3×3 mixed ANOVA revealed a statistically significant main effect of age group on thresholds, $F(1,38) = 33.67$, $p < .001$, with those aged fifty years or over requiring higher target contrast than younger observers.

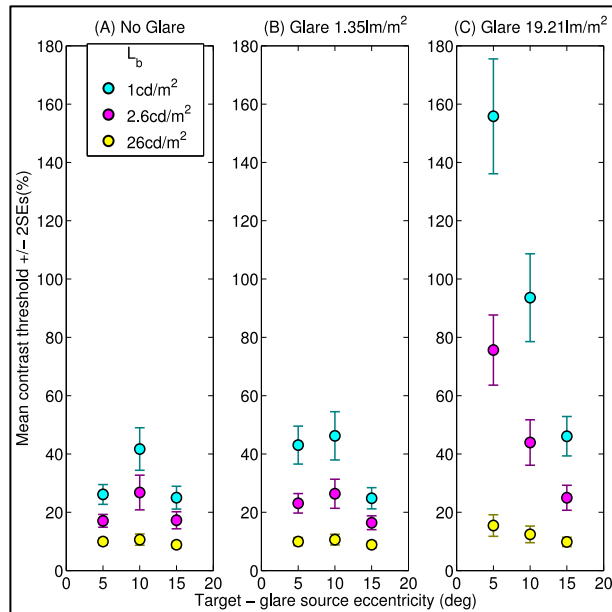


Figure 6.4. Mean FCS thresholds for 40 observers. The intensity of the glare source was set to produce a pupil plane illuminance of (A) 0, (B) 1.35 , and (C) 19.2 lm/m^2 . The error bars represent ± 2 standard errors of the mean. Target eccentricities are given in terms of their distance from the glare source, corresponding to -5° , 0° and $+5^\circ$ from fixation for the 5° , 10° and 15° locations respectively.

6. 3. 3. Disability glare –predictions of functional contrast thresholds

Whereas the pattern of results has thus far been in line with expectations, the question remains as to whether it is possible to predict reliably changes in visual performance due to the presence of glare, using scatter-based formulae. Scatter-based predictions of contrast thresholds were obtained using Equation 6.4 and are shown plotted against measured thresholds in Fig 6.5. In the presence of low intensity glare, 1.35 lm/m^2 , the scatter-based predictions appear to be reasonably accurate. Although the data become more dispersed as thresholds increase, showing that larger errors are associated with larger thresholds, the deviation from the $X = Y$ line is not biased. However, in the presence of high intensity glare, 19.21 lm/m^2 , at the lowest background luminance level, 1 cd/m^2 , there is a clear bias in the deviation of data points from the $X = Y$ line. This finding indicates that at low background luminance the predictions over-estimate contrast thresholds, and therefore the detriment caused

by the presence of high intensity glare. This can also be seen, albeit to a lesser extent, at the 2.6 cd/m² background luminance level.

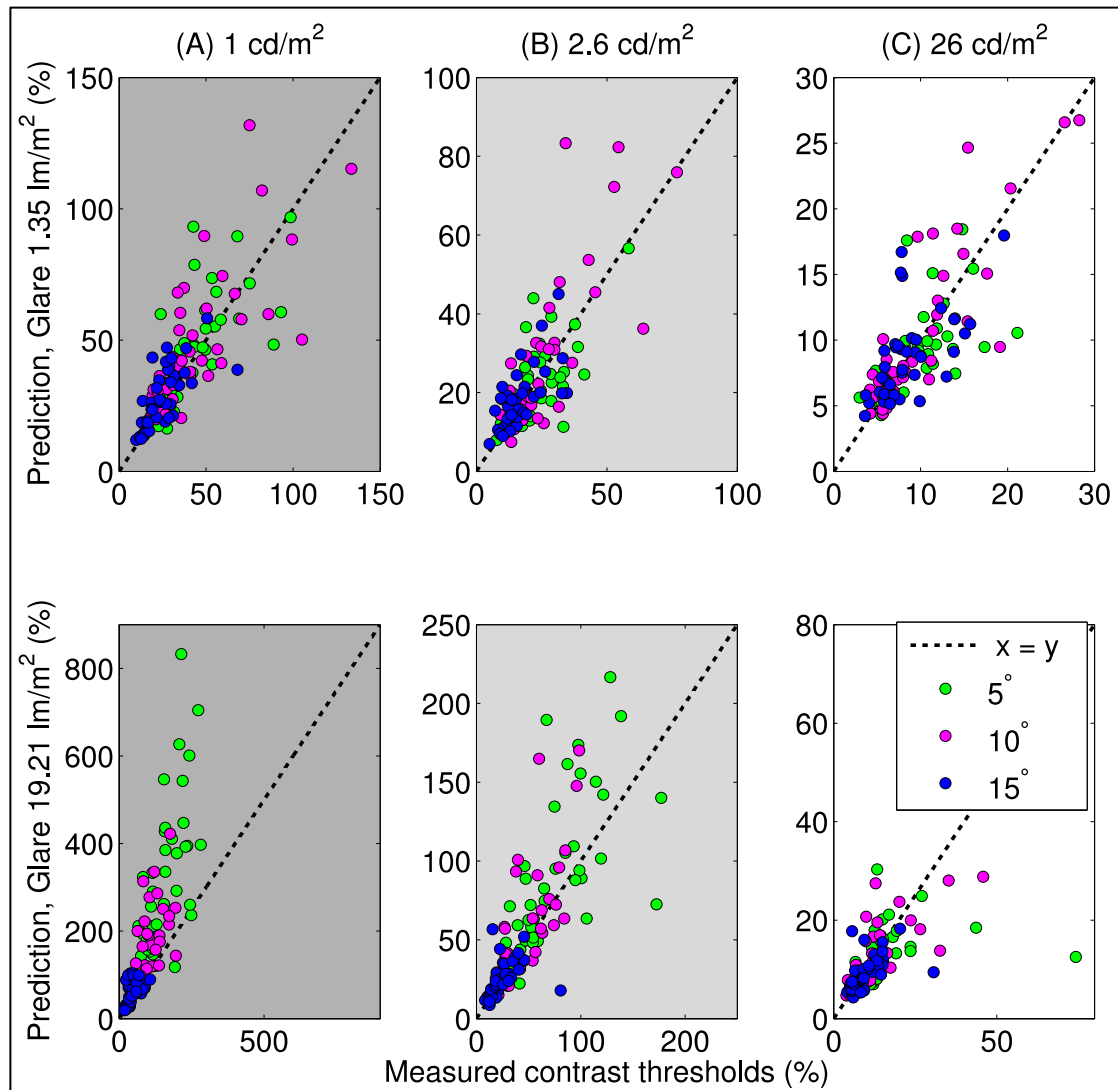


Figure 6.5. Relationship between measured thresholds and model predictions based solely on scattered light. Each data point represents the threshold for one participant in one of the 18 conditions, i.e. each participant is represented three times in each subplot. The $x = y$ line illustrates 100% accuracy of predictions; data points that fall above this line indicate an over-estimation of the contrast threshold in the presence of glare, i.e. better performance than expected. The largest over-estimation of thresholds was in the presence of high intensity glare at 1 cd/m² screen luminance.

In an attempt to improve upon the accuracy of the scatter-based predictions (Eq. 6.1 and 6.4) retinal sensitivity was incorporated using Equation 6.5. The curve that was used to find the multiplication factor in Equation 6.5 is shown in Figure 6.5. The new combined predictions used either local or global luminance, which was multiplied by pupil area in order to provide an estimation of the adaptation state of the retina in terms of retinal illuminance. Due to pupil constriction, the retinal illuminance in the presence of glare was sometimes lower than in the absence of glare.

To determine whether there was an effect of age group upon prediction accuracy, a $2 \times 2 \times 3 \times 3$ mixed ANOVA was carried out for each prediction. There was a significant main effect of age on prediction-accuracy for all three predictions, with scatter-based predictions exhibiting a larger effect, $F(1,35) = 18.57$, $p < .001$, than either local, $F(1,34) = 5.39$, $p < .05$, or global, $F(1,33) = 7.36$, $p < .05$ combined predictions. Whereas it was hoped that the accuracy of the new predictions would not be age-dependent, this result is not particularly surprising. Firstly, it has already been established that older participants tend to have higher contrast thresholds, which increases the scope for error; a lapse in concentration during the CAA test in the absence of glare would therefore lead to a larger error in the estimated contrast threshold in the presence of glare for an older observer. Secondly, the contrast threshold curve was based on data collected from one fifty year old participant, and it is entirely possible that the shape of the curve exhibits inter-observer variability and may also be a function of age. This, again, would lead to larger errors in the estimation of thresholds in the presence of glare.

The accuracy of the predictions for each condition is shown in Table 6.2. as root-mean-square (RMS) errors. Errors were calculated by subtracting measured thresholds from predicted thresholds. Upon inspection of the errors, differences in accuracy between the three predictions in the presence of low intensity glare (1.35 lm/m^2) appeared to be small. A $3 \times 3 \times 3$ repeated measures ANOVA (with prediction type, background luminance and eccentricity as factors) confirmed that there was no significant main effect of prediction type on the size of absolute discrepancies in the presence of low intensity glare. Similarly in the presence of high intensity glare, 19.21 lm/m^2 , and at photopic background luminance, 26 cd/m^2 , differences in accuracy seem to differ very little between the three predictions. A 3×3 ANOVA (with prediction type and eccentricity as factors) confirmed that there was no significant main effect of prediction-type on the size of absolute discrepancies at the 26 cd/m^2 background luminance level. However, in the presence of high intensity glare and at the background luminance level of 2.6 cd/m^2 , there was a greater variation in the size of errors between the three predictions; a 3×3 ANOVA revealed a significant main effect of prediction type, $F(2,76) = 6.06, p < .01$. Differences in errors between conditions are even more pronounced at the lowest, 1 cd/m^2 , background luminance, confirmed by a larger significant main effect $F(2,76) = 37.31, p < .001$.

Table 6.2. Root mean square error as a measure of the discrepancy between observed and predicted thresholds for each of the three models.

	<i>Low Glare</i>			<i>High Glare</i>		
<i>Pupil-plane illuminance</i>	<i>1.35 lm/m²</i>			<i>19.21 lm/m²</i>		
<i>Eccentricity</i>	<i>5°</i>	<i>10°</i>	<i>15°</i>	<i>5°</i>	<i>10°</i>	<i>15°</i>
<i>Screen luminance</i>	<i>RMS error associated with scatter-based model predictions</i>					
<i>1 cd/m²</i>	<i>15.97</i>	<i>19.56</i>	<i>9.41</i>	<i>213.30</i>	<i>90.15</i>	<i>23.80</i>
<i>2.6 cd/m²</i>	<i>8.44</i>	<i>12.64</i>	<i>6.30</i>	<i>41.33</i>	<i>28.18</i>	<i>13.16</i>
<i>26 cd/m²</i>	<i>3.32</i>	<i>3.32</i>	<i>3.12</i>	<i>11.42</i>	<i>5.84</i>	<i>4.45</i>
	<i>RMS error associated with 'local' combined model predictions</i>					
<i>1 cd/m²</i>	<i>15.69</i>	<i>19.31</i>	<i>12.25</i>	<i>104.51</i>	<i>62.21</i>	<i>27.35</i>
<i>2.6 cd/m²</i>	<i>7.92</i>	<i>13.13</i>	<i>6.58</i>	<i>30.57</i>	<i>25.95</i>	<i>13.11</i>
<i>26 cd/m²</i>	<i>3.31</i>	<i>3.16</i>	<i>3.06</i>	<i>11.55</i>	<i>5.93</i>	<i>4.53</i>
	<i>RMS error associated with 'global' combined model predictions</i>					
<i>1 cd/m²</i>	<i>17.58</i>	<i>18.24</i>	<i>9.84</i>	<i>128.30</i>	<i>49.86</i>	<i>20.03</i>
<i>2.6 cd/m²</i>	<i>8.07</i>	<i>13.13</i>	<i>6.21</i>	<i>31.91</i>	<i>24.23</i>	<i>13.19</i>
<i>26 cd/m²</i>	<i>3.31</i>	<i>3.16</i>	<i>3.06</i>	<i>11.54</i>	<i>5.94</i>	<i>4.52</i>

As the accuracy did not differ at low glare intensity or at photopic background luminance, RMS errors were recalculated at mesopic background luminance and in the presence of high intensity glare. At 2.6 cd/m² background luminance, the errors associated with scatter-based predictions, 27.56, were larger than for both local and

global combined predictions, 23.21 and 23.11 respectively. The difference in accuracy was even larger at 1 cd/m² background luminance, as scatter-based predictions yielded an RMS error of 109.08 as opposed to 64.69 and 66.07 for local and global combined predictions, respectively. As the results for both sets of combined predictions were similar, only the global set has been plotted against measured thresholds (Fig 6.6). The smaller error size for the new combined predictions suggests that by taking into account changes in retinal sensitivity, estimations of contrast thresholds in the presence of glare can be improved.

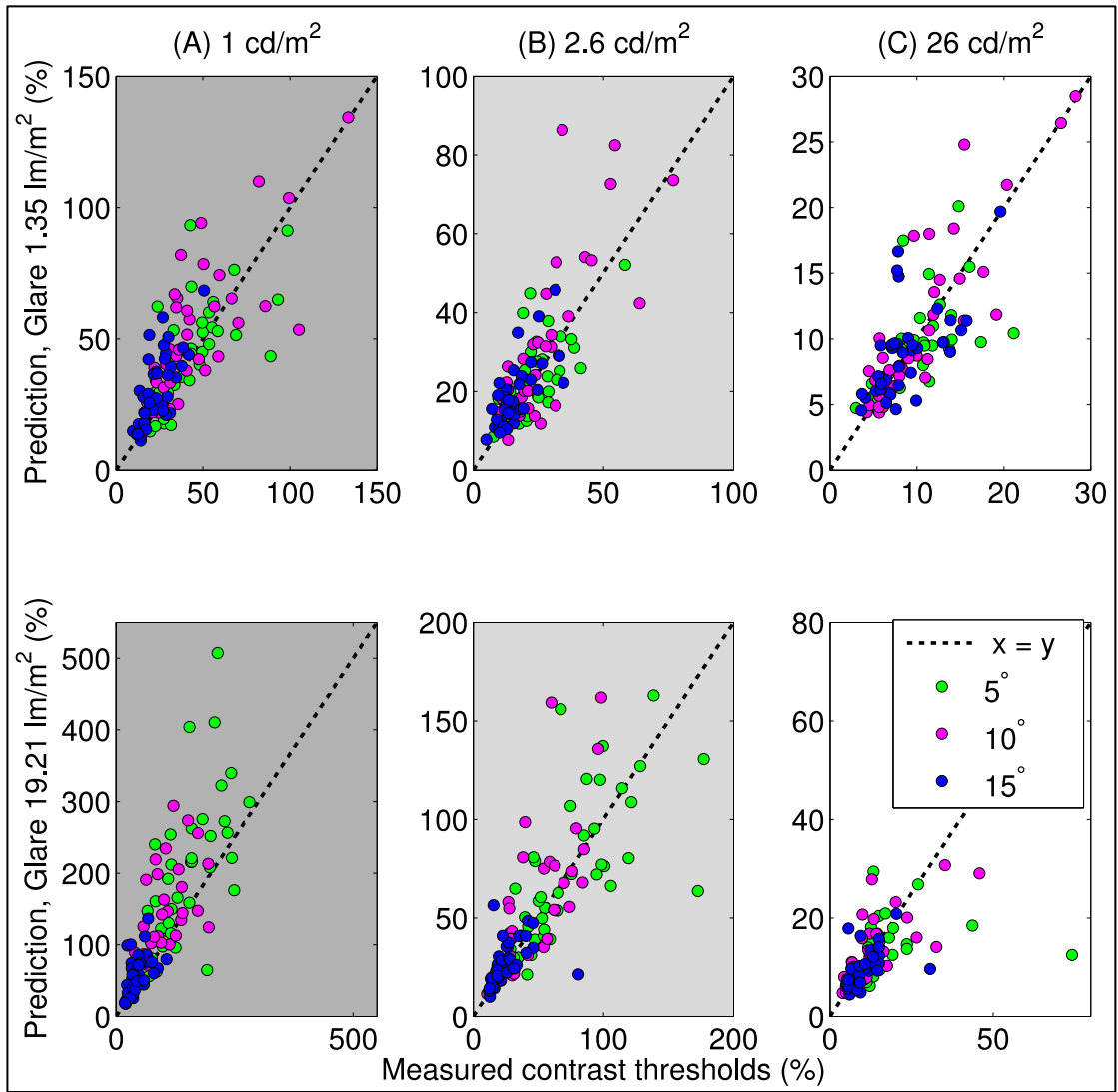


Figure 6.6. Relationship between measured thresholds and model predictions based on ‘global’ changes in retinal sensitivity combined with changes in scattered light. As in figure 6.5, the $x = y$ line illustrates 100% accuracy of predictions.

6. 4. Discussion

The current investigation aimed to address the question of whether visual performance can be accurately predicted based on measured forward light scatter within the eye. Previous work has demonstrated that predictions of visual performance based solely on scattered light are reasonably accurate in photopic lighting conditions (Mainster & Turner, 2012). In mesopic lighting conditions however, when most people report experiencing problems with glare (Mainster & Timberlake, 2003), the scatter based prediction becomes less reliable (de Waard et al., 1992; Fisher & Christie, 1965; van den Berg, 1991). Although it is well known that retinal sensitivity increases with luminance (Barbur & Stockman, 2010; Stockman et al., 2006), there has of yet been no serious attempt to model systematically its effect on visual performance under glare conditions.

Three predictions — one based solely on forward light scatter and two that were further combined with a model of retinal sensitivity — were used to estimate contrast sensitivity thresholds in the presence of glare. Upon assessment of each of the predictions, the largest discrepancies were found to be associated with those based solely on scattered light, with prediction accuracy at its poorest when the background luminance was low. As previously discussed, an increase in retinal illuminance in the mesopic range corresponds to a larger increase in contrast sensitivity under similar stimulus conditions than an identical increase in the photopic range (Barbur & Stockman, 2010); the reported similarity in accuracy between the scatter-based and combined predictions in the photopic range supports this observation. In the mesopic range, the superiority of the combined predictions in terms of accuracy indicates that the addition of light from the glare source is advantageous, despite the fact that the

additional light does not contribute to the illumination of the stimulus itself. The improved accuracy of the combined predictions lends support to the hypothesis that increased retinal sensitivity is at least partially capable of offsetting the disadvantage of reduced physical contrast in the presence of glare.

The two methods that were used to calculate retinal illuminance — local and global — yielded predictions with a similar level of accuracy. As such, it is unclear whether changes in retinal sensitivity to contrast are determined by local interactions at the target location or by mechanisms that operate across larger regions of the retina. Although the term ‘global’ has been used here to distinguish between the two sets of predictions, it should be noted that the retinal illuminance was calculated only across the area of the display. Prediction accuracy may be further improved by calculating mean luminance across the entire visual field, by applying a weighting function according to cortical representation of the retinal image, or indeed by using a combination of local and global measures. Any refinement to such a measure that increases prediction accuracy, is not only useful for the glare community, but may also elucidate mechanisms that determine the adaptation state of the retina.

Despite the improvement in prediction afforded by the incorporation of retinal sensitivity, neither set is entirely accurate, as there remains a significant over-estimation of thresholds in some conditions. The persistent over-estimation of thresholds, even after taking into account changes in retinal illuminance and sensitivity, may indicate the existence of an additional protective factor in the presence of glare.

The overestimation of contrast thresholds in the presence of glare was shown to be larger for observers aged fifty years and over. Given the well-established decline

in visual function with age (Haegerstrom-Portnoy et al., 1999), it seems unlikely that the discrepancy in the older group's performance would be due to additional protective factors. There are a number of other individual differences — initial thresholds, iris pigmentation (Ijspeert et al., 1990) and susceptibility to discomfort glare (Hopkinson, 1956), to name just a few — that could impact upon the relationship between retinal illuminance and contrast thresholds. Furthermore, it would be of great interest to investigate the extent to which the relationship is affected by various pathological conditions. Expanding the sample upon which the contrast threshold curve is based has the potential to improve the accuracy of the predictions, possibly by tailoring the formulae to specific age groups.

Although there may be several ways to improve upon the new combined predictions, the evidence presented here shows that retinal sensitivity to contrast is a critical factor in predicting visual performance. The lack of any noteworthy effect of the adjustment to predictions at the photopic lighting level is in keeping with this finding. In addition, the large effect seen in both of the mesopic lighting conditions makes the conclusions all the more robust. As such, it is demonstrated that the adjustment for retinal sensitivity in predictions of visual performance is particularly relevant to research dealing with high intensity glare under low ambient luminance conditions, such as those involving street lighting and car headlights. Future research investigating visual function in the presence of glare is likely to benefit from taking into account concurrent changes in retinal sensitivity.

Chapter 7.

Directional sensitivity of cone photoreceptors and scattered light within the eye

7.1 Introduction

As light travels through the eye, some will be scattered as a result of imperfections and inconsistencies in the ocular media. The scattering of light results in an image with lower contrast with respect to its adjacent background because some of the light from the centre of the object will fall onto the surrounding area. In the case of an image being projected through a medium onto a flat surface, it is possible to predict the loss in contrast, on the condition that the properties of the glare source, the scattering properties of the medium, and the relative position of the surface and the source are known. However, in the case of the human eye, there are several factors that make it more difficult to predict how the image will be perceived. Firstly, the retina is curved, and this may affect the distribution of back scatter, which contributes around 40% of the total scatter within the eye (Vos, 2003b). Secondly, the response of the photoreceptive cells depends on their type and location, as well as the overall amount of light on the retina (Stockman et al., 2006; Stockman & Sharpe, 2006). The rod and cone photoreceptors differ a great deal in their sensitivity to light of different intensities and wavelengths and in the way that they communicate with other cells within the retina. Another way in which the two types of photoreceptor differ is in their directional sensitivity to light, whereby a photon travelling along the axis of a cone or, to a far lesser extent, rod photoreceptor (Van Loo & Enoch, 1975; Walraven, 2009) is absorbed more readily than when approaching at an angle. This phenomenon was first observed by Stiles and Crawford in 1933 and has since been

known as the Stiles-Crawford (S-C) effect (Stiles & Crawford, 1933). By comparing the response of the human visual system with that of the predicted response based on light flux measured with a photometer, they found that using a large artificial pupil resulted in an over estimation of the visual response. This finding indicates that light entering through more eccentric parts of the pupil is less effective than light entering through the centre of the pupil. The fact that cone photoreceptors exhibit directional sensitivity is advantageous as it minimises the response to internal scatter within the eye ball (Le Grand, 1937), and reduces the effectiveness of aberrated rays that tend to come from the periphery of the pupil (Campbell, 1957; Charman, Jennings, & Whitefoot, 1978). It has been suggested that directional sensitivity of rods would be unnecessary and even disadvantageous at low light levels (Walraven, 2009), hence why they exhibit only a very small S-C effect.

The effect of directional sensitivity on visual function has been a matter for debate. Scattered light within the eye leads to a degradation in image quality mainly by reducing contrast on the retina. Because directional sensitivity will be most relevant when the pupil is dilated, one might expect that failing to account for the S-C effect would lead to an overestimation of the illuminance level on the retina. It has also been suggested that scattered light may be underestimated by psychophysical measures (Boynton et al., 1954). It is worth noting, however, that the S-C effect will impact equally the different parts of an image, so fluctuation in pupil size will not cause image contrast on the retina to change. On the other hand, retinal sensitivity to contrast is improved at higher levels of incident light on the retina (Barbur & Stockman, 2010; Blackwell, 1946); it is therefore possible that the S-C effect could lead to small changes in sensitivity to contrast.

It is of great interest to determine the extent to which the S-C effect impacts upon visual performance under different lighting conditions. In order to investigate this matter, functional contrast sensitivity (FCS) thresholds were measured under four measurement methods:

1. Constant display luminance with no correction for either pupil size changes or the S-C effect. This shall be referred to as the constant display luminance (CDL) method.
2. Fixed retinal illuminance based on the use of a 3.9 mm artificial pupil size. This shall be referred to as the artificial pupil (AP) method.
3. Natural pupil with constant retinal illuminance without correction for the S-C effect. This shall be referred to as the constant retinal illuminance (CRI) method.
4. Natural pupil and constant 'effective' retinal illuminance, which incorporates S-C correction. This shall be referred to as the constant retinal illuminance with apodization (CRIA) method.

The independent variable in the first and second methods is screen luminance, although by measuring the pupil diameter at each luminance level, it is also possible to calculate changes in FCS with retinal illuminance. The third and fourth methods use a closed loop technique, which adjusts the luminance of the screen to account for changes in pupil size, with or without pupil apodization.

The CDL and CRI methods both used natural viewing conditions without apodization, however differences in pupil size, and therefore the size of the S-C effect, may prevent the data sets yielding identical results. The AP and CRIA methods both ensure that retinal illuminance and the S-C effect remain constant. By applying a S-C correction to the thresholds obtained using the AP method, it is expected that the

two data sets will yield identical results; any large differences would indicate inaccuracy of the CRIA method.

Comparing methods one (CDL) and three (CRI) with methods two (AP) and four (CRIA) may reveal how the S-C effect affects effective retinal illuminance and whether the closed-loop, natural pupil technique with real time apodization is equivalent to using an artificial pupil in keeping retinal illuminance constant.

7. 2. Experimental design

7. 2. 1. Participants

One 26-year old female (EP) and one 34-year old male (GB) participant took part in the study; both were experienced observers. Each participant undertook an ocular examination, which was conducted by an optometrist on-site. The examination involved ophthalmoscopy and refraction. Both participants were free of ocular disease, damage, surgery or intraocular lenses and did not experience any other health issues. Uncorrected visual acuity was 20/30 or better and correction was not used as the target size was well above threshold.

This study was approved by the Senate Research and Ethics Committee at City University London, and adhered to the principles of the Declaration of Helsinki. All participants provided written consent to take part in the study.

7. 2. 2. Functional contrast sensitivity measurements

Contrast thresholds were measured under monocular viewing conditions using

the FCS test, which has been described previously (Chisholm et al., 2003). The right eye was used throughout.

In order to establish how retinal sensitivity to contrast depends on retinal illuminance under the stimulus conditions employed in Chapter 6, contrast thresholds were measured over a range of four log units. The four measurement methods used were as follows:

1. Constant display luminance (CDL) method
2. Artificial pupil (AP) method
3. Constant retinal illuminance (CRI) method
4. Constant retinal illuminance with apodization (CRIA) method

The FCS program when used on the P_SCAN system allows continuous monitoring of pupil size, with or without S-C apodization, and the corresponding control of screen luminance needed to maintain the effective retinal illuminance constant during the test. This closed-loop system was used for methods three and four.

In addition, method four incorporated S-C correction, i.e. the display luminance was increased to compensate for the loss in ‘effective’ retinal illuminance do to directional sensitivity of the cones. The relationship between pupil size and the magnitude of the Stiles-Crawford effect has been described previously (Applegate & Lakshminarayanan, 1993). Luminous efficiency, based on pupil radius, r , is given by:

Eq. 7. 1.
$$f(r) = 10^{0.05r^2}$$

The shape of this ‘apodization’ function in relation to the pupil of the eye is

shown as an inset to Figure 7.4. Constant retinal illuminance can be achieved using an artificial pupil, or when viewing the display with the natural pupil (Barbur & Stockman, 2010), by adjusting the luminance of the screen to account for changes in pupil size.

7. 2. 2. 1. *Apparatus.* Neutral density filters were mounted between the observer and the display by slotting them within the hood at a 45° angle; display luminance was calibrated with the filters in place to account for this. For the AP method, a 3.9mm artificial pupil was positioned in front of the eye. The artificial pupil was mounted within a rubber socket so that the observers could rest their faces against it directly, minimising head movements.

7. 2. 2. 2. *Stimuli.* An observer's view of the stimuli is shown in Figure 7. 1. A Landolt C target of positive luminance contrast was employed. The target was presented either at the centre of the display or $\pm 5^\circ$ from fixation, along the horizontal meridian. Each run consisted of three randomly interleaved staircases: one for each target location. One run yielded three contrast threshold measurements.

For each of the four measurement methods, there were eight luminance conditions, chosen deliberately to include the photopic, mesopic and scotopic ranges. For the first and second methods, the luminance of the display was set at the start of each run and remained constant throughout. The luminance values were chosen at logarithmic intervals: 31.62, 10, 3.16, 1, 0.32, 0.1, 0.03, and 0.01 cd/m^2 . The maximum luminance value was based on the upper limit of display. Neutral density filters were used to achieve the full range of luminance values. Retinal illuminance at

each luminance condition was calculated following a pilot run using the CDL method. In order to increase the validity of comparisons between the four methods, retinal illuminance values for the third and fourth methods were chosen on the basis of being comparable to method one. The maximum illuminance was based on the upper limit of the display and all values were at regular intervals: 3, 2.5, 2, 1.5, 1, 0.5, 0, and -0.5 log Td.

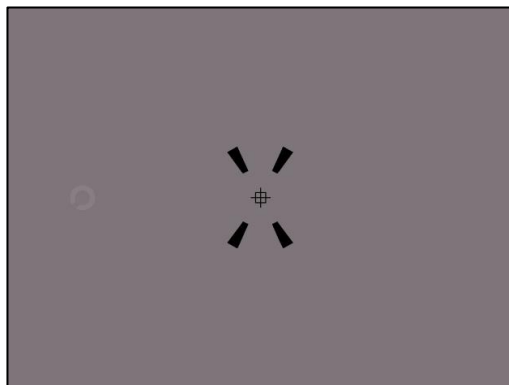


Figure 7.1. Observers' view of the experimental setup. The functional contrast sensitivity test was carried out on a CRT monitor. The Landolt C target was presented at three locations: at fixation and $\pm 5^\circ$. The three locations were interleaved randomly and the observer's task was to report the orientation of the gap. The gap size was set at 4' for foveal targets and 8' for peripheral targets.

Pupil size was measured continuously and used to calculate retinal illuminance.

A supra-threshold target gap size of 4' was chosen at the foveal location to ensure that small fluctuations of accommodation and differences in higher order ocular aberrations that can cause large inter-observer differences when assessing the limit of spatial resolution would not confound significantly the results of this study. Peripheral targets were scaled in size to maintain similar contrast visibility across the three target locations. The scaling factor was determined using threshold measurements for four young participants at a display luminance of 26 cd/m². Target gap size was set at 4' for central targets and 8' for peripheral targets.

7. 2. 2. 3. *Procedure.* During the FCS test, observers were given a minimum of three minutes to dark-adapt, with up to fifteen minutes in the lower lighting conditions. Observer EP completed two full runs of the FCS test; the main purpose of this was to assess intra-observer variability. As variability was found to be low, the second participant (GB) completed only one full run. The typical duration of a single test was 12 mins.

7. 2. 3. *Predictions of functional contrast thresholds in the presence of glare*

The model discussed in Chapter 6 was modified, using mean data from participant A, so as to account for the S-C effect in estimations of functional contrast sensitivity in the presence of glare.

In order to validate the closed-loop technique that allows free viewing of the display, contrast thresholds measured with the CRIA method were compared to thresholds measured using a fixed, artificial pupil of 3.9 mm diameter. In the AP method, S-C apodization was applied to the thresholds after testing; in the CRIA method, correction was applied in real time to the stimuli presented during the test. The two measures were expected to yield similar results, which would enable a function to be fitted to the combined data.

The presence or absence of the glare source causes a change in pupil size and ‘effective’ retinal illuminance through apodization. The equations derived to describe the retinal sensitivity to contrast as a function of effective retinal illuminance were used to compute the expected improvement in threshold as a result of changes in the retinal sensitivity to contrast. It was not practically possible to measure contrast thresholds over the full range of retinal illuminance levels in every subject

investigated in Chapter 6. Although, retinal sensitivity to contrast will undoubtedly exhibit some inter-subject variability, the region of interest, which involves the rapid increase in contrast thresholds in the mesopic range, is likely to remain largely unchanged. Nevertheless, this assumption may limit somewhat the accuracy of the predicted thresholds.

7. 3. Results

7. 3. 1. Absolute functional contrast thresholds

The results show an asymptotic decrease in thresholds with increasing retinal illuminance. Across conditions, foveal thresholds were higher than peripheral thresholds at the lowest light level and lower than peripheral thresholds at the highest light level (Table 1.); this was to be expected given the differing functionality of the rods and cones under scotopic and photopic conditions.

FCS thresholds are shown in Fig 7.2. A comparison of the four measurement methods shows that the pattern of results is similar. Using the CRIA method resulted in thresholds that were slightly lower than in the other three methods, which was to be expected given that this method compensated for the S-C effect by increasing the illuminance on the retina. However, the differences were small, as shown by the error bars in Fig 7.2.

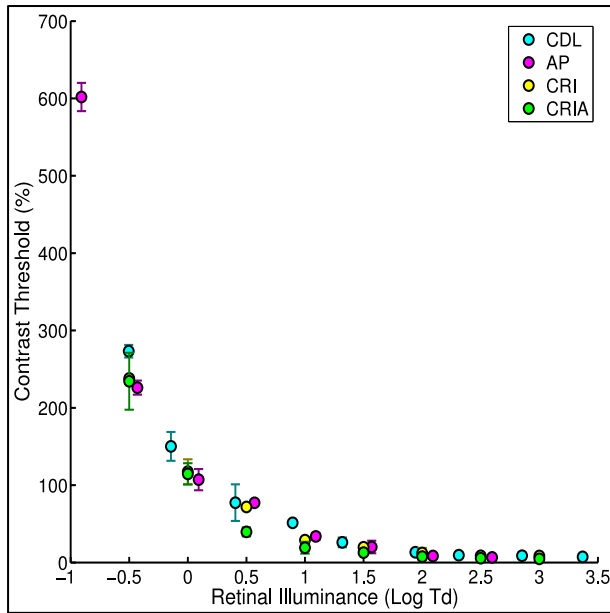


Figure 7.2. Mean foveal FCS thresholds for each of the four conditions, based on two measurements from observer EP. The error bars represent ± 2 standard deviations of the mean.

In the CDL and AP methods, screen luminance remained constant throughout the test. In the CRI and CRIA methods, pupil size measurements were used to adjust the screen luminance in order to maintain constant retinal illuminance.

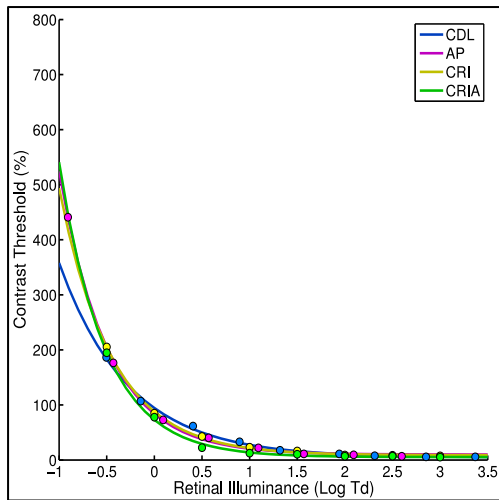
Pupil diameter was measured with each target presentation and the mean diameter was recorded. Natural pupil diameter did not fall below the 3.9 mm aperture used for the artificial pupil in the AP method, as shown by the minimum values in Table 7.1.

Table 7.1. Maximum and minimum pupil diameters and FCS thresholds for both observers.

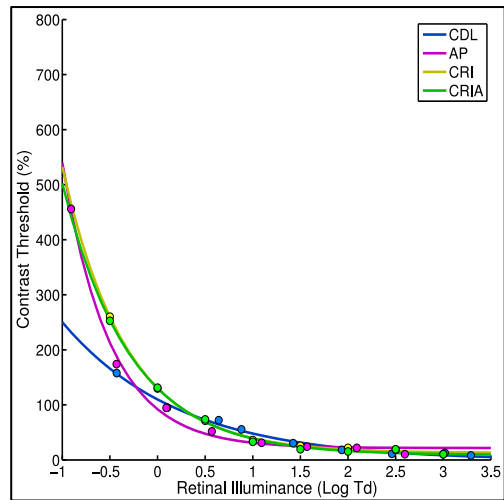
		Observer A	Observer B
Max natural pupil diameter (mm)		6.31	8.09
Min natural pupil diameter (mm)		4.48	5.57
	-5°	440.98	455.85
Max FCS threshold (%)	0°	601.83	693.36
	+5°	460.12	513.26
	-5°	6.76	10.44
Min FCS threshold (%)	0°	6.57	8.08
	+5°	11.97	20.22

As the pattern of results was similar for both observers (as shown in Fig 7.3), the mean data from the two runs completed by observer EP were used in the following analyses.

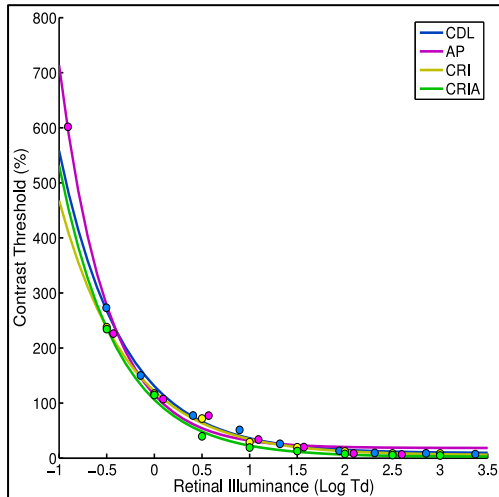
(A) Observer EP: -5° from fovea



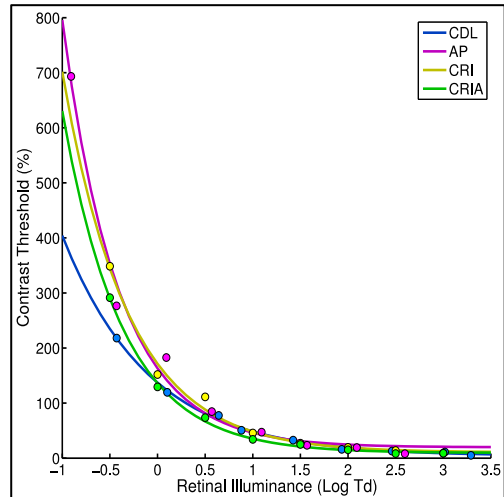
(D) Observer GB: -5° from fovea



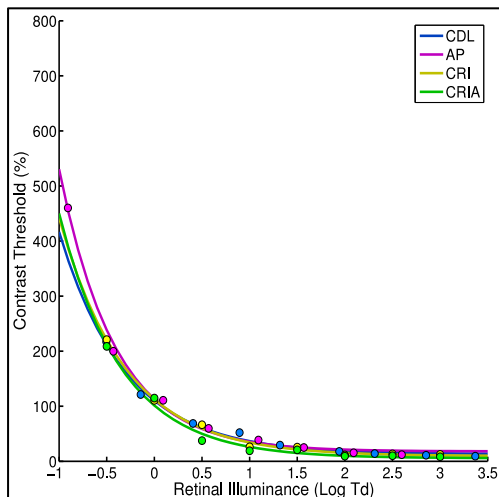
(B) Observer EP: 0° from fovea



(E) Observer GB: 0° from fovea



(C) Observer EP: +5° from fovea



(C) Observer GB: +5° from fovea

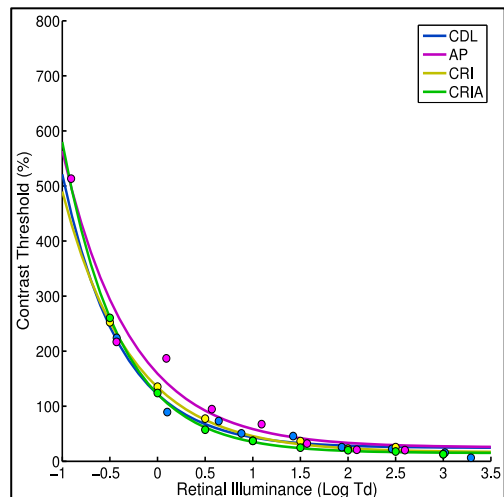


Figure 7.3. FCS thresholds as a function of retinal illuminance measured for a Landolt ring stimulus, measured at the fovea and at $\pm 5^\circ$ in the periphery. The graph shows thresholds measured using four different methods: The CDL method uses constant display luminance with no correction for either pupil size changes or the S-C effect. The AP method uses a 3.9 mm artificial pupil in order to maintain constant retinal illuminance. The CRI method uses a dynamic feedback loop to maintain constant retinal illuminance without the S-C effect whereas the CRIA method incorporates the Applegate apodization.

7. 3. 2. Modelling contrast sensitivity with the Stiles-Crawford effect

The AP method did not allow fluctuations in pupil size, thereby keeping the size of the S-C effect constant throughout the test. Applying the S-C apodization to the measured thresholds was expected to yield data equivalent to the CRIA method. The two data sets were in good agreement, which confirms that the closed loop technique designed to maintain constant, retinal illuminance with an apodized pupil is equivalent to what can be achieved using a fixed size, artificial pupil (Fig 7. 4). A function was fitted to the combined data, which are best described using an equation of the form:

$$\text{Eq. 7. 2.} \quad C_e = b_1 \times \text{exponent}(-b_2 \times \log(E)) + b_3$$

Where:

C_e is the expected contrast threshold at a given retinal illuminance, E .

E is the ‘effective’ retinal illuminance at the point of interest on the retina (Trolands).

b_1 , b_2 and b_3 are constants. The model was applied to measured data, both at the fovea and at 5° in the periphery, yielding different constants for the two retinal locations.

The foveal constants were $b_1 = 79.66$, $b_2 = 1.97$ and $b_3 = 18.37$; peripheral constants were $b_1 = 70.39$, $b_2 = 1.81$ and $b_3 = 14.17$.

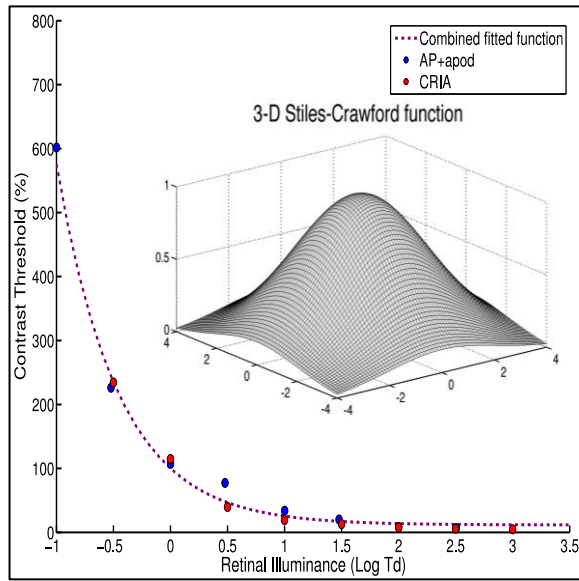


Figure 7.4. FCS thresholds as a function of retinal illuminance measured for a Landolt ring stimulus, measured at the fovea. The graph shows thresholds measured using a 3.9 mm fixed pupil diameter as well as using a dynamic feedback loop with the Applegate apodization applied to the data. The dotted line represents the function fitted to the combined data sets: $C_e = b_1 \times \text{exponent}(-b_2 \times \log(E)) + b_3$. The inset diagram shows the relationship between distance from the pupil and the effective light signal due to the S-C effect.

The difference between thresholds obtained using an artificial pupil with and without S-C correction is shown in Fig. 7.5.

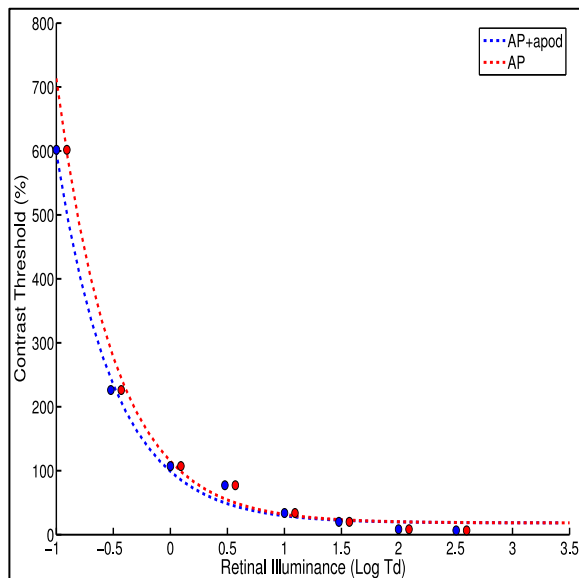


Figure 7.5. Functional contrast sensitivity thresholds as a function of retinal illuminance measured for a Landolt ring stimulus, measured at the fovea. The graph shows thresholds measured using a 3.9 mm fixed pupil diameter with and without the Applegate apodization applied to the data (post-hoc). The dotted line represents the function fitted to the combined data sets: $C_e = b_1 \times \text{exponent}(-b_2 \times \log(E)) + b_3$.

7. 3. 3. Disability glare –predictions of functional contrast thresholds

Predictions of FCS thresholds discussed in Chapter 6 were repeated using the

new S-C-corrected data, yielding new predictions of contrast thresholds, which take into account both retinal sensitivity and the S-C effect. RMS errors were used to assess the accuracy of each of the three predictions (Table 7.2). As the accuracy did not differ at low glare intensity or at photopic background luminance, RMS errors were recalculated at mesopic background luminance and in the presence of high intensity glare. As in chapter 6, the new predictions were more accurate than scatter (only)-based predictions; at 2.6 cd/m^2 background luminance, RMS errors associated with scatter-based predictions were 27.56, as opposed to local and global combined predictions, 23.60 and 23.66 respectively. The difference in accuracy was even larger at 1 cd/m^2 background luminance, as scatter-based predictions yielded an RMS error of 109.08 as opposed to 68.09 and 69.69 for local and global combined predictions, respectively. However, a comparison between RMS errors associated with the newest model and that in chapter 6 shows that the S-C apodization does not improve prediction accuracy.

Table 7.2. Root mean square error as a measure of the discrepancy between observed and predicted thresholds for each of the three models.

	Low Glare			High Glare		
Pupil-plane illuminance	1.35 lm/m ²			19.21 lm/m ²		
Eccentricity	5°	10°	15°	5°	10°	15°
Screen luminance	RMS error associated with scatter-based model predictions					
1 cd/m ²	15.97	19.56	9.41	213.30	90.15	23.80
2.6 cd/m ²	8.44	12.64	6.30	41.33	28.18	13.16
26 cd/m ²	3.32	3.32	3.12	11.42	5.84	4.45
	RMS error associated with 'local' combined model predictions					
1 cd/m ²	15.40	17.65	10.12	118.21	62.93	23.12
2.6 cd/m ²	7.73	12.79	6.39	30.08	25.79	12.93
26 cd/m ²	3.25	3.05	3.09	11.95	5.85	4.62
	RMS error associated with 'global' combined model predictions					
1 cd/m ²	16.38	17.44	8.56	134.21	55.47	19.38
2.6 cd/m ²	7.80	12.79	6.16	33.49	24.44	13.05
26 cd/m ²	3.26	3.05	3.09	11.95	5.84	4.62

Although the differences between the RMS errors shown here and those from Ch. 6 are small, there was a slight reduction in prediction accuracy in some conditions. Errors were, again, highest in the presence of high intensity glare, 19.21 lm/m², at the lowest background luminance level, 1 cd/m². In order to establish

whether there were any notable effects of apodization under this condition, a comparison of (A) the model from chapter 6, (B) the new model, which uses the combined fitted function from the AP method with the apodization applied post-hoc and CRIA methods (as shown in Fig. 7. 4.) is shown in Figure 7. 6. To determine whether the small differences in accuracy between the two models is owing to differences in the age of observers or to the S-C correction, a further comparison is made between (C) a model that uses the AP method only (as shown by the red line in Fig 7. 5.), and (D) a model that uses the AP method with the apodization applied post-hoc (as shown by the blue line in Fig 7. 5.) As the S-C effect is most relevant at the fovea, and because of the similarity between local and global predictions, only foveal local data have been plotted. The plots reveal only very small differences between the four methods used to calculate changes in retinal illuminance in the presence of glare. The comparison between (A) and (C) can be used to reveal differences accountable to the age of the observer upon which the retinal sensitivity curve is based; differences are small but (A) shows slightly less bias, suggesting that data based on the 50-year old observer is more representative. The comparison between (C) and (D) can be used to reveal differences accountable to the S-C correction; again, differences are very small but (D) shows slightly less bias, indicating that the S-C correction leads to a slight increase in accuracy.

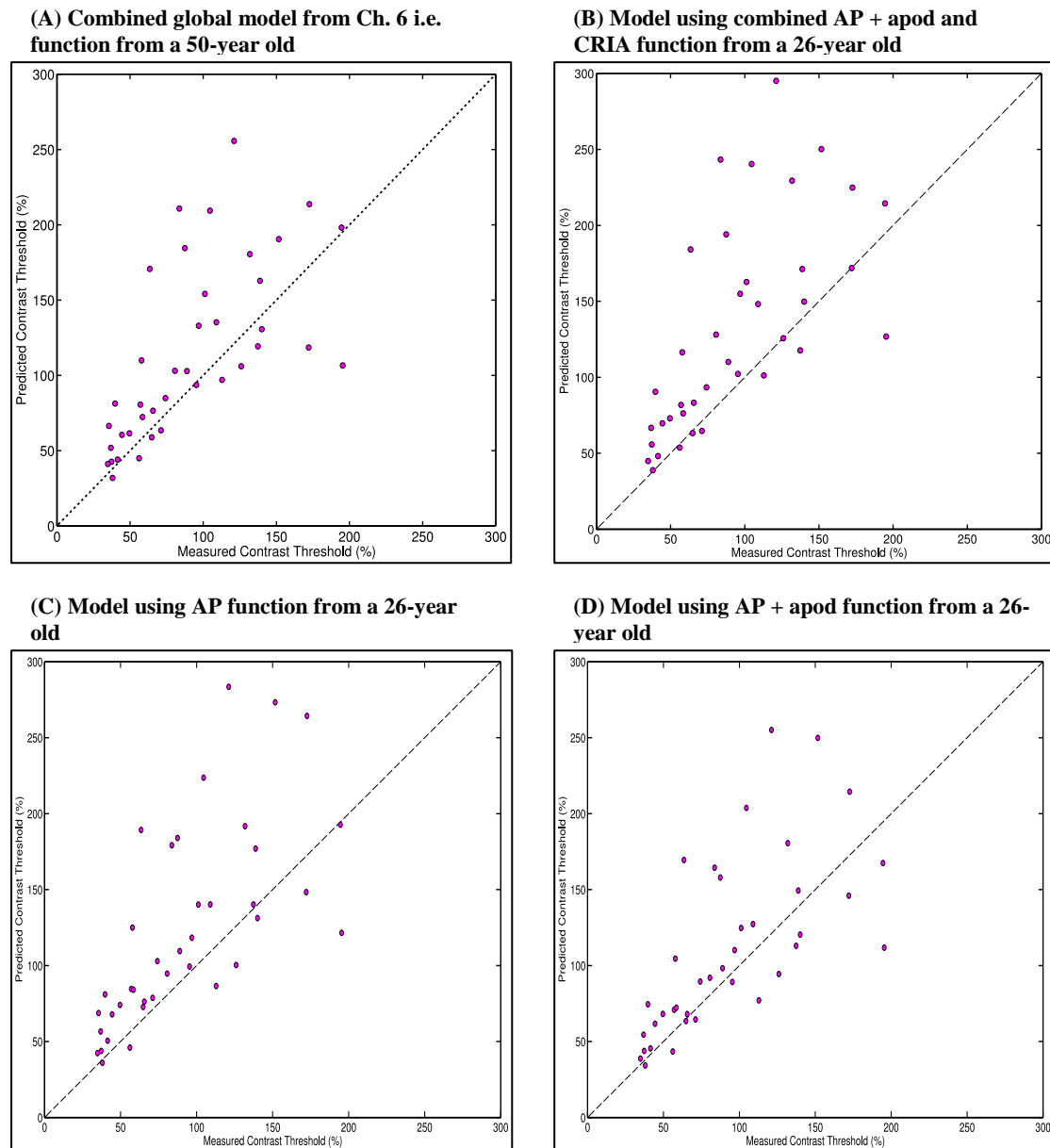


Figure 7.6. Comparison between (A) the global model predictions used in Chapter 6, (B) the new model predictions, which take into account the S-C effect. A further comparison is made between (C) non-apodized and (D) apodized data using a fixed artificial pupil size. The plots show the relationship between measured foveal thresholds and model predictions at 1 cd/m^2 screen luminance and in the presence of high glare (19.21 lm/m^2). Each data point represents the threshold for one participant at the foveal location, i.e. 10° from the glare source. The $x = y$ line illustrates 100% accuracy of predictions; data points that fall above this line indicate an over-estimation of the contrast threshold in the presence of glare, i.e. better performance than expected.

7. 4. Discussion

The aim of this investigation was to determine the extent to which directional sensitivity of the photoreceptors affects measured thresholds of FCS. In addition, a model that incorporates the Applegate apodization was applied to data collected in chapter 6 to predict the effects of disability glare on FCS thresholds, while taking the S-C effect into account. Although the S-C effect has been discussed in relation to retinal sensitivity, there have not been any attempts to compare directly its effect on measurements of sensitivity to contrast.

Four measurement methods were used to measure FCS thresholds at different retinal illuminance values ranging through scotopic, mesopic and photopic light levels. The CDL and CRI methods were expected to yield equivalent results; this was indeed the case. After the apodization was applied to the AP method, this method yielded equivalent results to the CRIA method, although the small aperture created by the artificial pupil naturally resulted in a shift in the range of retinal illuminance levels. The results of this comparison confirm that the closed loop technique designed to maintain constant, retinal illuminance with an apodized pupil is equivalent to what can be achieved using a fixed size, artificial pupil. The difference in thresholds afforded by the S-C correction was small, and was only distinguishable from the non-corrected data at 1 log Td retinal illuminance, which is in the mesopic range. The lack of any noteworthy effect is owing most likely to the fact that contrast on the retina is unaffected by changes in illuminance. Although retinal sensitivity responds to changes in light level, it is unlikely that changes in effective retinal illuminance as a direct result of the S-C effect would be large enough to elicit a noticeable change in sensitivity. Given these findings, the S-C effect does not appear to be a crucial

consideration in the measurement of sensitivity to contrast when dealing with normal observers. The S-C effect may, however, be more pertinent when using other measurement methods, such as in increment detection and resolution (Westheimer, 2008).

It was found that the new model, which takes into account scattered light, changes in retinal sensitivity with light level, and the S-C effect, was no more accurate in predicting the effects of glare on sensitivity to contrast than the model in chapter 6. The most likely explanation for the lack of an increase in accuracy concerns the age of the observer upon which the model was based. The mean age of the sample of forty observers was 42; the model discussed in chapter 6 was based on data (collected previously (Connolly & Barbur, 2009) from one 50-year old, whereas the current model was based on one 26-year old observer. Although the curves obtained using data from these two observers as well as the additional 34-year old were similar in appearance, the asymptotic nature of the curve lends itself to higher sensitivity to slight differences in the slope and intercept in the mesopic range. A comparison showed that predictions based on the 50-year old observer's retinal sensitivity curve were slightly more accurate than those of the 26-year old observer (both without apodization).

Given that the S-C effect becomes weaker with increasing eccentricity, and thereby decreasing cone density, from the fovea, it might be expected that the apodized threshold predictions would be less accurate at peripheral target locations but more accurate at the fovea. Directional sensitivity has the effect of reducing effective retinal illuminance; due to the asymptotic relationship between retinal illuminance and contrast sensitivity, a reduction in retinal illuminance would

correspond to a greater shift in the 'baseline' contrast used for predictions and would therefore be less likely to overestimate the degradation caused by glare. The comparison between predictions made using non-apodized and apodized data from the 26-year old observer (with a fixed artificial pupil size) did indeed show a slight reduction in bias, i.e. fewer data points fell above the $x = y$ line, although the effect was very small.

Taken together, the comparisons between the current model and that developed in Ch. 6 suggest that any slight reduction in accuracy is most likely to be caused by the assumption that the retinal sensitivity of one 26-year old observer is generalisable to a wider age range. The most accurate predictions would require that an individual's own retinal sensitivity curve was used to calculate changes in illuminance and contrast on the retina with the addition of glare; this would, however, involve many hours of testing for each participant and was not feasible in the current study.

Although the S-C correction did not affect significantly either the FCS thresholds themselves or the predictions of visual performance in the presence of glare, it is worth bearing in mind that the observers in question all had normal vision. It is possible that the S-C effect could have a larger impact on contrast thresholds for those with increased scattered light within the eye, when the discrepancy between actual and effective illuminance on the retina is larger. The situation is further complicated by the fact that some conditions associated with scattered light, such as retinitis pigmentosa, are also associated with reduced directional sensitivity (Birch, Sandberg, & Berson, 1982). Indeed, measurement of the waveguiding properties of photoreceptors can provide a good indication of retinal health (Carroll, Dubis,

Godara, Dubra, & Stepien, 2011; DeLint, Berendschot, T. T. J. M., & van Norren, 1998; Vohnsen, 2007).

Although the S-C effect undeniably has significant advantages as a tool for detecting retinal abnormalities in a clinical context, the results from this study indicate that the S-C effect is unlikely to affect significantly estimations of sensitivity to contrast in normal observers. The combined evidence from this study and the previous chapter shows that retinal sensitivity to contrast is a critical factor and that the S-C effect is relatively unimportant when predicting changes in sensitivity to contrast.

Chapter 8. Discussion and conclusions

8. 1. Summary of the results

The experiments carried out in Ch. 4 – 7 explored the effects of scattered light on different aspects of visual performance. Ch. 4 investigated the angular dependence of scattered light within the eye and addressed the question of whether its measurement is necessary. It was found that changes in angular distribution (parameter n) did not affect significantly the overall measured amount of scattered light within the eye (parameter k), although there was a correlation in the size of the errors associated with the two parameters. In Ch. 5, increased light scatter was produced in young observers using ‘fogging’ filters designed for photographic applications. The effects of increasing the amount of scattered light on visual acuity, contrast sensitivity and chromatic sensitivity were investigated as well as the impact light scatter may have on binocular summation. Increased light scatter caused little change in visual acuity and chromatic sensitivity, but led to significant losses in sensitivity to contrast. It was found that there was a significant benefit of binocular summation on contrast sensitivity, even when the image in one eye is degraded by adding scattered light.

Ch. 6 focused on how retinal sensitivity to contrast varies with light level in the presence of a bright light source. Visual performance was most affected at low light levels and in the presence of high intensity glare, although the detriment was less than predicted using predictions of contrast loss based on scattered light. By taking into account changes in retinal sensitivity that occur in the presence of glare, predictions of contrast thresholds were vastly improved, particularly at low light levels.

In Ch. 7, the impact of the Stiles-Crawford (S-C) effect (Stiles & Crawford, 1933) on sensitivity to contrast was investigated. The results show that the relationship between contrast thresholds and retinal illuminance can change significantly when the latter is calculated with and without pupil apodization, particularly when large differences in pupil size are involved. The experiments carried out also demonstrate that a closed-loop system designed to keep retinal illuminance constant with a natural pupil can be achieved by measuring the pupil of the eye continuously, by applying pupil apodization and by adjusting the luminance of the screen to cancel the effects of pupil size changes.

8. 2. Discussion of overall results

The aim of chapter Ch. 4 was to determine how fluctuations in the scatter index, n , affect the scatter parameter, k . Scattered light within the eye is measured using a flicker-cancellation technique and the empirical light scatter equation, $L_s = E k \theta_e^{-n}$, is used to determine its amount and angular distribution, which is proportional to k and n , respectively. The scatter parameter, k , and scatter index, n , are co-dependent, therefore fluctuations in the angular dependence will affect the calculation of the overall amount of light scatter. n is often assumed to have a value of 2 (van den Berg & Ijspeert, 1992; van den Berg, 1986) and, based on this assumption, k can be measured using a single annulus; it is, however, unclear whether measurements of overall light scatter obtained using this method are accurate. Measured values of n differed significantly from the value of 2, which is used for clinical measures of intraocular light scatter (Franssen et al., 2006; van den Berg & Spekreijse, 1987; van den Berg & Ijspeert, 1991). Despite this, comparisons between values of k and the integrated parameter, k' , obtained using measured values of n and under the

assumption that $n = 2$ revealed differences between the two data sets; these were, however, not statistically significant. On the other hand, there was a significant correlation between the deviation in n from the value of two and the error in the measured value of both k and k' calculated under the same assumption. It is therefore likely that the large variability in k values leads to the failure to find a significant difference between the two sets of k and k' values. The large variability was not surprising given the small size of the sample and large range of ages.

As expected, increased scattered light had little effect on visual acuity but a large effect on contrast sensitivity (van den Berg et al., 2013; Vos & van den Berg, 1999). In the presence of glare, there is an increase in the amount of light that is scattered within the eye and it was of interest to determine whether performance can be estimated under such conditions. Previous literature has found that estimations of contrast sensitivity based on the contrast losses due to scattered light hold reasonable accuracy (Paulsson & Sjöstrand, 1980; Whitaker, Elliott, & Steen, 1994); in agreement, the experiment carried out in Ch. 6 found good prediction accuracy at photopic levels. At mesopic levels, however, prediction accuracy was poor. Past authors have suggested that there may be a threshold to the disability glare effect (Fisher & Christie, 1965) or that the inaccuracy may be caused by higher surround field luminance (de Waard et al., 1992) or the adaptation state of the retina (van den Berg, 1991). Although the impact of mean luminance on retinal sensitivity has been studied extensively (Barbur & Stockman, 2010; Rovamo, Mustonen, & Näsänen, 1995; van Nes & Bouman, 1967), there has not yet been a quantitative account of the effect under glare conditions. The incorporation of changes in retinal sensitivity in the presence of glare succeeded in providing a more accurate estimation of visual performance. Prediction accuracy at photopic levels was similar, but at mesopic levels

was vastly improved, supporting previous qualitative explanations (van den Berg, 1991). Although it has been suggested that psychophysical measures of scattered light may be underestimated as a result of the S-C effect (Boynton et al., 1954), the equivalent veiling luminance technique (Le Grand, 1937) already takes such factors into account. As expected, the S-C effect was shown to have little impact on the accuracy of contrast thresholds, but can affect the relationship between contrast thresholds and retinal illuminance in the mesopic range when the pupil size is large (Ch. 7).

8. 3. Implications for underlying mechanisms

The findings from Ch. 4 and 6 revealed that the angular distribution of scattered light within the eye varies between observers and that the measured scatter index, n , can deviate significantly from the value of 2. Larger values of n correspond to a narrower spread of scattered light and lead to smaller estimations of k for a given amount of light scatter within the eye. Although previous literature has found little effect of age on the angular distribution of scattered light (Fisher & Christie, 1965), higher values of n , and thereby smaller scattering angles, were associated with older observers in Ch. 4. The same effect was shown in Ch. 6 but did not reach statistical significance. There are two main explanations for an increase in narrow-angle scatter with age.

Given our knowledge of the physical behaviour of light as it is scattered, it may be assumed that the increase in light scatter in older observers is caused by macromolecules that are larger than the wavelength of light (Coppens et al., 2006; Hemenger, 1988; Hemenger, 1992; Mainster & Turner, 2012; van den Berg &

Ijspeert, 1995; Whitaker et al., 1993; Wooten & Geri, 1987). This is supported by research conducted both in vivo (Costello et al., 2007; Spector et al., 1974; Thaung & Sjöstrand, 2002; van den Berg & Ijspeert, 1995; Wooten & Geri, 1987) and in vitro (Thaung & Sjöstrand, 2002; van den Berg & Ijspeert, 1995), which suggests that particles or cellular structures larger than the wavelength of light are responsible for the majority of intraocular scatter.

The use of young observers and fogging filters enabled us to isolate increases in scatter from other changes that occur with ageing. It may be that the small changes in angular distribution of scattered light with age are caused predominantly by age-related changes other than increased number and size of scattering particles within the lens.

It is well known that, as we age, the lens absorbs more short-wave light causing the lens to become progressively more yellow (Mellerio, 1971; Weale, 1963). It has been suggested that this phenomenon is due to increased path-length within the nucleus (Mellerio, 1971) and an increase in fluorogens, which results in increased spectral absorption and fluorescence (Bron, Vrensen, Koretz, Maraini, & Harding, 2000). Due to the wavelength dependency of scattered light, short-wave (i.e. blue) light scatters at a wider angle than long-wave (i.e. red) light; it would therefore be expected that, proportionally, a narrower scatter distribution would be observed in those whose lenses absorb more short-wave light.

Certainly the effects of lens-yellowing and changes in iris pigmentation (Coppens et al., 2006; Franssen et al., 2007; van den Berg et al., 1991) are much more likely to exhibit an effect on the wavelength of light reaching the retina than the process of light scattering.

Having gained an improved understanding of the physical behaviour of scattered light in the eye in Ch.s 4 and 5, the aim of the experiments in Ch.s 6 and 7 was to elucidate the mechanisms involved at the level of the retina. It was shown that visual performance was better than would be predicted based solely on contrast losses due to increased light scatter; this indicates that there are processes that take place at the level of the retina (or beyond) that are able to compensate at least partially for the detriment. It is well known that retinal sensitivity to contrast increases exponentially with increasing ambient lighting (Barbur & Stockman, 2010; Blackwell, 1946; Stockman & Sharpe, 2006; Stockman et al., 2006) and it has been shown previously that loss in sensitivity to contrast is greater at low light levels because the rods require larger contrast differences than cones (Pokorny & Smith, 2006). However, a model that takes this into account when calculating the effects of scattered light in the presence of glare has not yet been put forward. In Ch. 6 it was shown that by using a new model that incorporates concurrent changes in retinal sensitivity the estimations of visual performance under mesopic conditions were significantly improved. As expected, the scatter-based approach and the new combined predictions did not differ significantly under photopic conditions, as improvements in retinal sensitivity were expected to be minimal. Only when the ambient lighting was within the mesopic range, and the addition of light from the glare source brought the retinal illuminance up to photopic levels, were the predictions improved noticeably.

In Ch. 6, an attempt was made to determine whether the adaptation state of the retina was more accurately predicted by 'local' or 'global' changes in retinal illuminance. The results were, however, inconclusive as each of the methods yielded different levels of accuracy at different focal eccentricities. At the lowest background luminance, local predictions had a higher level of accuracy than either scatter-based

or global predictions at the smallest glare-source eccentricity, whereas global predictions prevailed at the other two eccentricities. The difference afforded by using global rather than local predictions was to reduce the retinal illuminance value at the location of the target closest to the glare source but increase retinal illuminance at the other two target locations. An increase in the estimation of retinal illuminance (in the presence of glare) leads to a reduction in the baseline threshold used to calculate performance in the presence of glare, which in turn results in a decrease in the predicted threshold. In other words, the best prediction in each case is the one in which the improvement in retinal sensitivity is assumed to be greatest. It is, as yet, unclear what implications this finding has on the mechanisms involved in retinal adaptation; one possibility is that the visual system possesses a further protective element, such as that which is responsible for observed contrast constancy for gratings of different spatial frequencies (Barlow & Mollon, 1982; Georgeson & Sullivan, 1975).

The differences afforded by incorporating the S-C effect in Ch. 7 were small. Although the expected 'effective' illuminance on the retina was lowered, the effect on the target and background would be identical; differences in effective image contrast would therefore be negligible. On the other hand, the adaptation state of the retina may undergo small changes; the direction of these changes would depend on differences in pupil size in the presence and absence of glare. The difference made by incorporating the S-C effect will be larger at lower light levels but the pupil size is likely to constrict, which would reduce the effectiveness of apodization. In any case, the findings presented here indicate that the impact of the S-C effect on forward scattered light is minimal.

8. 4. Implications for road lighting practice

In Ch. 6, it was demonstrated that changes in retinal sensitivity caused by glare under mesopic illumination lead to a deviation in contrast sensitivity from what would be predicted using estimations of scattered light alone. This finding has important implications for the lighting industry, and for road lighting in particular. Light from isolated sources, such as streetlights and car headlights, will have maximum impact on the adaptation state of the retina when the background luminance is low. Although the primary aim of road lighting is to illuminate directly the road and the immediately surrounding area, the current findings suggest that a secondary aim might be to increase the adaptation state of the retina.

As older drivers and those with increased intraocular scattered light frequently complain of visual difficulties while night-driving, any measure that could improve visibility would benefit not only the individuals concerned but would also improve safety for all other road users. The current work indicates that light within the visual field — even light that does not illuminate directly the scene — may help by increasing the adaptation state of the retina, thereby improving sensitivity to contrast. It is therefore possible that a measure as simple as leaving the internal dome light on while driving could help to elevate retinal adaptation.

Further research, perhaps using driving simulators, would be needed to establish the ideal luminance of the light used for adaptation under different lighting conditions and to determine the efficacy of such a technique.

8. 5. Implications for methodology and future directions

The deviation in measured n values from 2 was, in general, larger for older participants, which suggests that the measurement of angular distribution is more pertinent for those who are older than fifty years. By extension, it would be beneficial to measure angular dependence in all cases in which scatter levels are elevated, for example, cases of ocular damage or disease. Although the assumption that $n = 2$ for young normal observers is reasonable, the current findings would suggest that methods using this assumption may not be appropriate for clinical assessment of those with ocular abnormalities.

The other exploratory experiments carried out in Ch. 5 indicate that the effects of scattered light on visual acuity and chromatic sensitivity are small unless scatter levels are extremely high; contrast sensitivity, however, is impacted more by increases in scattered light, particularly at high spatial frequencies.

The findings in Ch. 7 showed that correction for the S-C effect has little impact on sensitivity to contrast and is not beneficial when incorporated into predictions of performance in the presence of glare. The accuracy of the predictions with and without apodization was almost identical when using data based on a fixed pupil size. One drawback of the retinal sensitivity curve in Ch. 7 is that the data are based on one 26-year old observer and may therefore not be generalisable to the whole sample of 40 observers. On the other hand, differences in accuracy between the predictions using the curve based on a 50-year old and a 26-year old were negligible. Given this finding, future research may benefit from using different contrast sensitivity curves based on the age of the population being studied.

In conclusion, Ch.s 6 and 7 show that retinal sensitivity to contrast is a crucial factor in the assessment of visual performance in the presence of glare and, as such, should be incorporated into future research in this area. Although the effects of retinal illuminance are not as large at high lighting levels, and are therefore less relevant when studying visual performance under photopic conditions, many situations that involve glare occur at low lighting levels (Mainster & Timberlake, 2003). Night-time drivers must often contend with bright lights in the field of view, either from street lights or approaching car headlights; it is therefore important for designers and manufacturers to have a good understanding of the visual system under mesopic conditions. It would therefore be beneficial for the lighting industry and the scientific community if research that focuses on visual performance at low light levels were to take into account the expected changes in retinal sensitivity as a result of scattered light.

8. 6. *Synopsis*

The aim of this thesis was to elucidate the effects of scattered light on various aspects of visual performance, particularly in relation to disability glare. Overall, the findings have shown that, with regard to young normal observers, there is little difference in the angular distribution and wavelength dependence of scattered light between observers. Increases in the amount of scattered light within the eye lead to only small decreases in visual acuity and chromatic sensitivity but large decreases in contrast sensitivity.

In the presence of glare, the amount of light that is scattered over the retina increases and observers require higher contrast in order to detect objects. The detriment to visual performance under low ambient lighting conditions and in the presence of glare is not, however, as large as would be expected based on the decreased image contrast on the retina due to scattered light. Concurrent increases in retinal sensitivity were shown to offset partially the negative effects of reduced contrast; this is thought to be due to changes in the adaptation state of the retina, i.e. from dark-adapted to light-adapted. Although changes in the magnitude of the S-C effect with varying pupil size could lead to changes in ‘effective’ retinal illuminance, the impact on measured contrast thresholds, and the estimation of visual performance in the presence of glare, was negligible.

By accounting for changes in retinal sensitivity in the presence of glare, predictions of visual performance can be improved significantly, particularly at low levels of ambient illumination.

References

- Aguirre, R. C., Colombo, E. M., & Barraza, J. F. (2011). Effect of glare on reaction time for peripheral vision at mesopic adaptation. *Journal of the Optical Society of America A*, *28*, 2187-2191.
- Alcon. (2014). *Myeyes.com*. <http://www.myeyes.com/cataracts/all-about-cataracts.shtml>
- Alexander, K. R., Fishman, G. A., & Derlacki, D. J. (1996). Intraocular light scatter in patients with retinitis pigmentosa. *Vision Research*, *36*, 3703-3709.
- Alexandridis, E., Leendertz, J. A., & Barbur, J. L. (1992.). Methods of studying the behaviour of the pupil. *Journal of Psychophysiology*, *5*, 223-239.
- American Academy of Ophthalmology. (2014). *Normal Fundus*.
<http://www.aao.org/theeyeshaveit/anatomy/normal-fundus.cfm>
- Applegate, R. A., & Lakshminarayanan, V. (1993). Parametric representation of stiles-crawford functions: Normal variation of peak location and directionality. *Journal of the Optical Society of America A*, *10*, 1611-1623.
- Augusteyn, R. C. (2010). On the growth and internal structure of the human lens. *Experimental Eye Research*, *90*, 643-654.
- Barbur, J. L., Edgar, D. F., & Woodward, E. G. (1995). Measurement of the scattering characteristics of the eye in relation to pupil size. *Non-invasive assessment of the visual system (technical digest series)*, (pp. 250-253). Washington D.C.: Optical Society of America.
- Barbur, J. L., Rodriguez-Carmona, M., & Harlow, A. (2006). Establishing the statistical limits of “normal” chromatic sensitivity. *CIE Proceedings 75 Years of the Standard Colorimetric Observer*. CIE Expert Symposium.

- Barbur, J. L., Chisholm, C. M., & Harlow, A. J. (1999). Effects of increased scattered light on visual performance. *Non-Invasive Assessment of the Visual System (Technical Digest Series)*, (p. 6-9). Washington D.C.: Optical Society of America.
- Barbur, J. L., de Cunha, D., Harlow, A., & Woodward, E. G. (1993). Methods for the measurement and analysis of light scattered in the human eye. *Non-Invasive Assessment of the Visual System (Technical Digest Series)*, (pp. 170-173). Washington D.C.: Optical Society of America.
- Barbur, J. L., Edgar, D. F., & Woodward, E. G. (2010). Measurement of the scattering characteristics of the eye in relation to pupil size. *Journal for Optical Society of America, 1*, 250-253.
- Barbur, J. L., Harlow, J. A., & Plant, G. T. (1994). Insights into the different exploits of colour in the visual cortex. *Proceedings of the Royal Society London B*, 258, 327-334.
- Barbur, J. L., & Ruddock, K. (1980). Spatial characteristics of movement detection mechanisms in human vision. *Biological Cybernetics*, 37, 77-92.
- Barbur, J. L., & Stockman, A. (2010). Photopic, mesopic and scotopic vision and changes in visual performance. In D. A. Dartt (Ed.), *Encyclopedia of the eye, vol 3* (pp. 323-331). Oxford: Academic Press.
- Barlow, H. B., & Mollon, J. D. (1982). Spatial and temporal resolution and analysis. In J. M. Woodhouse, & H. B. Barlow (Eds.), *The senses* (pp. 132-164). Cambridge: Cambridge University Press.
- Ben-Sira, I., Weinberger, D., Bodenheimer, J., & Yassur, Y. (1980). Clinical method for measurement of light backscattering from the in vivo human lens. *Investigative Ophthalmology & Vision Science*, 19, 435-438.

- Bioninja. (2012). *E5: The human brain*. <http://www.ib.bioninja.com.au/options/option-e-neurobiology-and-2/e5-the-human-brain.html>
- Birch, D. G., Sandberg, A. M., & Berson, E. L. (1982). The stiles-crawford effect in retinitis pigmentosa. *Investigative Ophthalmology & Vision Science*, *22*, 157-164.
- Blackwell, H. R. (1946). Contrast thresholds of the human eye. *Journal of the Optical Society of America*, *36*, 624-632.
- Boynton, R. M., Enoch, J. M., & Bush, W. R. (1954). Physical measures of stray light in excised eyes. *Journal of the Optical Society of America*, *44*, 879-886.
- Bron, A. J., Vrensen, G. F., Koretz, J., Maraini, G., & Harding, J. J. (2000). The ageing lens. *Ophthalmologica*, *214*, 86-104.
- Brown, W. R. J. (1951). The influence of luminance level on visual sensitivity to color differences. *Journal of the Optical Society of America*, *41*, 648-688.
- Campbell, F. W. (1957). The depth of field of the human eye. *Optica Acta*, *4*, 157-164.
- Carroll, J., Dubis, A. M., Godara, P., Dubra, A., & Stepien, K. E. (2011). Clinical applications of retinal imaging with adaptive optics. *US Ophthalmic Review*, *4*, 78-83.
- Cerviño, A., Gonzalez'Meijome, J. M., Linhares, J. M. M., Hosking, S. L., & Montes-Mico, R. (2008). Effect of sport-tinted contact lenses for contrast enhancement on retinal straylight measurements. *Ophthalmic and Physiological Optics*, *28*, 151-156.
- Charman, W. N., Jennings, J. A. M., & Whitefoot, H. (1978). The refraction of the eye in relation to spherical aberration and pupil size. *British Journal of Physiological Optics*, *32*, 78-93.

- Chisholm, C. M., Evans, A. D., Harlow, J. A., & Barbur, J. L. (2003). New test to assess pilot's vision following refractive surgery. *Aviation Space and Environmental Medicine*, 74, 551-559.
- Claffey, M. (2012). *Convergence of cones and rods*. <http://mikeclaffey.com/psyc2/notes-vision.html>
- Connolly, D. M., & Barbur, J. L. (2009). Low contrast acuity at photopic and mesopic luminance under mild hypoxia, normoxia, and hyperoxia. *Aviation Space and Environmental Medicine*, 80, 933-940.
- Coppens, J. E., Franssen, L., & van den Berg, T. J. T. P. (2006). Wavelength dependence of intraocular straylight. *Experimental Eye Research*, 82, 688-692.
- Costello, J. M., Johnsen, S., Gilliland, K. O., Freel, C. D., & Fowler, C. W. (2007). Predicted light scattering from particles observed in human age-related nuclear cataracts using mie scattering theory. *Investigative Ophthalmology & Vision Science*, 48, 303-312.
- Curcio, C. A., Allen, K. A., Sloan, K. R., Lerea, C. L., Hurley, J. B., Klock, I. B., et al. (1991). Distribution and morphology of human cone photoreceptors stained with anti-blue opsin. *The Journal of Comparative Neurology*, 312, 610-624.
- De Brouwere, D. (2008). Corneal light scattering following excimer laser surgery. *Unpublished Doctor of Philosophy, University of Crete*.
- De Brouwere, D., Ginis, H., Kymionis, G., Naoumidi, I., & Pallikaris, I. Forward scattering properties of corneal haze. *Optometry & Vision Science*, 85, 843-848.
- de Waard, P. W., IJspeert, J. K., van den Berg, T. J. T. P., & de Jong, P. T. V. M. (1992). Intraocular light scattering in age-related cataracts. *Investigative Ophthalmology & Vision Science*, 33, 618-625.

- DeLint, P. J., Berendschot, T. T. J. M., & van Norren, D. (1998). A comparison of the optical stiles-crawford effect and retinal densitometry in a clinical setting. *Investigative Ophthalmology & Vision Science*, 39, 1519-1523.
- DeMott, D. W., & Boynton, R. M. (1957). Retinal distribution of entoptic straylight. *Journal of the Optical Society of America*, 48, 13-22.
- DeMott, D. W., & Boynton, R. M. (1958). Sources of entoptic straylight. *Journal of the Optical Society of America*, 48, 120-125.
- Duree, G. (2011). *Optics for dummies*. Indianapolis, Indiana: Wiley Publishing, Inc.
- Elliott, D. B. Evaluating visual function in cataract. *Optometry & Vision Science*, 70, 896-902.
- Elliott, D. B., & Bullimore, M. A. (1993). Assessing the reliability, discriminative ability, and validity of disability glare tests. *Investigative Ophthalmology & Visual Science*, 34, 108-119.
- Elliott, D. B., Hurst, M. A., & Weatherill, J. (1990). Comparing clinical tests of visual function in cataract with the patient's perceived visual disability. *Eye*, 4, 712-717.
- Elliott, D. B., Mitchell, S., & Whitaker, D. (1991). Factors affecting light scatter in contact lens wearers. *Optometry and Vision Science*, 68, 629-633.
- Elliott, D. B., Fonn, D., Flanagan, J., & Doughty, M. (1993). The relative sensitivity of clinical tests to hydrophilic lens induced corneal thickness changes. *Optometry & Vision Science*, 70, 1044-1048.
- Enoch, J. M., & Fry, G. A. (1958). Characteristics of a model retinal receptor studied at microwave frequencies. *Journal of the Optical Society of America*, 48, 899-911.

- Enoch, J. M., & Hope, G. M. (1973). Directional sensitivity of the foveal and parafoveal retina. *Investigative Ophthalmology & Visual Science*, 12, 497-503.
- Ferris, F. L., Kassov, A., Bresnick, G. H., & Bailey, I. (1982). New visual acuity charts for clinical research. *American Journal of Ophthalmology*, 94, 91-96.
- Fisher, A. J., & Christie, A. W. (1965). A note on disability glare. *Vision Research*, 5, 565-580.
- Forrester, J., Dick, A., McMenamin, P., & Lee, W. (1996). *The eye: Basic sciences in practice*. London: W.B. Saunders Company Ltd.
- Franssen, L., Coppens, J. E., & van den Berg, T. J. T. P. (2006). Compensation comparison method for assessment of retinal straylight. *Investigative Ophthalmology & Vision Science*, 47, 768-776.
- Franssen, L., Taberner, J., Coppens, J. E., & van den Berg, T. J. T. P. (2007). Pupil size and retinal straylight in the normal eye. *Investigative Ophthalmology & Visual Science*, 48, 2375-2382.
- Freeman, M. H., & Hull, C. C. (2003). *Optics* (11th ed.). Eastbourne, England: Butterworth-Heinemann.
- Fry, G. A., & Alpern, M. (1953). The effect of a peripheral glare source upon the apparent brightness of an object. *Journal of the Optical Society of America*, 43, 189-195.
- Georgeson, M. A., & Sullivan, G. D. (1975). Contrast constancy. *Journal of Physiology*, 252, 627.
- Gibbs, K. (2013). *Diffraction*. http://www.schoolphysics.co.uk/age14-16/Wave%20properties/text/Diffraction_/index.html

- Gregory, R. L. (1966). *Eye and brain*. Verona, Italy: Officine Grafiche Arnoldo Mondadori.
- Haegerstrom-Portnoy, G., Schneck, M. E., & Brabyn, J. A. (1999). Seeing into old age: Vision function beyond visual acuity. *Optometry and Vision Science*, *76*, 141-158.
- Haegerstrom-Portnoy, G. (2005). The Glenn A. Fry award lecture 2003: Vision in elders- summary of findings of the SKI study. *Optometry & Vision Science*, *82*, 87-93.
- Hammond, B. R., Jr., Wooten, B. R., & Snodderly, M. D. (1998). Preservation of visual sensitivity of older subjects: Association with macular pigment density. *Investigative Ophthalmology & Visual Science*, *39*, 397-406.
- Harrison, J. M., Applegate, R. A., Yates, J. T., & Ballentine, C. (1993). Contrast sensitivity and disability glare in the middle years. *Journal of the Optical Society of America A*, *10*, 1849-1855.
- Hecht, S., Schlaer, S., & Pirenne, M. H. (1942). Energy, quanta, and vision. *The Journal of General Physiology*, *25*, 819-840.
- Hemenger, R. P. (1988). Small-angle intraocular light scatter: A hypothesis concerning its source. *Journal of the Optical Society of America A*, *5*, 577-582.
- Hemenger, R. P. (1992). Sources of intraocular light scatter from inversion of an empirical glare function. *Applied Optics*, *31*, 3687-3693.
- Hennelly, M. L., Barbur, J. L., Edgar, D. F., & Woodward, E. G. (1998). The effect of age on the light scattering characteristics of the eye. *Ophthalmic & Physiological Optics*, *18*, 197-203.
- Hennelly, M. L., Barbur, J. L., Edgar, D. F., & Woodward, E. G. (1997). Factors affecting the integrated straylight parameter in the normal human eye. *Investigative Ophthalmology & Visual Science*, *38*, S1014.

- Hodgkinson, I. J., & Greer, P. B. (1994). Point-spread function for light scattered in the human ocular fundus. *Journal of the Optical Society of America A*, *11*, 479-486.
- Holladay, L. L. (1926). The fundamentals of glare and visibility. *Journal of the Optical Society of America*, *12*, 271-319.
- Holladay, L. L. (1927). Action of a light source in the field of lowering visibility. *Journal of the Optical Society of America*, *14*, 1.
- Hopkinson, R. G. (1956). Glare discomfort and pupil diameter. *Journal of the Optical Society of America*, *46*, 649-656.
- Hubel, D. H. (1988). *Eye, brain and vision*. New York: Scientific American Press.
- Hume, R. (1978). Binocular summation: A study of contrast sensitivity, visual acuity and recognition. *Vision Research*, *18*, 579-585.
- Ijspeert, J. K., de Waard, P. W. T., van den Berg, T. J. T. P., & de Jong, P. T. V. M. (1990). The intraocular straylight function in 129 healthy volunteers; dependence on angle, age and pigmentation. *Vision Research*, *30*, 669-707.
- International Commission on Illumination. (1926). *Proceedings 6th Session (Geneva, 1924)*, pp. 67-69.
- International Commission on Illumination. (1952). *Proceedings 12th Session (Stockholm, 1951)*, pp. 37-39.
- International Commission on Illumination. (1987). *International lighting vocabulary, 4th edition*. CIE publication No. 17.4.
- International Commission on Illumination. (2002). *CIE collection on glare*. CIE publication No. 146.

- International Commission on Illumination. (2010). *Recommended system for mesopic photometry based on visual performance*. CIE publication No. 191.
- James, B., & Bron, A. (2011). *Ophthalmology lecture notes*. Chichester: Wiley-Blackwell.
- Jinabhai, A., O'Donnell, C., Radhakrishnan, H., & Nourrit, V. (2012). Forward light scatter and contrast sensitivity in keratoconic patients. *Contact Lens & Anterior Eye*, 35, 22-27.
- Kaufman, P. (2002). *Adler's physiology of the eye* (10th ed.). London: Elsevier.
- Kline, D. W., & Schieber, F. (1985). Vision & ageing. In J. E. Birren, & K. W. Schaie (Eds.), *Handbook of the psychology of ageing* (pp. 296-331). New York: Van Nostrand Reinhold.
- Kolb, H. (2014a). Inner plexiform layer. In H. Kolb, R. Nelson, E. Fernandez & B. Jones (Eds.), *Webvision: The organization of the retina and visual system*.
<http://webvision.med.utah.edu/>
- Kolb, H. (2014b). Simple anatomy of the retina. In H. Kolb, R. Nelson, E. Fernandez & B. Jones (Eds.), *Webvision: The organization of the retina and visual system*.
<http://webvision.med.utah.edu/>
- Kruijt, B., Franssen, L., Prick, L. J. M. M., van Vliet, J. M. J., & van den Berg, T. J. T. P. (2011). Ocular straylight in albinism. *Optometry & Vision Science*, 88, 585-592.
- Kvansakul, J. G. S. (2005). The measurement of scattered light in the eye and its effects on visual performance. *Unpublished Doctor of Philosophy, City University, London*.
- Landrum, J. T., & Bone, R. A. (2001). Lutein, zeaxanthin, and the macular pigment. *Archives of Biochemistry and Biophysics*, 385, 28-40.

- Le Grand, Y. (1937). Recherches sur la diffusion de la lumière dans l'oeil humain. *Optical Review*, 16, 240-266.
- LeClaire, J., Nadler, P., Weiss, S., & Miller, D. (1982). A new glare tester for clinical testing. *Archives of Ophthalmology*, 100, 153-158.
- Lohmann, C. P., Fitze, F., O'Brart, D., Muir, M. K., Timberlake, G., & Marshall, J. (1993). Corneal light scattering and visual performance in myopic individuals with spectacles, contact lenses, or excimer laser photorefractive keratectomy. *American Journal of Ophthalmology*, 115, 444-453.
- Luria, S. M. (1972). Vision with chromatic filters. *American Journal of Optometry and Archives of American Academy of Optometry*, 49, 818-829.
- Mainster, M. A., & Turner, P. L. (2012). Glare's causes, consequences, and clinical challenges after a century of ophthalmic study. *American Journal of Ophthalmology*, 153, 587-593.
- Mainster, M. A., & Timberlake, G. T. (2003). Why HID headlights bother older drivers. *British Journal of Ophthalmology*, 87, 113-117.
- Mellerio, J. (1971). Light absorption and scatter in the human lens. *Vision Research*, 11, 129-141.
- Michael, R., van Merl, J., Vrensen, G. F. J. M., & van den Berg, T. J. T. P. (2003). Changes in the refractive index of lens fibre membranes during maturation: Impact on lens transparency. *Experimental Eye Research*, 77, 93-99.
- Millodot, M. (1982). Image formation in the eye. In H. B. Barlow, & J. D. Mollon (Eds.), *The senses* (pp. 46-61) Cambridge: Cambridge University Press.

- Nave, C. R. (2012). *Hyperphysics*. <http://hyperphysics.phy-astr.gsu.edu/hbase/atmos/blusky.html>
- Norren, D. V., & Vos, J. J. (1974). Spectral transmission of the human ocular media. *Vision Research, 14*, 1237-1244.
- O'Brien, B. (1951). Vision and resolution in the central retina. *Journal of the Optical Society of America A, 41*, 882-894.
- Pardhan, S., & Gilchrist, J. (1991). The importance of measuring binocular contrast sensitivity in unilateral cataract. *Eye, 5*, 31-35.
- Paulsson, L. E., & Sjöstrand, J. (1980). Contrast sensitivity in the presence of a glare light. theoretical concepts and preliminary clinical studies. *Investigative Ophthalmology & Vision Science, 19*, 401-406.
- Pelli, D. G., Robson, J. G., & Wilkins, A. J. (1988). The design of a new letter chart for measuring contrast sensitivity. *Clinical Vision Sciences, 2*, 187-199.
- Perkins, E. S. (2014). *Human eye*. In *Encyclopædia Britannica*.
<http://www.britannica.com/EBchecked/topic/1688997/human-eye?oasmId=3421>
- Pokorny, J., & Smith, V. C. (2006). Visual acuity and contrast sensitivity. In S. J. Ryan, D. R. Hinton, A. P. Schachat & P. Wilkinson (Eds.), *Retina* (4th ed., pp. 209-225). London: Elsevier Publishers.
- Prager, T. C., Urso, R. G., Holladay, J. T., & Stewart, R. H. (1989). Glare testing in cataract patients: Instrument evaluation and identification of sources of methodological error. *Journal of Cataract and Refractive Surgery, 15*, 149-157.
- Quillan, D. A. (1999). Common causes of vision loss in elderly patients. *American Family Physician, 60*, 99-108.

- Raman, C. V. (1978). *Scattering of light*. Bangalore, India: The Indian Academy of Sciences.
- Rodriguez-Carmona, M., Harlow, J. A., Walker, G., & Barbur, J. L. (2005). The variability of normal trichromatic vision and the establishment of the "normal" range. *Proceedings of 10th Congress of the International Colour Association*, (pp. 979-982). Granada.
- Root, T. (2009). *OphthoBook*. North Charleston, SC: CreateSpace Independent Publishing Platform.
- Rovamo, J., Mustonen, J., & Näsänen, R. (1995). Neural modulation transfer function of the human visual system at various eccentricities. *Vision Research*, *35*, 767-774.
- Schlaer, S. (1937). The relationship between visual acuity and illumination. *The Journal of General Physiology*, *21*, 165-188.
- Schmidt, S. Y., & Peisch, R. D. (1986). Melanin concentration in normal human retinal pigment epithelium. *Investigative Ophthalmology & Visual Science*, *27*, 1063-1067.
- Schwiegerling, J. (2004). *Field guide to visual and ophthalmic optics*. Barnesandnoble.com: SPIE Press.
- Simpson, G. C. (1953). Ocular haloes and coronas. *British Journal of Ophthalmology*, *37*, 450-486.
- Snowden, R., Thompson, P., & Troscianko, T. (2006). *Basic vision*. New York: Oxford University Press.
- Song, S., Landsbury, A., Dahm, R., Liu, Y., Zhang, Q., & Quinlan, R. A. (2009). Functions of the intermediate filament cytoskeleton in the eye lens. *Journal of Clinical Investigation*, *119*, 1837-1848.

- Spector, A., Li, S., & Sigelman, J. (1974). Age-dependent changes in the molecular size of human lens proteins and their relationship to light scatter. *Investigative Ophthalmology & Vision Science*, *13*(10), 795-798.
- STAAR Surgical Company. (2014). *Visian ICL*. <http://visianinfo.com/cataracts-intraocular-lens>.
- Steen, R., Whitaker, D., Elliot, D. B., & Wild, J. M. (1994). Age-related effects of glare on luminance and color contrast sensitivity. *Optometry and Vision Science*, *71*, 792-796.
- Stiles, W. S. (1929a). The effect of glare on the brightness difference threshold. *Proceedings of the Royal Society of London 104B*, 322-355.
- Stiles, W. S. (1929b). The nature and effects of glare. *The Illuminating Engineering Society*, *22*, 304-312.
- Stiles, W. S. (1930). The scattering theory on the effect of glare on the brightness difference threshold. *Proceedings of the Royal Society of London 105B*, 131-146.
- Stiles, W. S., & Crawford, B. H. (1933). The luminous efficiency of rays entering the eye pupils at different points. *Proceedings of the Royal Society of London 112B*, 428-450.
- Stiles, W. S., & Crawford, B. H. (1934). The liminal brightness increment for white light for different conditions of the foveal and parafoveal retina. *Proceedings of the Royal Society London, 116B*, 55-102.
- Stiles, W. S., & Crawford, B. H. (1937). The effect of a glaring light source on extrafoveal vision. *Proceedings of the Royal Society of London 122B*, 255-280.
- Stockman, A., Langendorfer, M., Smithson, H. E., & Sharpe, L. T. (2006). Human cone light adaptation: From behavioral measurements to molecular mechanisms. *Journal of Vision*, *6*, 1194-1213.

- Stockman, A., & Sharpe, L. T. (2006). Into the twilight zone: The complexities of mesopic vision and luminous efficiency. *Ophthalmic & Physiological Optics*, 26, 225-239.
- Stringham, J. M., Garcia, P. V., Smith, P. A., McLin, L. N., & Foutch, B. K. (2011). Macular pigment and visual performance in glare: Benefits for photostress recovery, disability glare, and visual discomfort. *Investigative Ophthalmology & Visual Science*, 52, 7406-7415.
- Strutt, J. (1971). On the light from the sky, its polarization and colour. *Philosophical Magazine*, 41, 107-120.
- Thaug, J., & Sjöstrand, J. (2002). Integrated light scattering as a function of wavelength in donor lenses. *Journal of the Optical Society of America A*, 19, 152-157.
- Tiffen. (2015). *4K diffusion test film*. <http://tiffen.com/tiffen-filters/4k-diffusion-test-film>.
- Trattler, W. (2014). *Corneal crosslinking for Keratoconus and LASIK complications*. <http://www.allaboutvision.com/conditions/corneal-crosslinking.htm>.
- Troelstra, A. (1968). Detection of time-varying light signals as measured by the pupillary response. *Journal of the Optical Society of America*, 5, 685-690.
- Trokel, S. (1962). The physical basis for the transparency of the crystalline lens. *Investigative Ophthalmology*, 1, 493-501.
- Troxler, D. (1804). Über das verschwinden gegebener gegenstände innerhalb unseres gesichtskreises. In K. Himly, & J. A. Schmidt (Eds.), *Ophthalmologische Bibliothek*, 2, 1-53.
- van den Berg, T. J. T. P. (1995). Analysis of intraocular straylight, especially in relation to age. *Optometry & Vision Science*, 72, 52-59.

- van den Berg, T. J. T. P. (1986). Importance of pathological intraocular light scatter for visual disability. *Documenta Ophthalmologica: Advances in Ophthalmology*, 61, 327-333.
- van den Berg, T. J. T. P. (1991). On the relation between glare and straylight. *Documenta Ophthalmologica*, 78, 177-181.
- van den Berg, T. J. T. P., & Coppens, J. E. (2005). *Method and device for measuring retinal straylight* (WO2005023103 ed.) NL1024232C.
- van den Berg, T. J. T. P., Franssen, L., Kruijt, B., & Coppens, J. E. (2013). History of ocular straylight measurement: A review. *Zeitschrift Fur Medizinische Physik*, 23(1), 6-20.
- van den Berg, T. J. T. P., Hagenouw, M. P. J., & Coppens, J. E. (2005). The ciliary corona: Physical model and simulation of the fine needles radiating from point light sources. *Investigative Ophthalmology & Visual Science*, 46, 2627-2632.
- van den Berg, T. J. T. P., & IJspeert, J. K. (1991). Intraocular straylight, studied using the direct compensation technique. *CIE Proceedings 22nd session, division I*, (pp. 83-84). Vienna.
- van den Berg, T. J. T. P., IJspeert, J. K., & de Waard, P. W. (1991). Dependence of intraocular straylight on pigmentation and light transmission through the ocular wall. *Vision Research*, 31, 1361-1367.
- van den Berg, T. J. T. P., & Spekreijse, H. (1987). Measurement of the straylight function of the eye in cataract and other optical media disturbances by means of a direct compensation method. *Investigative Ophthalmology & Vision Science (Suppl)*, 28, 397.
- van den Berg, T. J. T. P., & Ijspeert, J. K. (1992). Clinical assessment of intraocular stray light. *Applied Optics*, 31, 3694-3696.

- van den Berg, Thomas J.T.P. (1995). Age related changes in clarity of the ocular media. *Proceedings of the 3rd International Symposium, Lighting for Aging Vision and Health*, (pp. 27-37). New York: Lighting Research Institute.
- van den Berg, T. J. T. P., & Ijspeert, J. K. (1995). Light scattering in donor lenses. *Vision Res.*, *35*, 169-177.
- van der Heijde, G. L., Weber, J., & Boukes, R. (1985). Effects of straylight on visual acuity in pseudophakia. *Documenta Ophthalmologica*, *59*, 81-84.
- Van Loo, J. A., & Enoch, J. M. (1975). The scotopic stiles-crawford effect. *Vision Research*, *15*, 1005-1009.
- van Nes, F. L., & Bouman, M. A. (1967). Spatial modulation transfer in the human eye. *Journal of the Optical Society of America*, *57*, 401-406.
- Vaughan, D., & Asbury, T. (1983). *General ophthalmology* (10th ed.). Los Altos, California: Lange Medical Publications.
- Veraart, G. N., van den Berg, T. J. T. P., Ijspeert, J. K., & Lopes Cardozo, O. (1992). Stray light in radial keratotomy and the influence of pupil size and straylight angle. *American Journal of Ophthalmology*, *114*, 424-428.
- Vitorpamplona. (2010). *Wikimedia commons*.
http://commons.wikimedia.org/wiki/File:Shack_hartmann.jpg.
- Vohnsen, B. (2007). Photoreceptor waveguides and effective retinal image quality. *Journal of the Optical Society of America A*, *24*, 597-607.
- Vos, J. J. (1964). Contribution of the retina to entoptic scatter. *Journal of the Optical Society of America*, *54*, 95-100.

- Vos, J. J. (2003a). On the cause of disability glare and its dependence on glare angle, age and ocular pigmentation. *Clinical and Experimental Optometry*, 86, 363-370.
- Vos, J. J. (2003b). Reflections on glare. *Lighting Research and Technology*, 35, 163-176.
- Vos, J. J., & Boogaard, J. (1963). Contribution of the cornea to entoptic scatter. *Journal for Optical Society of America*, 53, 869-873.
- Vos, J. J., & van den Berg, T. J. T. P. (1999). Report on disability glare. *CIE Collection: Vision and Colour, Physical Measurement of Light and Radiation*, 135, 1-9.
- Walkey, H. C., Harlow, J. A., & Barbur, J. L. (2006a). Changes in reaction time and search time with background luminance in the mesopic range. *Ophthalmic and Physiological Optics*, 26, 288-299.
- Walkey, H. C., Harlow, J. A., & Barbur, J. L. (2006b). Characterising mesopic spectral sensitivity from reaction times. *Vision Research*, 46, 4232-4243.
- Walkey, H. C., Barbur, J. L., Harlow, J. A., Hurden, A., Moorhead, I. R., & Taylor, J. A. (2005). Effective contrast of colored stimuli in the mesopic range: A metric for perceived contrast based on achromatic luminance contrast. *Journal of the Optical Society of America A*, 22, 17-28.
- Walraven, P. L. (2009). The virtual pupil. *Journal of Modern Optics*, 56, 2251-2253.
- Wandell, B. A. (1995). *Foundations of vision*. Sunderland, Massachusetts: Sinaur Associates, Inc.
- Weale, R. A. (1963). *The aging eye*. London: Lewis.

- Weiter, J. J., Delori, F. C., Wing, G. L., & Fitch, K. A. (1986). Retinal pigment lipofuscin and myelin and choroidal melanin in human eyes. *Investigative Ophthalmology & Visual Science*, 27, 145-152.
- Westheimer, G. (2008). Directional sensitivity of the retina: 75 years of Stiles–Crawford effect. *Proceedings of the Royal Society London B*, 275, 2777-2786.
- Westheimer, G., & Liang, J. (1995). Influence of ocular light scatter on the eye's optical performance. *J. Opt. Soc. Am. A*, 12, 1417-1424.
- Whitaker, D., Elliott, D. B., & Steen, R. (1994). Confirmation of the validity of the psychophysical light scattering factor. *Investigative Ophthalmology & Vision Science*, 35, 317-321.
- Whitaker, D., Steen, R., & Elliott, D. B. (1993). Light scatter in the normal young, elderly, and cataractous eye demonstrates little wavelength dependency. *Optometry & Vision Science*, 70, 963-968.
- Wolfe, J. M., Kluender, K. R., & Levi, D. M. (2006). In Bartushuk L. M., Herz R. S., Klatzky R. L. and Lederman S. J. (Eds.), *Sensation & perception*. Sunderland, Massachusetts: Sinaur Associates, Inc.
- Wolff, E. (1946). The muco-cutaneous junction of the lid margin and the distribution of the tear fluid. *Transactions of the Ophthalmological Societies of the United Kingdom*, 291-308.
- Wolff, E. (1954). *The anatomy of the eye and orbit*. (4th ed., pp. 49). London: H.K. Lewis and Co.

Wolffsohn, J. S. P., FAAO, Cochrane, A. L. P., FAAO, Khoo, H. B., Yoshimitsu, Y. B., & Wu, S. B. (2000). Contrast is enhanced by yellow lenses because of selective reduction of short-wavelength light. *Optometry and Vision Science*, 77, 73-81.

Wooten, B. R., & Geri, G. A. (1987). Psychophysical determination of intraocular light scatter as a function of wavelength. *Vision Research*, 27, 1291-1298.

Wopereis, J. (2010). *Center for microscopy and imaging (CMI), Smith College*.
<http://131.229.88.77/microscopy/images/var12.jpg>.

Xia, J. Z., Wang, Q., Tatarkova, S., Aerts, T., & Clauwaert, J. (2010). Structural basis of eye lens transparency: Light scattering by concentrated solutions of bovine alpha-crystallin proteins. *Biophysical Journal*, 71, 2815-2822.

Yebra, A., García, J. A., Nieves, J. L., & Romero, J. (2001). Chromatic discrimination in relation to luminance level. *Color Research and Application*, 26, 123-131.